Lecture notes: Composite Mechanics

Martin Fagerström[†]

[†]Division of Material and Computational Mechanics, Department of Applied Mechanics
Chalmers University of Technology, Göteborg, Sweden
e-mail: martin.fagerstrom@chalmers.se

Chapter 1

Elastic anisotropy

1.1 Basics of tensors and index notation

A 3-dimensional vector $\mathbf{a}$ in the 3D space spanned by the base vectors $\mathbf{e}_1, \mathbf{e}_2, \mathbf{e}_3$ can be represented in the following way:

$$\mathbf{a} = a_1\mathbf{e}_1 + a_2\mathbf{e}_2 + a_3\mathbf{e}_3 \tag{1.1}$$

where $a_i,\ i = 1, 2, 3$ are the vector components. This can of course also be written as a sum according to:

$$\mathbf{a} = \sum_{i=1}^{3} a_i\mathbf{e}_i \tag{1.2}$$

Now, in order to simplify things, we can drop the summation sign whenever two indices are the same (i in the vector form above). Thus, we use the short notation according to:

$$\mathbf{a} = \sum_{i=1}^{3} a_i\mathbf{e}_i = a_i\mathbf{e}_i \tag{1.3}$$

meaning that any index (e.g. i) can take the numbers 1-3 and when two identical indices are present, this implicitly means a summation over that index from 1 to 3.

We can also introduce the matrix representation of the vector $\mathbf{a}$ according to:

$$[\mathbf{a}]_{\mathbf{e}_1,\mathbf{e}_2,\mathbf{e}_3} = \begin{bmatrix} a_1 \\ a_2 \\ a_3 \end{bmatrix} \tag{1.4}$$

where the subscripts indicate that the representation is made with respect to the coordinate system with base vectors $\mathbf{e}_i$.

In the same way, we can write a second order tensor $\mathbf{T}$ as

$$\begin{aligned} \mathbf{T} = & T_{11}\mathbf{e}_1 \otimes \mathbf{e}_1 + T_{12}\mathbf{e}_1 \otimes \mathbf{e}_2 + T_{13}\mathbf{e}_1 \otimes \mathbf{e}_3 \\ & + T_{21}\mathbf{e}_2 \otimes e_1 + T_{22}\mathbf{e}_2 \otimes \mathbf{e}_2 + T_{23}\mathbf{e}_2 \otimes \mathbf{e}_3 \\ & + T_{31}\mathbf{e}_3 \otimes e_1 + T_{32}\mathbf{e}_3 \otimes \mathbf{e}_2 + T_{33}\mathbf{e}_3 \otimes \mathbf{e}_3 \\ = & \sum_{i=1}^{3}\sum_{j=1}^{3} T_{ij}\mathbf{e}_i \otimes \mathbf{e}_j = \{ \text{ index notation } \} = T_{ij}\mathbf{e}_i \otimes \mathbf{e}_j \end{aligned} \tag{1.5}$$

where $\otimes$ is the so-called *open product* between two vectors (resulting in a second order tensor) defined as

$$\mathbf{A} = \mathbf{a} \otimes \mathbf{b},\ \Rightarrow A_{ij} = a_i b_j. \tag{1.6}$$

Please note that $\otimes$ on matrix form can be visualised as the multiplication of a column vector and a row vector into a matrix. Furthermore, in Eq. (1.5) there are two indices i and j present precisely two times meaning that a summation should be conducted both for $i = 1, 2, 3$ and $j = 1, 2, 3$. And consequently, the matrix representation of the second order tensor $\mathbf{T}$ is given by:

$$[\mathbf{T}]_{\mathbf{e}_1,\mathbf{e}_2,\mathbf{e}_3} = \begin{bmatrix} T_{11} & T_{12} & T_{13} \\ T_{21} & T_{22} & T_{23} \\ T_{31} & T_{32} & T_{33} \end{bmatrix} \tag{1.7}$$

1.2 Repetition of strains

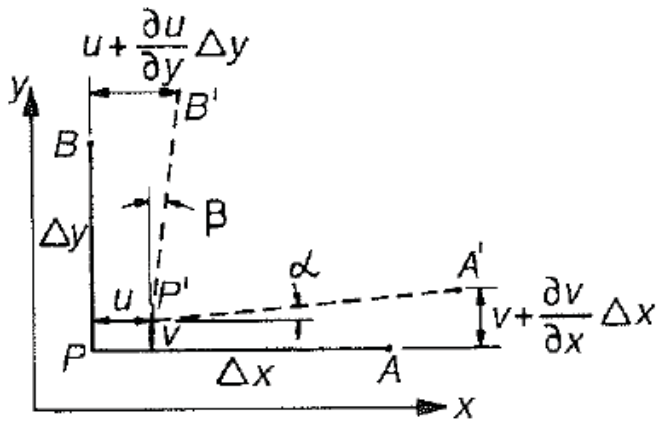

Figure 1.1: Deformation sketch (from Agarwal et al., figure A2-2).

A point P is subjected to the displacement field $\mathbf{u}$ with components in the x-direction $u(x, y, z)$, the y-direction $v(x, y, z)$ and the z-direction $w(x, y, z)$. To identify the normal (longitudinal) and shear strains at this point, we study the change of length and angle of two infinitesimal and perpendicular line segments PA and PB, cf. Figure 1.1.

The normal strain in the x-direction at point P is obtained as the ratio between the increase of length of PA in the x-direction due to deformation and the original length of PA. Thus, we obtain the longitudinal strain in the x-direction, ε_x as:

$$\varepsilon_x = \lim_{\Delta x \to 0} \frac{|P^{'}A^{'}|_x - |PA|_x}{|PA|_x} = \lim_{\Delta x \to 0} \frac{\Delta x + u(x + \Delta x, y, z) - u(x, y, z) - \Delta x}{\Delta x} = \frac{\partial u(x, y, z)}{\partial x} \tag{1.8}$$

In the same manner, we obtain the longitudinal strain in the y-direction, ε_y, as the ratio between the increase of length of PB in the y-direction due to deformation and the original length of PB:

$$\varepsilon_y = \lim_{\Delta y \to 0} \frac{|P^{'}B^{'}|_y - |PB|_y}{|PB|_y} = \lim_{\Delta y \to 0} \frac{\Delta y + v(x, y + \Delta y, z) - v(x, y, z) - \Delta y}{\Delta y} = \frac{\partial v(x, y, z)}{\partial y} \tag{1.9}$$

Finally, we obtain the shear strain (or shear angle) as the sum of change of angles of PA and PB due to deformation as:

$$\gamma_{xy} = \gamma_{yx} = \alpha + \beta = \lim_{\Delta x \to 0,\ \Delta y \to 0} \frac{v + \frac{\partial v}{\partial x}\Delta x - v}{\Delta x} + \frac{u + \frac{\partial u}{\partial y}\Delta y - u}{\Delta y} = \frac{\partial v}{\partial x} + \frac{\partial u}{\partial y} \tag{1.10}$$

where it was used that $\tan\alpha \approx \alpha,\ \tan\beta \approx \beta$ for small strains.

Now, generalising these results to three dimensions, the remaining strains are found as:

$$\varepsilon_z = \frac{\partial w(x, y, z)}{\partial z} \tag{1.11}$$

$$\gamma_{xz} = \gamma_{zx} = \frac{\partial w}{\partial x} + \frac{\partial u}{\partial z} \tag{1.12}$$

$$\gamma_{yz} = \gamma_{zy} = \frac{\partial w}{\partial y} + \frac{\partial v}{\partial z} \tag{1.13}$$

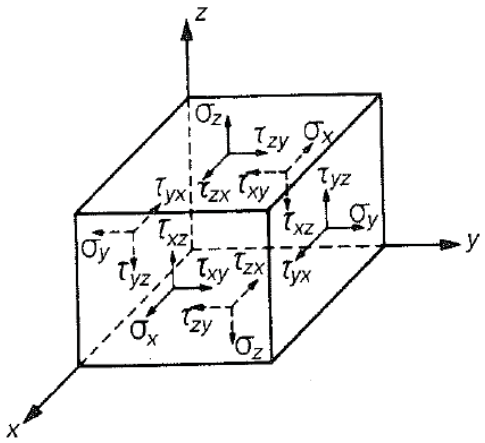

Figure 1.2: Three-dimensional stress components (from Agarwal et al. figure A2-5).

Generally speaking, the strain is represented by a *symmetric* second order tensor $\boldsymbol{\varepsilon} = \varepsilon_{ij}\mathbf{e}_i \otimes \mathbf{e}_j$ where $\mathbf{e}_i$ is the ith base vector. However, in this course we will restrict mainly to cartesian x,y,z-coordinate systems thereby limiting ourselves to the fact that the strain tensor can be represented (with respect to this coordinate system) by its cartesian matrix representation $[\boldsymbol{\varepsilon}]_{xyz}$ according to:

$$[\boldsymbol{\varepsilon}]_{xyz} = \begin{bmatrix} \varepsilon_x & \varepsilon_{xy} & \varepsilon_{xz} \\ \varepsilon_{xy} & \varepsilon_y & \varepsilon_{yz} \\ \varepsilon_{xz} & \varepsilon_{yz} & \varepsilon_z \end{bmatrix} = \begin{bmatrix} \varepsilon_x & \frac{1}{2}\gamma_{xy} & \frac{1}{2}\gamma_{xz} \\ \frac{1}{2}\gamma_{xy} & \varepsilon_y & \frac{1}{2}\gamma_{yz} \\ \frac{1}{2}\gamma_{xz} & \frac{1}{2}\gamma_{yz} & \varepsilon_z \end{bmatrix} \tag{1.14}$$

Please note that we in the following will omit the subscript xyz for convenience.

1.3 Repetition of stress

Generally, the stress at a point in a body is described by the nine components in the stress tensor σ_{ij} according to

$$\boldsymbol{\sigma} = \sigma_{ij}\mathbf{e}_i \otimes \mathbf{e}_j \tag{1.15}$$

where (again) $\mathbf{e}_i$ is the ith base vector. The stress tensor may be represented by a matrix representation considering a particular coordinate system. If we again limit ourselves to the cartesian x, y, z-system (as in Figure 1.2), the matrix representation of the stress tensor may be expressed as

$$[\boldsymbol{\sigma}] = \begin{bmatrix} \sigma_{xx} & \tau_{xy} & \tau_{xz} \\ \tau_{yx} & \sigma_{yy} & \tau_{yz} \\ \tau_{zx} & \tau_{zy} & \sigma_{zz} \end{bmatrix} = \{\sigma_{ij} = \sigma_{ji}\} = \begin{bmatrix} \sigma_{xx} & \tau_{xy} & \tau_{xz} \\ \tau_{xy} & \sigma_{yy} & \tau_{yz} \\ \tau_{xz} & \tau_{yz} & \sigma_{zz} \end{bmatrix} \tag{1.16}$$

Please note that it in the last equality was used that the (Cauchy) stress tensor is symmetric, which can be realised by studying the moment equilibrium of an infinitesimal parallelepiped element (at point $P(x, y, z)$) with sides $\Delta x, \Delta y$ and Δz respectively, cf. any basic course in solid mechanics or Appendix A-2 in the course book.

1.4 Coordinate transformation of stress and strain components

Later, we will consider the transformation of the stress and strain components between a fibre oriented coordinate system and a global reference coordinate system. For that purpose, we will need the transformation law for a 2D plane stress case for which the two coordinate systems differ by a rotation about the z axis, cf. Figure 1.3. Here, we will show two ways to derive the expressions for the coordinate transformations based on *i) coordinate transformation of the stress components by consideration of force equilibrium* and *ii) coordinate transformation by change of basis for tensors.*

1.4.1 Coordinate transformation of stress components by consideration of force equilibrium

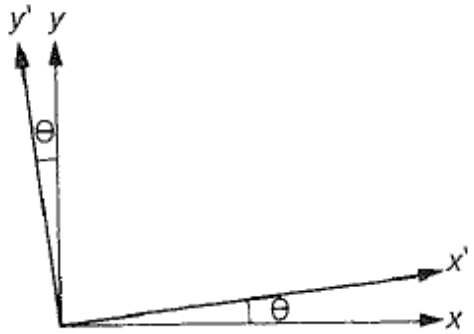

Figure 1.3: Definition of coordinate systems xyz and $x^{'}y^{'}z^{'}$ where the latter has been rotated $+\theta$ degrees around the common z axis ($z^{'}$ axis) (from Agarwal et al., Figure A2-3).

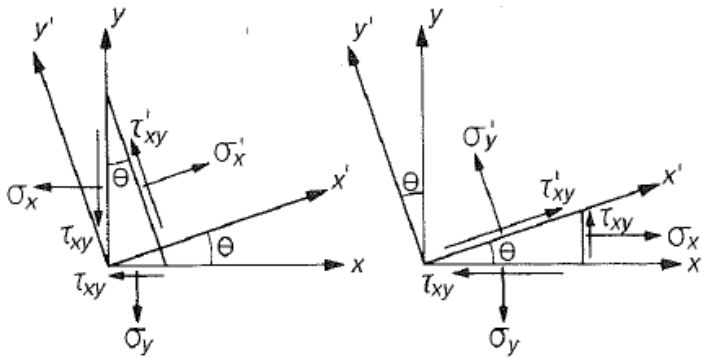

Figure 1.4: (from Agarwal et al., Figure A2-8).

In order to express the stress components in the $x'y'z'$ coordinate system (which is rotated $+\theta$ degrees around the z axis relative to the xyz coordinate system, cf. Figure 1.3) in terms of the components with respect to the xyz system, we consider the equilibrium of two infinitesimal triangular elements as in Figure 1.4. Considering the left part of the figure, with the diagonal area A and $A_x = A\cos\theta$ and $A_y = A\sin\theta$ we can via force equilibrium in the x' direction conclude that:

$$\begin{aligned}\sigma_x^{'}A &= \sigma_x\cos\theta A_x + \sigma_y\sin\theta A_y + \tau_{xy}\cos\theta A_y + \tau_{xy}\sin\theta A_x \\ &= A\left(\sigma_x\cos^2\theta + \sigma_y\sin^2\theta + 2\tau_{xy}\cos\theta\sin\theta\right)\end{aligned} \Rightarrow \tag{1.17}$$

$$\sigma_x^{'} = \sigma_x\cos^2\theta + \sigma_y\sin^2\theta + 2\tau_{xy}\cos\theta\sin\theta \tag{1.18}$$

In the same way, if we consider the equilibrium in the y' direction we obtain:

$$\begin{aligned}\tau_{xy}^{'}A &= -\sigma_x\sin\theta A_x + \sigma_y\cos\theta A_y + \tau_{xy}\cos\theta A_x - \tau_{xy}\sin\theta A_y \\ &= A\left(-\sigma_x\sin\theta\cos\theta + \sigma_y\cos\theta\sin\theta + \tau_{xy}\cos^2\theta - \tau_{xy}\sin^2\theta\right)\end{aligned} \Rightarrow \tag{1.19}$$

$$\tau_{xy}^{'} = (\sigma_y - \sigma_x)\sin\theta\cos\theta + \tau_{xy}\left(\cos^2\theta - \sin^2\theta\right) \tag{1.20}$$

Finally, if we do the same for the right part of the figure we obtain after some derivations:

$$\sigma_y^{'} = \sigma_x\sin^2\theta + \sigma_y\cos^2\theta - 2\tau_{xy}\sin\theta\cos\theta \tag{1.21}$$

$$\tau_{xy}^{'} = (\sigma_y - \sigma_x)\sin\theta\cos\theta + \tau_{xy}\left(\cos^2\theta - \sin^2\theta\right) \tag{1.22}$$

We see that Eq. (1.20) and Eq. (1.22) give the same result. Combining Eqs. (1.18),(1.21) and (1.22) into Voigt matrix form we finally obtain:

$$\left\{ \begin{array}{c} \sigma_x^{'} \\ \sigma_y^{'} \\ \tau_{xy}^{'} \end{array} \right\} = [T_1] \left\{ \begin{array}{c} \sigma_x \\ \sigma_y \\ \tau_{xy} \end{array} \right\} \tag{1.23}$$

where the stress transformation matrix $[T_1]$ is defined as:

$$[T_1] = \left[\begin{array}{ccc} \cos^2\theta & \sin^2\theta & 2\sin\theta\cos\theta \\ \sin^2\theta & \cos^2\theta & -2\sin\theta\cos\theta \\ -\sin\theta\cos\theta & \sin\theta\cos\theta & \cos^2\theta - \sin^2\theta \end{array} \right] \tag{1.24}$$

It should be remarked that the coordinate transformation could just as well have been determined by using the transformation laws of a second order tensor under change of basis, cf. Appendix A-1, which yields the same transformation matrix as in Eqs. (1.24).

1.4.2 Coordinate transformation of stress components by by change of basis for tensors

In order to derive the expression for a coordinate transformation of the stress tensor, we first note that the new base vectors of the rotated coordinate system, given a rotation θ about the z-axis as in Figure 1.3, are obtained as:

$$\mathbf{e}'_x = \mathbf{R} \cdot \mathbf{e}_x \Leftrightarrow \mathbf{e}_x = \mathbf{R}^t \cdot \mathbf{e}'_x \tag{1.25}$$
$$\mathbf{e}'_y = \mathbf{R} \cdot \mathbf{e}_y \Leftrightarrow \mathbf{e}_y = \mathbf{R}^t \cdot \mathbf{e}_y \tag{1.26}$$
$$\mathbf{e}'_z = \mathbf{R} \cdot \mathbf{e}_z = \mathbf{e}_z \tag{1.27}$$

with the given inter-relationships ($\mathbf{e}'_i \cdot \mathbf{e}_j = R_{ij}$):

$$\mathbf{e}'_x \cdot \mathbf{e}_x = \cos(\theta) \tag{1.28}$$
$$\mathbf{e}'_x \cdot \mathbf{e}_y = \sin(\theta) \tag{1.29}$$
$$\mathbf{e}'_x \cdot \mathbf{e}_z = 0 \tag{1.30}$$
$$\mathbf{e}'_y \cdot \mathbf{e}_x = -\sin(\theta) \tag{1.31}$$
$$\mathbf{e}'_y \cdot \mathbf{e}_y = \cos(\theta) \tag{1.32}$$
$$\mathbf{e}'_y \cdot \mathbf{e}_z = 0 \tag{1.33}$$
$$\mathbf{e}'_z \cdot \mathbf{e}_x = 0 \tag{1.34}$$
$$\mathbf{e}'_z \cdot \mathbf{e}_y = 0 \tag{1.35}$$
$$\mathbf{e}'_z \cdot \mathbf{e}_z = 0 \tag{1.36}$$

whereby the transformation tensor $\mathbf{R}$ becomes:

$$\mathbf{R} = \left[\begin{array}{ccc} \cos(\theta) & \sin(\theta) & 0 \\ -\sin(\theta) & \cos(\theta) & 0 \\ 0 & 0 & 1 \end{array} \right]. \tag{1.37}$$

Now, if we consider a change of base for a tensor, say the stress tensor, we have that:

$$\boldsymbol{\sigma} = \sigma_{ij}\mathbf{e}_i \otimes \mathbf{e}_j = \sigma_{ij}(R^t_{ik}\mathbf{e}'_k) \otimes (R^t_{jl}\mathbf{e}'_l) = \underbrace{R_{ki}\sigma_{ij}R^t_{jl}}_{\sigma'_{kl}} \mathbf{e}'_k \otimes \mathbf{e}'_l \tag{1.38}$$

By restricting to plane stress, i.e. only accounting for components in the x- and y-directions, Eq. (1.38) can be written on matrix form as:

$$\left[\begin{array}{cc} \sigma'_{xx} & \tau'_{xy} \\ \tau'_{yx} & \sigma'_{yy} \end{array} \right] = \left[\begin{array}{cc} \cos(\theta) & \sin(\theta) \\ -\sin(\theta) & \cos(\theta) \end{array} \right] \left[\begin{array}{cc} \sigma_{xx} & \tau_{xy} \\ \tau_{yx} & \sigma_{yy} \end{array} \right] \left[\begin{array}{cc} \cos(\theta) & -\sin(\theta) \\ \sin(\theta) & \cos(\theta) \end{array} \right] \tag{1.39}$$

which, if in turn rewritten on contracted Voigt form, becomes identical to Eqs. (1.23)-(1.24) (**show this!**).

1.4.3 Coordinate transformation of strain components

Since the strain tensor $\boldsymbol{\varepsilon}$ is an ordinary second order tensor exactly as the stress tensor, they both follow the same transformation laws. Hence, we can start by concluding that:

$$\begin{aligned}
\varepsilon_x^{'} &= \varepsilon_x \cos^2\theta + \varepsilon_y \sin^2\theta + 2\varepsilon_{xy}\cos\theta\sin\theta && (1.40)\\
\varepsilon_y^{'} &= \varepsilon_x \sin^2\theta + \varepsilon_y \cos^2\theta - 2\varepsilon_{xy}\sin\theta\cos\theta && (1.41)\\
\varepsilon_{xy}^{'} &= (\varepsilon_y - \varepsilon_x)\sin\theta\cos\theta + \varepsilon_{xy}\left(\cos^2\theta - \sin^2\theta\right) && (1.42)
\end{aligned}$$

Now, since we have that $\varepsilon_{xy} = \frac{1}{2}\gamma_{xy}, \varepsilon_{xz} = \frac{1}{2}\gamma_{xz}$ and $\varepsilon_{yz} = \frac{1}{2}\gamma_{yz}$ we also have that $\varepsilon_{xy}^{'} = \frac{1}{2}\gamma_{xy}^{'}, \varepsilon_{xz}^{'} = \frac{1}{2}\gamma_{xz}^{'}$ and $\varepsilon_{yz}^{'} = \frac{1}{2}\gamma_{yz}^{'}$ which finally yields:

$$\begin{aligned}
\varepsilon_x^{'} &= \varepsilon_x \cos^2\theta + \varepsilon_y \sin^2\theta + \gamma_{xy}\cos\theta\sin\theta && (1.43)\\
\varepsilon_y^{'} &= \varepsilon_x \sin^2\theta + \varepsilon_y \cos^2\theta - \gamma_{xy}\sin\theta\cos\theta && (1.44)\\
\gamma_{xy}^{'} &= 2(\varepsilon_y - \varepsilon_x)\sin\theta\cos\theta + \gamma_{xy}\left(\cos^2\theta - \sin^2\theta\right) && (1.45)
\end{aligned}$$

or

$$\begin{Bmatrix} \varepsilon_x^{'} \\ \varepsilon_y^{'} \\ \gamma_{xy}^{'} \end{Bmatrix} = [T_2] \begin{Bmatrix} \varepsilon_x \\ \varepsilon_y \\ \gamma_{xy} \end{Bmatrix} \tag{1.46}$$

with

$$[T_2] = \begin{bmatrix} \cos^2\theta & \sin^2\theta & \sin\theta\cos\theta \\ \sin^2\theta & \cos^2\theta & -\sin\theta\cos\theta \\ -2\sin\theta\cos\theta & 2\sin\theta\cos\theta & \cos^2\theta - \sin^2\theta \end{bmatrix}. \tag{1.47}$$

Please note that it is often more convenient to use numbers rather than characters when indicating the components of a vector or tensor. Hence, we will in the following use that the x**-direction corresponds to the 1-direction** (or the direction of base vector $\mathbf{x}_1$), **the** y**-directions corresponds to the 2-direction** and **the** z**-direction corresponds to the 3-direction**. Consequently, we get $\sigma_{xx} \rightarrow \sigma_{11},\ \sigma_{yy} \rightarrow \sigma_{22}, \tau_{xy} \rightarrow \tau_{12}$ etc.

1.5 Hooke's law and stiffness and compliance matrices

The most general linear relationship that relates the (Cauchy) stress $\boldsymbol{\sigma}$ with the linear strain $\boldsymbol{\varepsilon}$ under the assumption of 'small' strains can on component form be expressed as the *generalised Hooke's law* as

$$\sigma_{ij} = E_{ijkl}\varepsilon_{kl} \tag{1.48}$$

which for *e.g* σ_{11} yields (i=1; j=1; summation over k=1,2, 3 and l= 1,2,3):

$$\sigma_{11} = E_{1111}\varepsilon_{11} + E_{1112}\varepsilon_{12} + E_{1113}\varepsilon_{13} + E_{1121}\varepsilon_{21} + E_{1122}\varepsilon_{22} + E_{1123}\varepsilon_{23} + E_{1131}\varepsilon_{31} + E_{1132}\varepsilon_{32} + E_{1133}\varepsilon_{33} \tag{1.49}$$

This can for all components of stress be written on Voigt matrix form as:

$$\begin{Bmatrix} \sigma_{11} \\ \sigma_{22} \\ \sigma_{33} \\ \tau_{23} \\ \tau_{31} \\ \tau_{12} \\ \tau_{32} \\ \tau_{13} \\ \tau_{21} \end{Bmatrix} = \begin{bmatrix} E_{1111} & E_{1122} & E_{1133} & E_{1123} & E_{1131} & E_{1112} & E_{1132} & E_{1113} & E_{1121} \\ E_{2211} & E_{2222} & E_{2233} & E_{2223} & E_{2231} & E_{2212} & E_{2232} & E_{2213} & E_{2221} \\ E_{3311} & E_{3322} & E_{3333} & E_{3323} & E_{3331} & E_{3312} & E_{3332} & E_{3313} & E_{3321} \\ E_{2311} & E_{2322} & E_{2333} & E_{2323} & E_{2331} & E_{2312} & E_{2332} & E_{2313} & E_{2321} \\ E_{3111} & E_{3122} & E_{3133} & E_{3123} & E_{3131} & E_{3112} & E_{3132} & E_{3113} & E_{3121} \\ E_{1211} & E_{1222} & E_{1233} & E_{1223} & E_{1231} & E_{1212} & E_{1232} & E_{1213} & E_{1221} \\ E_{3211} & E_{3222} & E_{3233} & E_{3223} & E_{3231} & E_{3212} & E_{3232} & E_{3213} & E_{3221} \\ E_{1311} & E_{1322} & E_{1333} & E_{1323} & E_{1331} & E_{1312} & E_{1332} & E_{1313} & E_{1321} \\ E_{2111} & E_{2122} & E_{2133} & E_{2123} & E_{2131} & E_{2112} & E_{2132} & E_{2113} & E_{2121} \end{bmatrix} \begin{Bmatrix} \varepsilon_{11} \\ \varepsilon_{22} \\ \varepsilon_{33} \\ \varepsilon_{23} \\ \varepsilon_{31} \\ \varepsilon_{12} \\ \varepsilon_{32} \\ \varepsilon_{13} \\ \varepsilon_{21} \end{Bmatrix} \tag{1.50}$$

Please distinguish between the matrix form of a tensor $[\boldsymbol{\sigma}]$ resulting in a 3x3 matrix and the Voigt matrix form of the same tensor $\{\boldsymbol{\sigma}\}$ resulting in a 9x1 (or rather 6x1 due to symmetry) vector.

Please also note that the first row of Eq. (1.50) is the same as the expression for σ_{11} in Eq. (1.49), but with the terms in a different order. The index ordering of Eq. (1.50) is often used in the literature and hence also adopted in the current course.

At a first glance it appears as if there in the most general elastic case are 81 elastic constants describing the relation between stress and strain. Fortunately, due to symmetry arguments it can, cf. below, be shown that in the most general elastically anisotropic case, 21 independent components are necessary to describe the relation between $\boldsymbol{\sigma}$ and $\boldsymbol{\varepsilon}$.

1.5.1 Reduction of 27 constants due to symmetry of the strain tensor

Since $\boldsymbol{\varepsilon}$ is symmetric ($\varepsilon_{kl} = \varepsilon_{lk}$) we also have that

$$E_{ijkl} = E_{ijlk}. \tag{1.51}$$

In order to see how this reduces the amount of independent constants of $\mathbf{E}$, we first conclude that the two first indices i and j can be combined in 9 different ways. Secondly, for each combination of i and j, we can find three pairs of identical components of $\mathbf{E}$ ($E_{ij12} = E_{ij21}, E_{ij13} = E_{ij31}, E_{ij23} = E_{ij32}$) whereby three components (for each combination of i and j) can be replaced by their counterpart, leading to a reduction of 9 x 3 = 27 constants (54 left).

1.5.2 Reduction of additionally 18 constants due to symmetry of the stress tensor

Since $\boldsymbol{\sigma}$ is symmetric ($\sigma_{ij} = \sigma_{ji}$) we also have that

$$E_{ijkl} = E_{jikl}. \tag{1.52}$$

With the respect to the first reduction we note that to two last indices (k and l) can be combined in six independent ways. And for each of these combinations, there are as in the previous case three pairs of equal components ($E_{12kl} = E_{21kl}, E_{13kl} = E_{31kl}, E_{23kl} = E_{32kl}$). This leads to a reduction with another 18 constants (36 left).

1.5.3 Further reduction of 15 constants based on thermodynamical arguments

Assume the existence of a strain energy density function $U = U(\varepsilon_{ij})$ with the property:

$$\frac{\partial U}{\partial \varepsilon_{ij}} = \sigma_{ij} = E_{ijkl}\varepsilon_{kl} \Rightarrow \tag{1.53}$$

$$\frac{\partial}{\partial \varepsilon_{kl}}\left(\frac{\partial U}{\partial \varepsilon_{ij}}\right) = E_{ijkl} \tag{1.54}$$

Interchanging order of taking the derivative results in:

$$\frac{\partial}{\partial \varepsilon_{ij}}\left(\frac{\partial U}{\partial \varepsilon_{kl}}\right) = E_{klij} \tag{1.55}$$

which finally yields:

$$E_{jikl} = E_{klij} \tag{1.56}$$

This results in a reduction with additionally 15 components. **Thus, finally we end up with 21 independent components in the most general anisotropic case for linear elasticity.**

1.6 Specially orthotropic material

Orthotropic materials have properties that exhibit symmetry with respect to certain planes. Or, as an alternative interpretation, the elastic constants do not change when the direction perpendicular (or normal) to the plane of symmetry is reversed.

An example is a composite laminate reinforced with fibres. Thus, we let x_1 and x_2 be two base vectors in the lamina plane and x_3 to be the base vector pointing out of plane. Then, it can be realised that the lamina experience the same properties in the $\pm x_1$-direction meaning that one plane of symmetry is the x_2x_3-plane. In the same way it can be realised that the properties are also the same in $\pm x_2$-direction (x_1x_3-plane is plane of symmetry) and in the $\pm x_3$-direction (x_1x_2-plane is plane of symmetry) respectively. Based on these symmetry arguments, it can be shown that a total number of 9 elastic constants are enough to describe the constitutive relation between stresses and strains, cf. the course book. Hence, $\mathbf{E}$ can be expressed (with due consideration to the symmetry arguments) on Voigt form as:

$$[\mathbf{E}] = \begin{bmatrix} E_{1111} & E_{1122} & E_{1133} & 0 & 0 & 0 \\ E_{1122} & E_{2222} & E_{3322} & 0 & 0 & 0 \\ E_{1133} & E_{2233} & E_{3333} & 0 & 0 & 0 \\ 0 & 0 & 0 & E_{2323} & 0 & 0 \\ 0 & 0 & 0 & 0 & E_{1313} & 0 \\ 0 & 0 & 0 & 0 & 0 & E_{1212} \end{bmatrix} \tag{1.57}$$

or equivalently with a more contracted notation as $\sigma_i = C_{ij}\varepsilon_j,\ i,j = 1,2,3,4,5,6$

$$\begin{Bmatrix} \sigma_1 \\ \sigma_2 \\ \sigma_3 \\ \tau_{23} \\ \tau_{13} \\ \tau_{12} \end{Bmatrix} = \begin{bmatrix} C_{11} & C_{12} & C_{13} & 0 & 0 & 0 \\ C_{12} & C_{22} & C_{23} & 0 & 0 & 0 \\ C_{13} & C_{23} & C_{33} & 0 & 0 & 0 \\ 0 & 0 & 0 & C_{44} & 0 & 0 \\ 0 & 0 & 0 & 0 & C_{55} & 0 \\ 0 & 0 & 0 & 0 & 0 & C_{66} \end{bmatrix} \begin{Bmatrix} \varepsilon_1 \\ \varepsilon_2 \\ \varepsilon_3 \\ \gamma_{23} \\ \gamma_{13} \\ \gamma_{12} \end{Bmatrix} \tag{1.58}$$

Please note that the forms of Eqs. (1.57) and (1.58) are obtained when the coordinate axes are placed along the normals to the symmetry planes. In general, if this is not the case, the $[\mathbf{E}]$ and $[\mathbf{C}]$ matrices are full. But in this case, the components are not independent and there is still only necessary to have nine independent material constants to describe the constitutive response.

1.7 Transversely isotropic material

A transversely isotropic material has one plane of isotropy. As an example consider a unidirectional fibre reinforced composite. For this material, the mechanical properties in all directions perpendicular to the longitudinal (fibre) direction are considered the same. Since a transversely isotropic material has more planes of symmetry, the number of independent elastic constants will be further reduced.

If we consider the fibre direction to coincide with the x_1-direction, making the x_2x_3-plane the plane of isotropy, it can be shown that:

$$C_{22} = C_{33},\ C_{12} = C_{13},\ C_{55} = C_{66},\ C_{44} = \frac{C_{22} - C_{23}}{2} \tag{1.59}$$

whereby the Voigt form of the relation between the stresses and strains can be written as:

$$\begin{Bmatrix} \sigma_1 \\ \sigma_2 \\ \sigma_3 \\ \tau_{23} \\ \tau_{13} \\ \tau_{12} \end{Bmatrix} = \begin{bmatrix} C_{11} & C_{12} & C_{12} & 0 & 0 & 0 \\ C_{12} & C_{22} & C_{23} & 0 & 0 & 0 \\ C_{12} & C_{23} & C_{22} & 0 & 0 & 0 \\ 0 & 0 & 0 & \frac{C_{22}-C_{23}}{2} & 0 & 0 \\ 0 & 0 & 0 & 0 & C_{66} & 0 \\ 0 & 0 & 0 & 0 & 0 & C_{66} \end{bmatrix} \begin{Bmatrix} \varepsilon_1 \\ \varepsilon_2 \\ \varepsilon_3 \\ \gamma_{23} \\ \gamma_{13} \\ \gamma_{12} \end{Bmatrix} \tag{1.60}$$

Thus, only five independent elastic constants are necessary to describe the constitutive response of a transversely isotropic material.

1.8 Constitutive relations for a fibre reinforced lamina

In order to establish the constitutive relations for a unidirectional composite (or a single unidirectional lamina/ply of a composite laminate), we make the basic assumption that it is in the **state of plane stress**. Thus, if a coordinate system $x_1x_2x_3$ is placed such that the x_1-axis points in the direction of the fibres and the x_3-axis points out of the lamina plane we have $\sigma_3 = \tau_{23} = \tau_{13} = 0$ and Eq. (1.60) is reduced to

$$\left\{ \begin{array}{c} \sigma_1 \\ \sigma_2 \\ \tau_{12} \end{array} \right\} = \underbrace{\left[\begin{array}{ccc} Q_{11} & Q_{12} & 0 \\ Q_{12} & Q_{22} & 0 \\ 0 & 0 & Q_{66} \end{array} \right]}_{[\mathbf{Q}]} \left\{ \begin{array}{c} \varepsilon_1 \\ \varepsilon_2 \\ \gamma_{12} \end{array} \right\} \tag{1.61}$$

or equivalently in terms of longitudinal and transverse stresses and strains ($\sigma_1 \to \sigma_L, \sigma_2 \to \sigma_T, \sigma_{12} \to \sigma_{LT}$ etc.

$$\left\{ \begin{array}{c} \sigma_L \\ \sigma_T \\ \tau_{LT} \end{array} \right\} = [\mathbf{Q}] \left\{ \begin{array}{c} \varepsilon_L \\ \varepsilon_T \\ \gamma_{LT} \end{array} \right\} \tag{1.62}$$

The plane stress assumption is generally a valid assumption since in the majority of the structural applications, composite laminates are loaded in the plane of the laminate. And even if there are normal stresses present in the out-of-plane direction (e.g. caused by internal or external pressure) these stresses are often much smaller than the in-plane stresses.

To arrive at the general relation between stresses and strains, i.e. to establish the expressions for the components of $[\mathbf{Q}]$ we note that it can be considered as the superposition of load cases in which only one of the in-plane stress components are non-zero. Thus, as a starting point, we consider each of these states individually.

1.8.1 Longitudinal stress σ_L nonzero

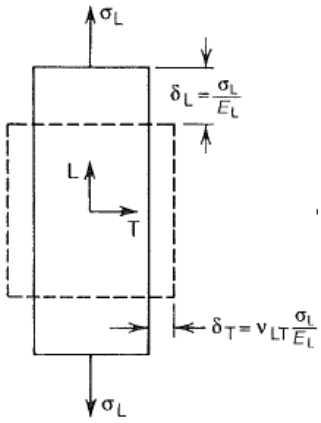

Figure 1.5: Deformation due to nonzero longitudinal stress (from Agarwal et al., Figure 5-3).

The resulting strains when only the longitudinal stress σ_L acts on the lamina are:

$$\varepsilon_L = \frac{\sigma_L}{E_L} \tag{1.63}$$

$$\varepsilon_T = -\nu_{LT}\varepsilon_L = -\nu_{LT}\frac{\sigma_L}{E_L} \tag{1.64}$$

$$\gamma_{LT} = 0 \tag{1.65}$$

where E_L is the longitudinal stiffness and ν_{LT} is the so-called major Poisson's ratio relating the longitudinal stress to the transverse strain.

1.8.2 Transverse stress σ_T nonzero

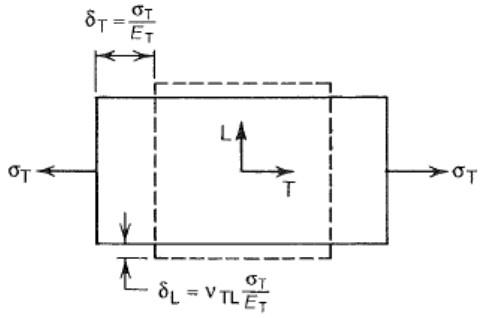

Figure 1.6: Deformation due to nonzero transverse stress (from Agarwal et al., Figure 5-3).

The resulting strains when only the transverse stress σ_T acts on the lamina are:

$$\varepsilon_T = \frac{\sigma_T}{E_T} \tag{1.66}$$

$$\varepsilon_L = -\nu_{TL}\varepsilon_T = -\nu_{TL}\frac{\sigma_T}{E_T} \tag{1.67}$$

$$\gamma_{LT} = 0 \tag{1.68}$$

where E_T is the transverse stiffness and ν_{TL} is the so-called minor Poisson's ratio relating the transverse stress to the longitudinal strain.

1.8.3 Shear stress τ_{LT} nonzero

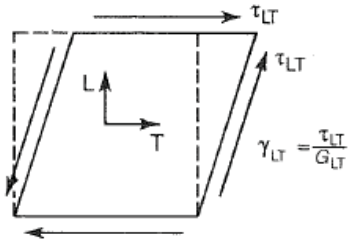

Figure 1.7: Deformation due to nonzero shear stress (from Agarwal et al., Figure 5-3).

The resulting strains when only the shear stress τ_{LT} acts on the lamina are:

$$\varepsilon_L = 0 \tag{1.69}$$

$$\varepsilon_T = 0 \tag{1.70}$$

$$\gamma_{LT} = \frac{\tau_{LT}}{G_{LT}} \tag{1.71}$$

where G_{LT} is the shear modulus of the lamina.

1.8.4 Total constitutive relation

If we superimpose the strains from these three states one obtains:

$$\varepsilon_L = \frac{\sigma_L}{E_L} - \nu_{TL}\frac{\sigma_T}{E_T} \tag{1.72}$$

$$\varepsilon_T = \frac{\sigma_T}{E_T} - \nu_{LT}\varepsilon_L = \frac{\sigma_T}{E_T} - \nu_{LT}\frac{\sigma_L}{E_L} \tag{1.73}$$

$$\gamma_{LT} = \frac{\tau_{LT}}{G_{LT}} \tag{1.74}$$

or on Voigt matrix form

$$\begin{Bmatrix} \varepsilon_L \\ \varepsilon_T \\ \gamma_{LT} \end{Bmatrix} = \begin{bmatrix} \frac{1}{E_L} & -\frac{\nu_{TL}}{E_T} & 0 \\ -\frac{\nu_{LT}}{E_L} & \frac{1}{E_T} & 0 \\ 0 & 0 & \frac{1}{G_{LT}} \end{bmatrix} \begin{Bmatrix} \sigma_L \\ \sigma_T \\ \tau_{LT} \end{Bmatrix} \tag{1.75}$$

If we invert this relation, we obtain:

$$\begin{Bmatrix} \sigma_L \\ \sigma_T \\ \tau_{LT} \end{Bmatrix} = \underbrace{\begin{bmatrix} \frac{E_L}{1-\nu_{LT}\nu_{TL}} & \frac{\nu_{TL}E_L}{1-\nu_{LT}\nu_{TL}} & 0 \\ \frac{\nu_{LT}E_T}{1-\nu_{LT}\nu_{TL}} & \frac{E_T}{1-\nu_{LT}\nu_{TL}} & 0 \\ 0 & 0 & G_{LT} \end{bmatrix}}_{[\mathbf{Q}]} \begin{Bmatrix} \varepsilon_L \\ \varepsilon_T \\ \gamma_{LT} \end{Bmatrix} \tag{1.76}$$

If we make use of the fact that the lamina/ply is transversely isotropic we can also conclude that the matrix $[\mathbf{Q}]$ is symmetric whereby

$$\frac{\nu_{TL}E_L}{1-\nu_{LT}\nu_{TL}} = \frac{\nu_{LT}E_T}{1-\nu_{LT}\nu_{TL}} \Rightarrow \nu_{LT}E_T = \nu_{TL}E_L \tag{1.77}$$

1.9 Constitutive relations in terms of global coordinates

In order to make use of the relation (1.76) in analyses of composite laminates, constitutive relations need to be transformed from fibre oriented coordinate axes LT to global coordinate axes xy. To do so, consider a lamina with fibres oriented by a rotation angle $+\theta$ around the out-of-plane coordinate axis according to Figure 1.8. It can be shown that the stresses and strains can be transformed from the fibre oriented coordinate system to the global coordinate system as:

$$\begin{Bmatrix} \sigma_L \\ \sigma_T \\ \tau_{LT} \end{Bmatrix} = [T_1] \begin{Bmatrix} \sigma_x \\ \sigma_y \\ \tau_{xy} \end{Bmatrix} \tag{1.78}$$

$$\begin{Bmatrix} \varepsilon_L \\ \varepsilon_T \\ \gamma_{LT} \end{Bmatrix} = [T_2] \begin{Bmatrix} \varepsilon_x \\ \varepsilon_y \\ \gamma_{xy} \end{Bmatrix} \tag{1.79}$$

where $[T_1]$ and $[T_2]$ are the stress transformation matrix and the strain transformation matrix respectively defined in Eq. (1.24) and Eq. (1.47).

Thus, the relation between stresses and strains in the global coordinates is obtained as

$$\begin{Bmatrix} \sigma_x \\ \sigma_y \\ \tau_{xy} \end{Bmatrix} = \underbrace{[T_1]^{-1}[\mathbf{Q}][T_2]}_{[\overline{\mathbf{Q}}]} \begin{Bmatrix} \varepsilon_x \\ \varepsilon_y \\ \gamma_{xy} \end{Bmatrix} \tag{1.80}$$

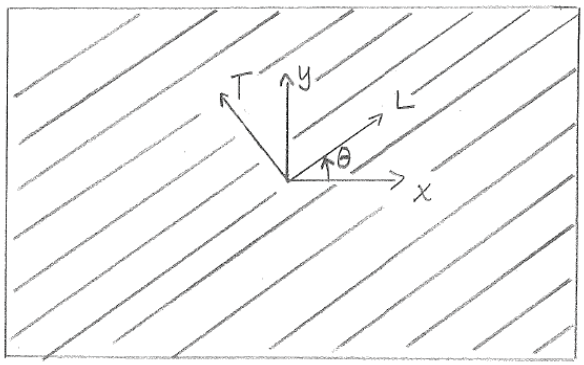

Figure 1.8: UD lamina with fibres oriented $+\theta$ degrees.

Chapter 2

Lamina theory

2.1 Volume and weight fractions

A very important factor influencing the properties of a composite is the relative portions of the matrix and the fibre materials. This can be characterised in (at least) two different ways: by weight fractions, W_i or volume fractions V_i where i stands for either the matrix (m) or the fibre (f) material. The weight fractions are easier to determine from the manufacturing or by subsequent experiments (due to mass conservation), whereas the volume fractions is used exclusively in the theoretical analysis of the properties of the composite material.

2.1.1 Weight fraction

If the total weight of the composite material is denoted w_c and the total weights of the matrix and fibre material are denoted w_m and w_f respectively, we have that

$$w_c = w_m + w_f \tag{2.1}$$

and the weight fractions of matrix material (W_m) and fibre material (W_f) can be defined as:

$$W_m = \frac{w_m}{w_c},\ W_f = \frac{w_f}{w_c} \tag{2.2}$$

2.1.2 Volume fractions

If the total volumes of the matrix and fibre material are denoted v_m and v_f respectively, and if one in the initial stage neglects the existence of pores in the composite material, the total volume of the composite material may be expressed as

$$v_c = v_m + v_f. \tag{2.3}$$

Consequently, the volume fractions of matrix material (v_m) and fibre material (v_f) can be defined as:

$$V_m = \frac{v_m}{v_c},\ V_f = \frac{v_f}{v_c} \tag{2.4}$$

Since the weight fractions are easier to determine from experiments, relations between these weight fractions and the volume fractions are of importance. Introducing ρ_c, ρ_m and ρ_f for the density of the composite material, the matrix material and the fibre material, the relation between the volume and weight fractions are obtained as

$$W_f = \frac{w_f}{w_c} = \frac{\rho_f v_f}{\rho_c v_c} = \frac{\rho_f}{\rho_c} V_f \tag{2.5}$$

$$W_m = \frac{\rho_m}{\rho_c} V_m \tag{2.6}$$

Remains then to determine the density of the composite material (neglecting the existence of pores). To do this, we first note that the total volume of the composite may be written as

$$v_c = \frac{w_c}{\rho_c} = \frac{w_m}{\rho_m} + \frac{w_f}{\rho_f} = \frac{w_f\rho_m + \rho_f w_m}{\rho_f\rho_m}. \tag{2.7}$$

From this expression, we can obtain ρ_c as

$$\rho_c = \frac{w_c\rho_m\rho_f}{w_f\rho_m + \rho_f w_m} = \frac{1}{\frac{w_f}{w_c\rho_f} + \frac{w_m}{w_c\rho_m}} = \frac{1}{(W_f/\rho_f) + (W_m/\rho_m)}. \tag{2.8}$$

It should be remarked that in the presence of voids, the actual composite density is somewhat lower. In general, this discrepancy might be rather small (less than 1% for a good composite) but a difference of up to 5% can be expected for a poorly produced composite. However, the actual effect of a higher amount of voids may have significant influence on some of the properties such as a lowered fatigue resistance and strength.

2.2 Analytical and semi-empirical methods for predicting lamina properties of unidirectional composites

The properties of a composite material depend on the properties of its constituents, their concentrations, distributions and orientations as well as their physical and chemical interaction. The most direct method to determine the properties of a composite material is **by experimental methods**. In many cases, rather simple methods can be used to determine e.g. longitudinal stiffness and (tensile) strength of a lamina. However, the experimental results obtained are only valid for that particular fibre matrix system in terms of volume fractions, constituent properties and production method. If any one of these are changed, new experiments need to be performed in order to establish the properties of the new system. Such extensive testing may be very time consuming and costly, whereby analytical or semi-empirical models can be a very valuable tool to predict some of the properties. Some of the available models, to obtain homogenised properties of the composite, will be discussed below in this section.

2.2.1 Longitudinal properties

2.2.1.1 Longitudinal stiffness prediction based on the constant stress assumption - the Voigt assumption

To predict the longitudinal stiffness of a unidirectional composite lamina, the fibres are assumed as uniform in properties and size and parallel throughout the composite, cf. Figure 2.1. Furthermore, prefect bonding between the matrix and the fibres is assumed. This implies that the longitudinal strains experienced by the fibres ε_{fL}, the matrix ε_{mL} and the composite ε_{cL} are the same:

$$\varepsilon_{fL} = \varepsilon_{mL} = \varepsilon_{cL} \tag{2.9}$$

This is in general homogenisation theory denoted the Voigt assumption which serves as an upper limit of the possible stiffness of a composite in any direction, given a certain fibre volume fraction.

Based on the assumptions above, the longitudinal load P_c carried by the composite will be shared between the fibres P_f and the matrix P_m so that

$$P_c = \sigma_c A_c = P_f + P_m = \sigma_f A_f + \sigma_m A_m \tag{2.10}$$

where σ_c, σ_f and σ_m are the stresses experienced by the composite, the fibres and the matrix respectively, and where A_c, A_f and A_m are the corresponding total cross sectional areas. From Eq. (2.10), we can get the expression for the composite stress σ_c which, by using the fact that the area fractions equals the volume fractions of a unidirectional composite, takes the form

$$\sigma_c = \sigma_f\frac{A_f}{A_c} + \sigma_m\frac{A_m}{A_c} = \sigma_f V_f + \sigma_m V_m. \tag{2.11}$$

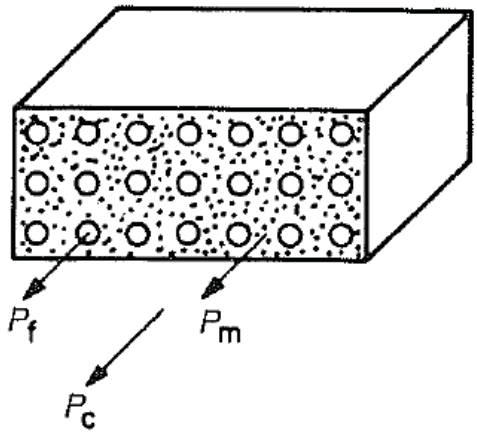

Figure 2.1: Model for predicting longitudinal behaviour of unidirectional composite (from Agarwal et al., Figure 3-3).

If we now assume that both the fibres and the matrix behaves linear elastic ($\sigma = E\varepsilon$) we obtain the expression of the longitudinal elastic stiffness (modulus) of the composite as

$$E_L = E_f V_f + E_m V_m \tag{2.12}$$

which generally is denoted the *rule of mixtures* (ROM). For a composite of n constituents, the expression for the longitudinal stiffness can be generalised as

$$E_L = \sum_{i=1}^{n} E_i V_i. \tag{2.13}$$

From Eqs. (2.12)-(2.13) and in Figure 2.2 it can be seen that, for the case of significantly stiffer fibres (compared to the matrix), most of the (longitudinal) load is carried by the fibres already at rather low fibre volume fractions.

It should be remarked that Eqs. (2.12)-(2.13) are only valid as long as both the matrix and the fibre material behaves linear elastic. This may however constitute only a small portion of the stress-strain behaviour and generally, the longitudinal deformation of a unidirectional composite proceed in four stages:

1. The matrix and the fibres both deform linear elastically
2. The fibres still deform linear elastically whereas the matrix deforms nonlinearly elastic or even plastically
3. The fibres and the matrix both deform in a nonlinear fashion
4. The fibres break followed by composite failure

Whereas stage 3 can be observed only for ductile fibres, stage 2 may occupy the largest portion of the composite stress-strain curve (which is no longer linear) and the longitudinal composite stiffness (modulus) relating an incremental change in strain to the corresponding change in stress ($\Delta\sigma_L = E_L^{\Delta}\Delta\varepsilon_L$) must be predicted at each composite strain level ε_c as

$$E_L^{\Delta} = E_f V_f + \left(\frac{\partial \sigma_m}{\partial \varepsilon_m}\right)_{\varepsilon_c} V_m \tag{2.14}$$

where $\left(\frac{\partial \sigma_m}{\partial \varepsilon_m}\right)_{\varepsilon_c}$ is the slope of the matrix stress-strain curve at strain ε_c. However, in practice, the non-linearity of the stress-strain curve for the matrix material has low effect on the composite stiffness, especially at significant fibre fraction. Thus, in many cases Eq. (2.12) is a good approximation.

It should be remarked that the rule of mixtures is accurate for longitudinal *tensile* stiffness. But **when loaded in compression, the response of the composite observed in experiments may deviate from the analytical predictions (ROM)**. This because the combined compressive properties is strongly dependent on the matrix material properties, such as its shear stiffness (cf. buckling), whereas the tensile response is much more governed by the fibre properties.

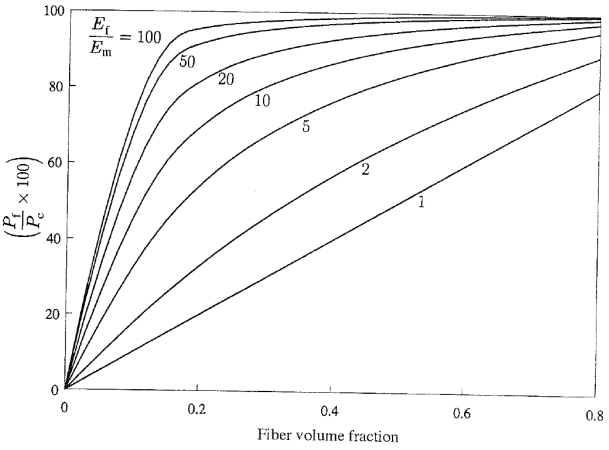

Figure 2.2: Graph showing the percentage of the total force carried by the fibres in a unidirectional composite as function of fibre volume fraction (from Agarwal et al., Figure 3-5).

2.2.1.2 Tensile strength

Failure initiates when the fibres are subjected to their fracture strain, assuming that the fibre failure strain ε_f^* is less than the matrix failure strain, which is generally the case. In most practicable applications with a sufficiently high volume fraction of fibres and where the matrix material behaves linearly elastic up to fibre failure, the failure stress of the composite σ_{cu} (cu for composite ultimate) can be expressed by the rule of mixtures as:

$$\begin{aligned}
\sigma_{cu}A &= \sigma_{fu}A_f + (\sigma_m)_{\varepsilon_f^*} A_m \Rightarrow \\
\sigma_{cu} &= \sigma_{fu}\frac{A_f}{A} + (\sigma_m)_{\varepsilon_f^*}\frac{A_m}{A} \Rightarrow \left\{ \frac{A_f}{A} = V_f,\ \frac{A_m}{A} = V_m \right\} \Rightarrow \\
\sigma_{cu} &= \sigma_{fu}V_f + (\sigma_m)_{\varepsilon_f^*} V_m = \left\{ \text{matrix linear elastic up to } \varepsilon_f^* \right\} = \sigma_{fu}\left(V_f + \frac{E_m}{E_f}V_m \right) \qquad (2.15)
\end{aligned}$$

where σ_{fu} is the fibre fracture stress (or ultimate strength of the fibres) and $(\sigma_m)_{\varepsilon_f^*}$ is the stress in a matrix subjected to the strain at which the fibres fail (ε_f^*), cf Figure 2.3.

It can be seen that Eq. (2.15) predicts a lower composite strength for the composite compared to the unreinforced matrix material for a certain level of fibre volume fraction (below V_{crit}). V_{crit} is defined as when the failure strength of the composite equals the failure strength of the unreinforced matrix material, i.e.

$$\sigma_{fu}V_{crit} + (\sigma_m)_{\varepsilon_f^*}\underbrace{(1 - V_{crit})}_{'V_m'} = \sigma_{mu} \Rightarrow V_{crit} = \frac{\sigma_{mu} - (\sigma_m)_{\varepsilon_f^*}}{\sigma_{fu} - (\sigma_m)_{\varepsilon_f^*}}. \qquad (2.16)$$

However, for most practical applications (V_{crit}) is 'really small'. Consider e.g. the common composite material consisting of carbon fibres and epoxy matrix (or resin) material. From mean values of the respective strength for carbon fibres (cf. Table 1-1 in Agarwal et al.) $\sigma_{fu} \approx 2.3$ GPa and epoxy (cf. Table 2-11 in Agarwal et al.) $\sigma_{mu} \approx 92.5$ MPa and assuming that the epoxy is linear elastic up to the

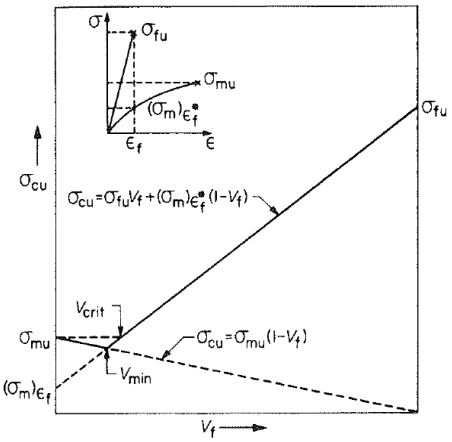

Figure 2.3: Graph showing the composite longitudinal failure stress σ_{cu} as function of fibre volume fraction (from Agarwal et al., Figure 3-7).

failure strain of the fibres $\varepsilon_f^* = 2.3 \cdot 10^9/315 \cdot 10^9 = 0.0073 \rightarrow (\sigma_m)_{\varepsilon_f^*} = \underbrace{3.425 \cdot 10^9}_{E_{epoxy}} \cdot 0.0073 = 25$ MPa, we can obtain V_{crit} as:

$$V_{crit} = \frac{92.5 \cdot 10^6 - 25 \cdot 10^6}{2.3 \cdot 10^9 - 25 \cdot 10^6} \approx 0.03 \tag{2.17}$$

That is, the critical volume fraction of fibres V_{crit} is about 3% which is considerably lower than in any practical applications (50-60%).

2.2.1.3 Compressive strength

It is unlikely that the fibres themselves would break due to compressive stresses. But when being subjected to compressive loads the fibres acts as long columns and either so-called micro-buckling or fibre kinking can occur. Of course, the buckling load of a fibre embedded into a matrix is significantly larger than for a free fibre or fibre bundle. But still, fibre (bundle) buckling can occur even when the corresponding matrix stresses are in the elastic range. However, for practical fibre volume fractions ($V_f > 0.4$), fibre buckling of often preceded by other failure phenomena to be discussed further in the chapter covering failure.

2.2.2 Factors influencing longitudinal stiffness and strength

There are a number of factors that may influence the longitudinal stiffness and strength of a composite leading, in some cases, to significant deviations from the predictions discussed above.

- Misorientation of fibres

  Fibre orientation directly influences the properties of the composite. Naturally, the contribution from the fibres is maximised only when the fibres are aligned with the loading direction. As a consequence, the stiffness and strength will be reduced when the fibres are not parallel to the loading direction. However, the discrepancy is small and no corrections have to be made if the misalignment is small, i.e. limited to a few degrees. It should be remarked that in the general case, a composite material is often composed of a number of unidirectional lamina with different orientations stacked on top of each other. For this type of composite structure – a laminate – there are several appropriate theories (co-called laminate theories) available to described the structural response, cf. Chapter 3 and Chapters 6-8 in the course book.

- Fibres of nonuniform strength

  First of all, it should be remarked that any reduction of the fibre strength directly results in a lowered strength of the composite material. Consequently, a composite of high strength is obtained when the fibres are uniform in strength. Reasons for a non-uniform distribution may be due to at least the following two reasons:

1. A variation of cross section as function of length
2. As a result of initial damage due to handling of the fibres before manufacturing the composite

In addition, the fibre strength decreases as the fibre length increases. This is due to the fact that statistically, the existence of any strength reducing factor (flaw) increases with length and the fibre will always first break at its weakest link. In any case, it should be remarked that fibres start to break at loads lower than the composite strength and that this accumulates up to final failure. Thus, for detailed predictions of the composite strength, statistical methods need to be incorporated which, however, is considered as out of scope in the current course.

- Discontinuous fibres

  When the length of the fibres are in the same order of size as the length over which the load is transmitted through the matrix material, we speak of discontinuous fibre reinforcements. In these materials, the end effects (variation of stress along the fibre and stress concentrations) cannot be neglected and must be dealt with. This is however not included in the current course. Interested students are referred to Chapter 4 in the course book for reference.

- Interfacial conditions

  - More pronounced importance for discontinuous-reinforced-fibre composites.
  - Influences the transversal strength.
  - Good adhesion between fibre and matrix enhances water resistance.
  - A lower interface strength may lead to a higher composite ductility and, hence, a high fracture toughness.

- Residual stresses

  Originates predominantly from the manufacturing process due to e.g.

  - a variation between thermal expansion coefficients for the fibre and the matrix material,
  - a significant difference in temperature at manufacturing and temperature at use, cf. also Computer Assignment 1, and
  - chemical shrinkage in the manufacturing process

  It should be remarked that the existence of residual stresses significantly impact the response and the properties (strength) of the composite material and should be included in an advanced assessment analysis of a composite structure. How this is to be incorporated practically is not always straightforward, but this should definitively be kept in mind! The residual stresses in composites is much more importance for the component performance than say in the case of traditional metal components in which the residual stress often decrease with time due to local (and often 'harmless') plastic deformations leading to stress relaxation.

2.2.3 Transverse properties

2.2.3.1 Transverse stiffness prediction based on the constant stress assumption - the Reuss assumption

In order to derive a simple expression for predicting the transverse stiffness of a lamina, let us consider a lamina with unidirectional (UD) continuous fibre reinforcements loaded by a transversal tensile stress σ_c. Schematically, we study a Representative Volume Element (RVE) as a generic block consisting of fibre material bonded to matrix material, as shown in Figure 2.4.

For this case, the elongation of the composite in the loading direction (δ_c) is obtained by the sum of the elongation of the matrix material and of the fibre material in the loading direction according to

$$\delta_c = \varepsilon_{cT} L_2 = \varepsilon_{fT} L_f + \varepsilon_{mT} L_m \tag{2.18}$$

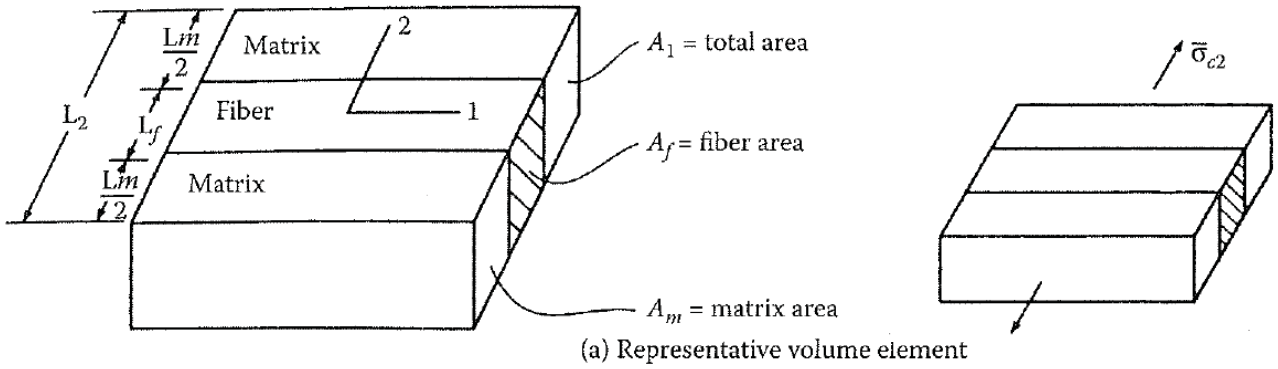

Figure 2.4: Model for predicting transverse stiffness of unidirectional composite (from Gibson, *Principles of Composite Material Mechanics 2nd ed.*, 2007).

where ε_{cT}, ε_{fT} and ε_{mT} are the transversal strains in the composite RVE, the fibre materials and the matrix material respectively. Furthermore, since the RVE do not change along the longitudinal direction, the length fractions must equal the volume fractions such that

$$\varepsilon_{cT} = \varepsilon_{fT} V_f + \varepsilon_{mT} V_m. \tag{2.19}$$

By using Hooke's law, (and neglecting any Poisson strains) this can be written as

$$\frac{\sigma_c}{E_T} = \frac{\sigma_f}{E_f} V_f + \frac{\sigma_m}{E_m} V_m. \tag{2.20}$$

If we now finally assume that the stress in each of the constituents (fibre and matrix) is the same (the so-called Reuss assumption), i.e. we have that

$$\sigma_c = \sigma_f = \sigma_m, \tag{2.21}$$

we end up with the 'inverse rule of mixtures' for the transverse modulus as

$$\frac{1}{E_T} = \frac{V_f}{E_f} + \frac{V_m}{E_m} \tag{2.22}$$

It should be remarked that by assuming equal stress in both fibres and matrix, the resulting expression for the (transverse) stiffness can be shown to be the lower bound given a certain fibre volume fraction, cf. also Figure 2.5.

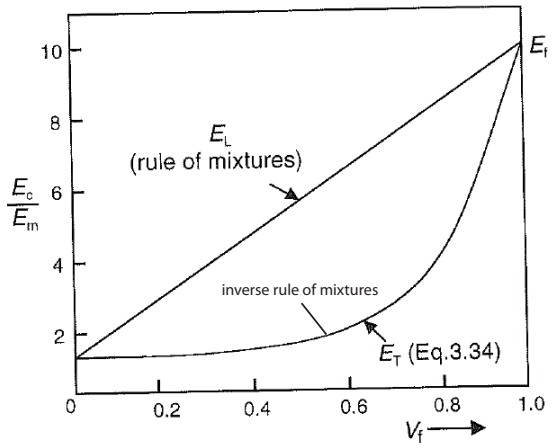

Figure 2.5: Longitudinal and transverse stiffness as function of fibre volume fraction (from Agarwal et al., Figure 3-9a). Please note that the rule of mixtures (Voigt assumption) serves as an upper limit of the composite stiffness whereas the inverse rule of mixtures (Reuss assumption) serves as the lower bound

2.2.3.2 Halpin-Tsai semi-empirical model for transverse stiffness prediction

The inverse rule of mixtures may lead to poor predictions (and an underestimation of the transverse stiffness) since, in reality, the stresses are not equal in the matrix and fibre material.

To improve the predictions, Halpin and Tsai developed simple and generalised equations to fit more advanced micromechanical models for transverse stiffness. The Halpin-Tsai equation for the transverse composite stiffness (modulus) can be written as

$$\frac{E_T}{E_m} = \frac{1 + \xi\eta V_f}{1 - \eta V_f},\ \eta = \frac{(E_f/E_m) - 1}{(E_f/E_m) + \xi} \tag{2.23}$$

in which ξ is a measure of the reinforcements and relates to the fibre geometry. Please note the special cases

$$\xi = 0: \qquad E_T = \frac{1}{\frac{V_m}{E_m} + \frac{V_f}{E_f}} \text{ (inverse rule of mixtures)} \tag{2.24}$$

$$\xi = \infty: \qquad E_T = V_m E_m + V_f E_f \text{ (Rule of mixtures)} \tag{2.25}$$

Thus, it is clear that ξ can be viewed as a curve fitting parameter since the real transverse stiffness will lie between the two limiting cases (closer to the inverse rule of mixture prediction). Halpin and Tsai have proposed $\boldsymbol{\xi = 2}$ **for circular or quadratic cross sections** and $\xi = 2\frac{a}{b}$ for rectangular cross sections in which a and b are side lengths of the cross section and where a is to be taken as the side length in the loading direction.

Predictions made by the Halpin-Tsai equations have proven to be adequate in many practical situations, cf. Figure 2.6 for a comparison made against experimental data for a boron-epoxy lamina reported by Whitney and Riley (*J. IAAA*, 4:1537, 1966), and it generally gives a better prediction than the prediction obtained based on the equivalence of stress in the fibre and the matrix material (the inverse rule of mixtures).

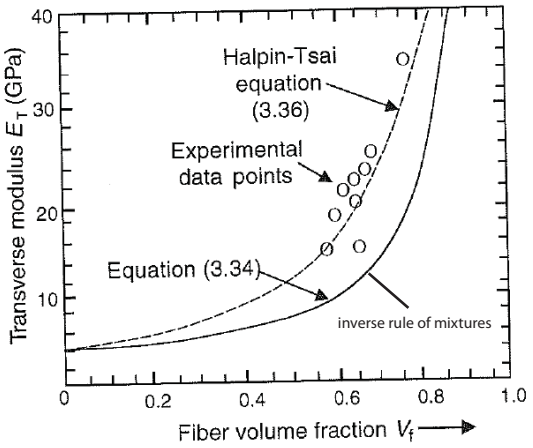

Figure 2.6: Transverse stiffness predicted by the inverse rule of mixtures and the Halpin-Tsai equation compared with experimental data reported by Whitney and Riley for boron-epoxy (from Agarwal et al., figure 3-9b).

2.2.3.3 Transverse strength

The transverse strength of a composite is reduced by the existence of fibres. The reason is that due to their geometry, the fibres cannot carry a large portion of the load which instead is distributed between the fibre and the matrix material. Instead, the existence of fibres place restrictions on the transverse deformations, causing strain and stress concentrations in their vicinity, cf. Figure 2.7 which results in an overall decreased strength in comparison to the unreinforced matrix material.

Thus, the composite transverse failure strength σ_{TU} can be expressed as

$$\sigma_{TU} = \frac{\sigma_{mu}}{S} \tag{2.26}$$

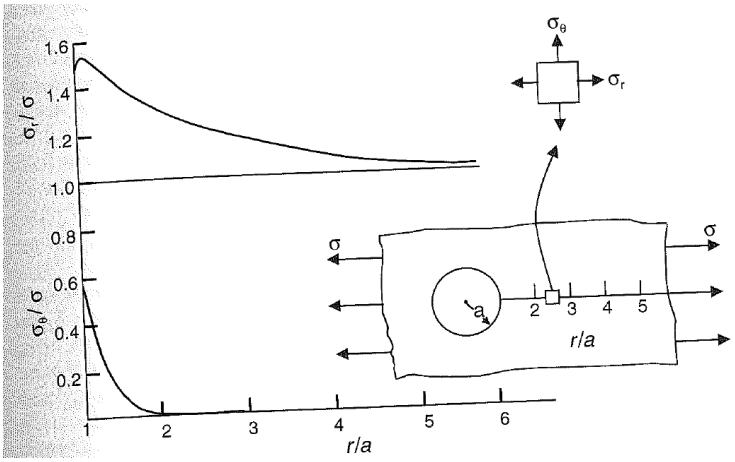

Figure 2.7: Stress distribution in matrix surrounding a single cylindrical inclusion $E_F/E_m = 10, \nu_m = 0.35, \nu_f = 0.3$ (from Agarwal et al., figure 3-12a).

in which S is a strength reduction factor. This reduction factor can be predicted by several methods.

The strength-of-materials method

Based on the strength-of-materials method, the factor S is assumed e.g. to be equal to the stress concentration factor SCF which can be predicted by neglecting Poisson effects, cf. Greszczuk *Society of Plastics Industry, 21st Annual Conference*, 1966 for details, as:

$$SCF = \frac{1 - V_f\left(1 - (E_m/E_f)\right)}{1 - (4V_f/\pi)^{1/2}\left(1 - (E_m/E_f)\right)}. \tag{2.27}$$

Based on Finite Element Analysis

Another alternative is to analyse the stress distribution in a UD lamina by FEM, cf. the results in shown in Figure 2.8 obtained by e.g. Chen and Lin (*Mater. Res. Stand. MTRSA*, 9:29-33, 1969).

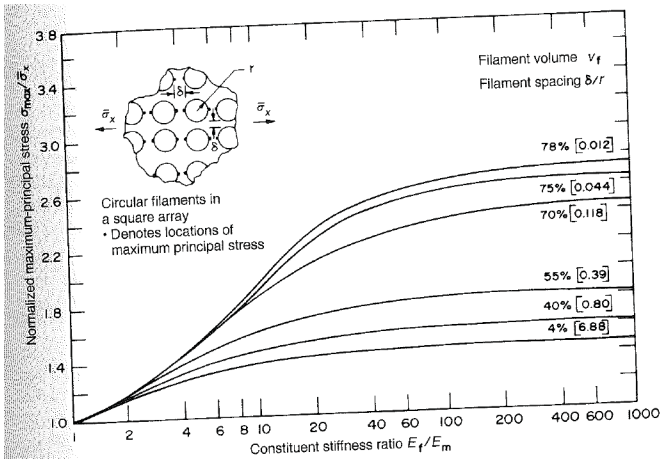

Figure 2.8: Principal stress in matrix surrounding multiple fibres obtained by FEM by Chen and Lin $\nu_m = 0.35, \nu_f = 0.2$ (from Agarwal et al., figure 3-12b).

2.2.4 Shear modulus

The derivations of a simple rule for predicting the in-plane shear stiffness of a lamina is similar to those for the transverse stiffness (E_L). Study Section 3.4 in the course book on your own.

2.2.4.1 Major results

Inverse rule of mixtures:

$$G_{LT} = \frac{1}{V_f/G_f + V_m/G_m} \tag{2.28}$$

Improved predictions by means of Halpin-Tsai:

$$\frac{G_{LT}}{G_m} = \frac{1+\xi\eta V_f}{1-\eta V_f},\ \eta = \frac{(G_f/G_m)-1}{(G_f/G_m)+\xi},\ \boldsymbol{\xi = 1} \tag{2.29}$$

2.2.5 Poisson's ratio

Study subsection 3.5 in the course book on your own.

2.2.5.1 Major results

Major Poisson's ratio ν_{LT}

For this case, the underlying assumptions in the derivations are:

- The longitudinal strain is the same in both constituents (as for the stiffness prediction)
- The Poisson's ratios for each constituent is (transversely) isotropic
- The total transverse contraction is the sum of the transverse contraction of the fibres and matrix respectively

Major Poisson's ratio ν_{LT} relating the longitudinal stress to the transverse strain:

$$\nu_{LT} = \nu_f V_f + \nu_m V_m \tag{2.30}$$

Minor Poisson's ratio ν_{TL}

For this case it is used that the stiffness matrix of a linear elastic material is symmetric.

Minor Poisson's ratio ν_{TL} relating the transverse stress to the longitudinal strain:

$$\frac{\nu_{LT}}{E_L} = \frac{\nu_{TL}}{E_T} \Rightarrow \nu_{TL} = \nu_{LT}\frac{E_T}{E_L} \tag{2.31}$$

2.3 Expansion coefficients

Study 3.7.1 and 3.7.2 in the course book on your own.

For the thermal case, the underlying assumptions (not explained in the text) in the derivations are:

- The fibres are assumed to be isotropic and linear elastic
- The matrix is assumed to be isotropic and linear elastic
- The strains in the longitudinal direction are the same in the matrix and in the fibres (Voigt assumption)
- The stresses in the transverse direction are constant, i.e. the Reuss assumption is used
- The homogenised macroscopic stresses in the lamina are zero, i.e. the assumption $\sigma_L = \sigma_T = 0$ is used.

Major results

Thermal expansion coefficients (cf. Scharpery, *J. Compos Mater.*, 2:280-404, 1968 for details):

$$\alpha_L = \frac{1}{E_L}\left(\alpha_f E_f V_f + \alpha_m E_m V_m\right) \tag{2.32}$$

$$\alpha_T = \left(1+\nu_f\right)\alpha_f V_f + \left(1+\nu_m\right)\alpha_m V_m - \alpha_L \nu_{LT} \tag{2.33}$$

Moisture expansion coefficients:

$$\beta_L \approx 0 \quad \text{(given that the fibres are much stiffer than the moisture absorbing matrix)} \tag{2.34}$$

$$\beta_T = \frac{\rho_c}{\rho_m}\left(1+\nu_m\right)\beta_m \quad \text{(cf. e.g. Tsai and Hahn, } \textit{Introduction to Composite Materials}\text{, 1980)} \tag{2.35}$$

2.4 Hygrothermal degradation of polymer matrix properties influencing the composite parameters (included for your information and understanding)

Review of Subsection 5.1-5.2 in Gibson (*Principles of Composite Material Mechanics 2nd ed.*, 2007):

Increased temperature of a polymer causes a gradual degradation of the stiffness up to a certain point, the so-called 'glass transition' temperature at which the matrix behaviour transforms from being glassy to being rubbery, cf. also Figure 2.9

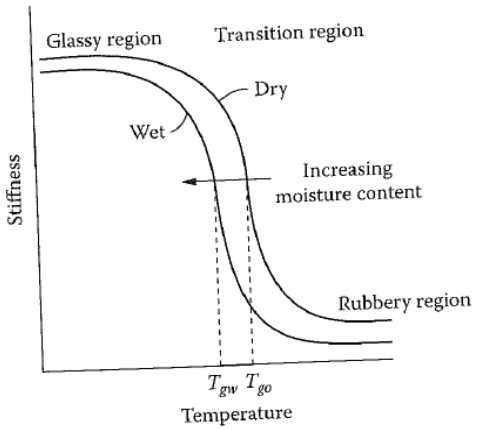

Figure 2.9: Variation of stiffness for a typical polymer showing the glass transition temperature T_g and the effect of absorbed moisture on T_g. Note: T_{g0} = 'dry', T_{g0} = 'wet' (from Gibson, figure 5.1.).

In addition, increased moist absorption **in the matrix** leads to a lowered glass transition temperature and a decrease in stiffness. Moist saturation 3-4 % leads to a lowered glass temperature of approx 20%, c.f also Figure 2.10 how the stress-strain curve for 3501-5 epoxy resin is affected by temperature and moist and Figure 2.11 how this in turn influence the stress-strain of a AS/3501-5 graphite/epoxy composite (same matrix material!) with fibre volume fraction $V_f = 0.63$.

The hygrothermal degradation of a composite strength and/or stiffness is often estimated by empirical models. Chamis and Sinclair (*Composite Materials: Testing and Design (Sixth Conference)*, ASTM STP 787, pp. 498–512, 1982) and Chamis (*Engineer's Guide to Composite Materials*, pp. 3-8–3-24, 1987) have demonstrated such a procedure. In their approach, the degraded stiffness E_m (or strength) is approximated by the nominal stiffness E_m^0 multiplied by a degradation factor F_m such that:

$$E_m \rightarrow F_m E_m^0 \tag{2.36}$$

and the degraded value E_m is then used in e.g. the Halpin-Tsai equation to approximate the temperature and moisture dependent transverse stiffness of the composite. As for the degradation factor, the following

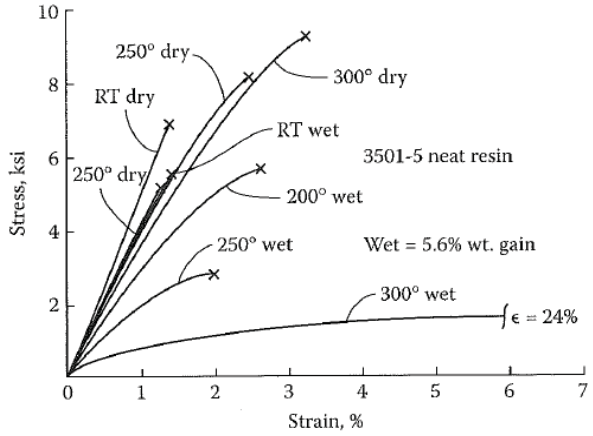

Figure 2.10: Stress-strain curves for 3501-5 epoxy resin at different temperatures and moisture contents (from Gibson, figure 5.2.)

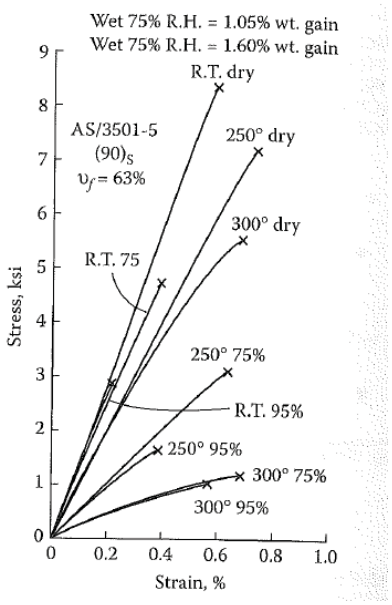

Figure 2.11: Stress-strain curves for AS/3501-5 graphite/epoxy composite with fibre volume fraction $V_f = 0.63$ at different temperatures and moisture contents (from Gibson, figure 5.3.)

expression is proposed:

$$F_m = \left[\frac{T_{gw} - T}{T_{g0} - T_0}\right]^{1/2} \tag{2.37}$$

where T_{g0} is the 'dry' glass transition temperature of the matrix material (i.e. without moisture), T_{gw} is the 'wet' glass transition temperature that depends on the moisture concentration, T_0 is the reference temperature at which the nominal matrix stiffness is measured (E_0) and T is the current temperature. Furthermore, Chamis used data for six different epoxy resins to fit the parameters of an empirical curve in order to get an approximate expression for T_{gw} **for epoxy resin** as:

$$T_{gw}[C] \quad = \quad \left(50M_r^2 - 10M_r + 1.0\right) T_{g0}[C] + \frac{32\left(50M_r^2 - 10M_r\right)}{1.8}. \tag{2.38}$$

where M_r is moist contents in weight percent ($4\% \rightarrow M_r = 0.04$), cf. also Figure 2.12 for tabulated data for some matrix materials. Please note that the somewhat strange format of the expression for T_{gw} stems from the fact that the parameters obtained by Chamis where found for temperatures measured in Fahrenheit whereas the expression in Eq. (2.38) is valid for temperatures measured in Celsius. Thus, it

has been used that

$$T[F] = T[C] * 1.8 + 32 \tag{2.39}$$

Hygrothermal Properties for Various Polymer Matrix Materials

Material	Supplier	Saturation Moisture Content, M_m (Weight %)	T_{go} (Dry) [°F (°C)]	T_{gw} (Wet) [°F (°C)]	Maximum Service Temperature (Dry) [°F (°C)]
Hexply® F655 bismaleimide	Hexcel	4.1	550(288)	400(204)	400(204)
Hexply 8551-7 epoxy	Hexcel	3.1	315(157)	240(116)	200(93)
Hexply 8552 epoxy	Hexcel	—	392(200)	309(154)	250(121)
Hexply 954-3A cyanate	Hexcel	—	400(204)	—	—
CyCom® 2237 polyimide	Cytec	4.4	640(338)	509(265)	550(208)
CyCom 934 epoxy	Cytec	—	381(194)	320(160)	350(177)
Avimid® R polyimide	Cytec	2.8	581(305)	487(253)	550(288)
Derakane® 411-350 vinylester	Ashland	1.5	250(120)	—	220(105)
Ultem® 2300 polyetherimide	General Electric	0.9	419(215)	—	340(171)
Victrex 150G polyetherether-ketone	Victrex plc	0.5	289(143)	—	356(180)

Figure 2.12: Hygrothermal properties of various polymer matrix materials (from Gibson, Table 5.1.).

Chapter 3

Laminate theory

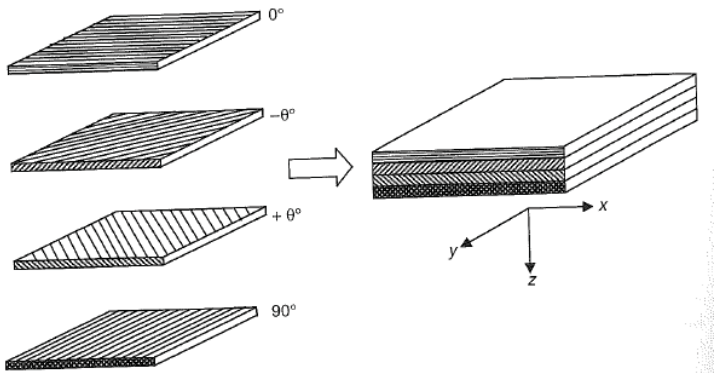

Figure 3.1: A four-ply laminate (from Agarwal et al, figure 6-1.)

3.1 Laminate strains

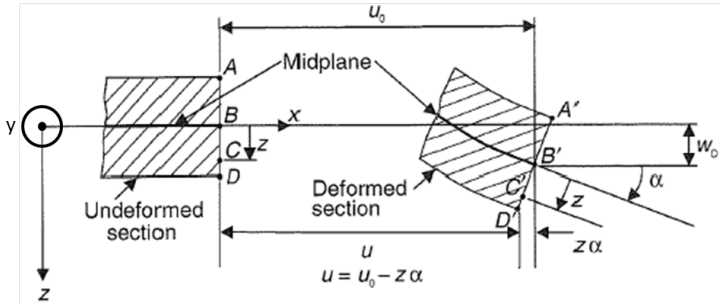

Figure 3.2: Deformation during bending of the laminate in the xz plane (adapted from Agarwal et al, figure 6-2.)

Consider first the deformation of a laminate in the xz-plane, cf. Figure 3.2. In this case, the displacement u in the x-direction of a point C that is located on the undeformed normal ABCD, at a distance z from the midplane, is given by

$$u = u_0 - z\sin\alpha \approx u_0 - z\alpha \tag{3.1}$$

where u_0 is the midplane displacement in the x-direction and α is the slope of the deformed section $A'B'C'D'$ or the (negative) rotation of the normal $ABCD$ around the y-axis due to deformation. Similarly, the displacement v of a corresponding point when the laminate is deformed in the yz-plane, cf. Figure 3.3, can be obtained as

$$v = v_0 - z\beta \tag{3.2}$$

where v_0 is the midplane displacement in the y-direction and β is the slope of the deformed section $A'B'C'D'$ or the (positive) rotation of the normal $ABCD$ around the x-axis due to deformation in the yz-plane).

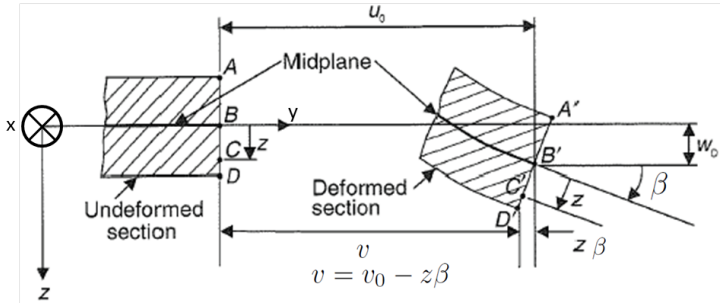

Figure 3.3: Deformation during bending of the laminate in the yz plane (adapted from Agarwal et al, figure 6-2.)

From these kinematical expressions for the displacements, we can derive the in-plane strains as

$$\varepsilon_x = \frac{\partial u}{\partial x} = \frac{\partial u_0}{\partial x} - z\frac{\partial \alpha}{\partial x} \tag{3.3}$$

$$\varepsilon_y = \frac{\partial v}{\partial y} = \frac{\partial v_0}{\partial y} - z\frac{\partial \beta}{\partial y} \tag{3.4}$$

$$\gamma_{xy} = \frac{\partial u}{\partial y} + \frac{\partial v}{\partial x} = \frac{\partial u_0}{\partial y} + \frac{\partial v_0}{\partial x} - z\left(\frac{\partial \alpha}{\partial y} + \frac{\partial \beta}{\partial x}\right) \tag{3.5}$$

The preceding strain-displacement relation can be written as

$$\left\{ \begin{array}{c} \varepsilon_x \\ \varepsilon_y \\ \gamma_{xy} \end{array} \right\} = \left\{ \begin{array}{c} \varepsilon_x^0 \\ \varepsilon_y^0 \\ \gamma_{xy}^0 \end{array} \right\} + z \left\{ \begin{array}{c} k_x \\ k_y \\ k_{xy} \end{array} \right\} \tag{3.6}$$

or

$$\{\boldsymbol{\varepsilon}\} = \{\boldsymbol{\varepsilon}^0\} + z\{\mathbf{k}\} \tag{3.7}$$

where the midplane strains $\boldsymbol{\varepsilon}^0$ and plate *curvatures* $\mathbf{k}$ are defined as

$$\{\boldsymbol{\varepsilon}^0\} = \left\{ \begin{array}{c} \varepsilon_x^0 \\ \varepsilon_y^0 \\ \gamma_{xy}^0 \end{array} \right\} = \left\{ \begin{array}{c} \dfrac{\partial u_0}{\partial x} \\ \dfrac{\partial v_0}{\partial y} \\ \dfrac{\partial u_0}{\partial y} + \dfrac{\partial v_0}{\partial x} \end{array} \right\} \tag{3.8}$$

and

$$\{\mathbf{k}\} = \left\{ \begin{array}{c} k_x \\ k_y \\ k_{xy} \end{array} \right\} = - \left\{ \begin{array}{c} \dfrac{\partial \alpha}{\partial x} \\ \dfrac{\partial \beta}{\partial y} \\ \dfrac{\partial \alpha}{\partial y} + \dfrac{\partial \beta}{\partial x} \end{array} \right\} \tag{3.9}$$

It should be remarked that the definition (and notation) of the curvatures differs in the literature. In these notes, we follow the notations used in the course book. **Please note that we assume that adjacent lamina across the thickness of the laminate do not slip over each other. Hence, the strain varies linearly through the thickness even though the properties vary, cf. Figure 3.4.** Please also note that both $\boldsymbol{\varepsilon}^0$ and $\mathbf{k}$ are functions of x and y only.

If we now assume that the normal ABCD remains planar and perpendicular to the midplane also after deformation (the Kirchhoff assumption), it can be found that

$$\alpha = \frac{\partial w_0}{\partial x} \tag{3.10}$$

$$\beta = \frac{\partial w_0}{\partial y} \tag{3.11}$$

whereby one obtains the plate curvature as

$$\left\{ \begin{array}{c} k_x \\ k_y \\ k_{xy} \end{array} \right\}_{Kirchhoff} = - \left\{ \begin{array}{c} \dfrac{\partial^2 w_0}{\partial x^2} \\ \dfrac{\partial^2 w_0}{\partial y^2} \\ 2\dfrac{\partial^2 w_0}{\partial x \partial y} \end{array} \right\} \tag{3.12}$$

where w_0 is the vertical displacement of the midplane (in the z-direction).

Please note that laminate theory based on the Kirchhoff assumption, which also implies that the transverse shear strains γ_{xz} and γ_{yz} are negligible, is often denoted *Classical Lamination Theory, CLT*.

3.2 Laminate stresses

For a material with identical properties through the thickness, the stresses will, as the strains, vary linearly. Thus, within each lamina, the stresses are a linear function of z. However, since the properties in general are different for each lamina – the properties are considered constant within each lamina – the stress distribution through the thickness will be discontinuous but piecewise linear in each lamina, cf. Figure 3.4.

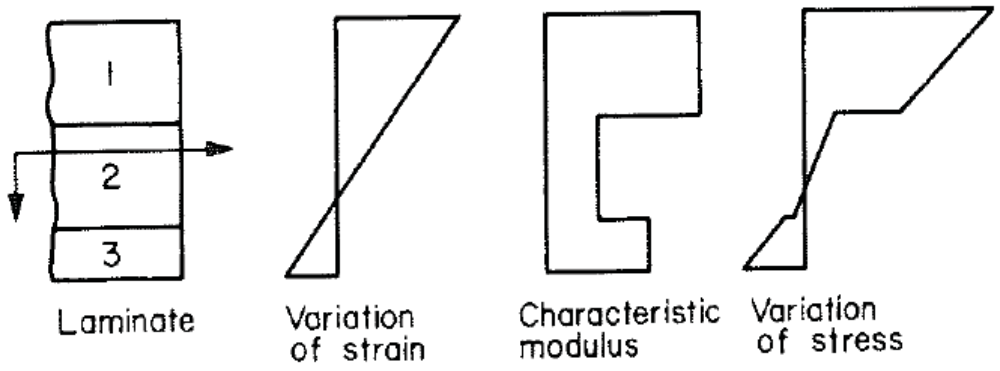

Figure 3.4: Principal variation of stresses and strains in a composite laminate consisting of three unidirectional laminae/plies with different orientation (from Agarwal et al, figure 6-3.)

Given the relation between stresses and strains from Chapter 1:

$$\left\{ \begin{array}{c} \sigma_x \\ \sigma_y \\ \tau_{xy} \end{array} \right\} = \left[\begin{array}{ccc} \overline{Q}_{11} & \overline{Q}_{12} & \overline{Q}_{16} \\ \overline{Q}_{12} & \overline{Q}_{22} & \overline{Q}_{26} \\ \overline{Q}_{16} & \overline{Q}_{26} & \overline{Q}_{66} \end{array} \right] \left\{ \begin{array}{c} \varepsilon_x \\ \varepsilon_y \\ \gamma_{xy} \end{array} \right\} \tag{3.13}$$

we can now obtain the stresses at any point in lamina k as

$$\left\{ \begin{array}{c} \sigma_x \\ \sigma_y \\ \tau_{xy} \end{array} \right\}_k = \left[\begin{array}{ccc} \overline{Q}_{11} & \overline{Q}_{12} & \overline{Q}_{16} \\ \overline{Q}_{12} & \overline{Q}_{22} & \overline{Q}_{26} \\ \overline{Q}_{16} & \overline{Q}_{26} & \overline{Q}_{66} \end{array} \right]_k \left\{ \begin{array}{c} \varepsilon_x^0 \\ \varepsilon_y^0 \\ \gamma_{xy}^0 \end{array} \right\} + z \left[\begin{array}{ccc} \overline{Q}_{11} & \overline{Q}_{12} & \overline{Q}_{16} \\ \overline{Q}_{12} & \overline{Q}_{22} & \overline{Q}_{26} \\ \overline{Q}_{16} & \overline{Q}_{26} & \overline{Q}_{66} \end{array} \right]_k \left\{ \begin{array}{c} k_x \\ k_y \\ k_{xy} \end{array} \right\} \tag{3.14}$$

3.3 Resultant forces and moments

For convenience, we define the stress resultants in terms of normal forces (per unit length) and moments (per unit length), obtained by integration of stresses through the thickness of the laminate, as (cf. Figure 3.5 below for sign conventions):

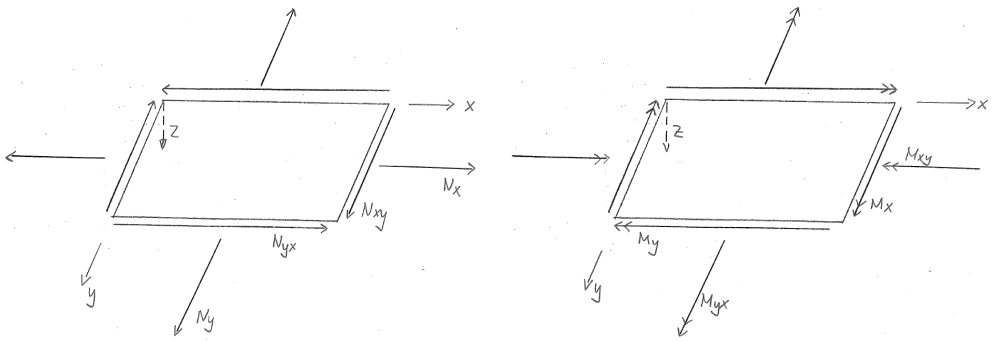

Figure 3.5: Sign convention for resultant forces and moments.

Resulting force per unit length in x-direction:

$$N_x = \int_{-h/2}^{h/2} \sigma_x \, dz \tag{3.15}$$

Resulting force per unit length in y-direction:

$$N_y = \int_{-h/2}^{h/2} \sigma_y \, dz \tag{3.16}$$

Resulting in-plane shear force per unit length:

$$N_{xy} = N_{yx} = \int_{-h/2}^{h/2} \tau_{xy} \, dz \tag{3.17}$$

Resulting moment per unit length, acting on the edge with normal in the x-axis direction causing a (positive) rotation around the y-axis (integration of stress times moment arm):

$$M_x = \int_{-h/2}^{h/2} \sigma_x z \, dz \tag{3.18}$$

Resulting moment per unit length, acting on the edge with normal in the y-axis direction causing a (negative) rotation around the x-axis (integration of stress times moment arm):

$$M_y = \int_{-h/2}^{h/2} \sigma_y z \, dz \tag{3.19}$$

Resulting moment per unit length, acting on the edge with normal in the x-axis direction causing a (negative) rotation around the x-axis (integration of stress times moment arm):

$$M_{xy} = \int_{-h/2}^{h/2} \tau_{xy} z \, dz \tag{3.20}$$

Resulting moment per unit length, acting on the edge with normal in the y-axis direction causing a (positive) rotation around the y-axis (integration of stress times moment arm):

$$M_{yx} = M_{xy} \tag{3.21}$$

Let us now consider an orthotropic laminate consisting of n laminae (plies), cf. Figure 3.6. Grouping the normal forces (per unit length) in a vector one obtains:

$$\{\mathbf{N}\} = \begin{Bmatrix} N_x \\ N_y \\ N_{xy} \end{Bmatrix} = \int_{-h/2}^{h/2} \begin{Bmatrix} \sigma_x \\ \sigma_y \\ \tau_{xy} \end{Bmatrix} dz = \sum_{k=1}^{n} \int_{h_{k-1}}^{h_k} \begin{Bmatrix} \sigma_x \\ \sigma_y \\ \tau_{xy} \end{Bmatrix}_k dz \tag{3.22}$$

where h_k is the z-coordinate of the upper (in positive z-direction) part of lamina k.

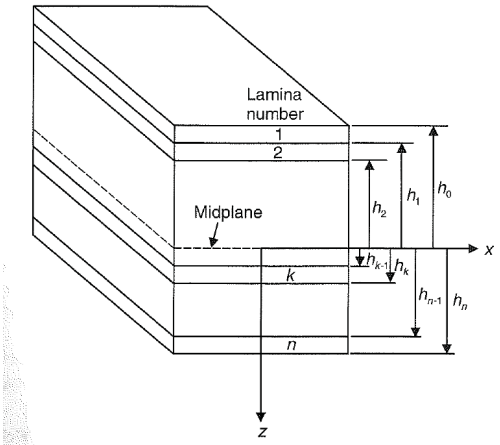

Figure 3.6: Description of a multilayered laminate geometry (from Agarwal et al, figure 6-5).

Now, combining Eq. (3.14) and Eq. (3.22), $\mathbf{N}$ can be written as:

$$\{\mathbf{N}\} = \sum_{k=1}^{n} \int_{h_{k-1}}^{h_k} \left[\overline{\mathbf{Q}}\right]_k \left\{\boldsymbol{\varepsilon}^0 + z\mathbf{k}\right\} dz \tag{3.23}$$

Realising that the midplane strains $\boldsymbol{\varepsilon}^0$, the curvatures $\mathbf{k}$ and the material properties $\overline{Q}_{ij}$ are constant within each lamina, we can further rewrite the expression for the normal forces as:

$$\begin{aligned} \{\mathbf{N}\} &= \sum_{k=1}^{n} \left(\left[\overline{\mathbf{Q}}\right]_k \int_{h_{k-1}}^{h_k} dz \, \{\boldsymbol{\varepsilon}^0\} + \left[\overline{\mathbf{Q}}\right]_k \int_{h_{k-1}}^{h_k} z \, dz \, \{\mathbf{k}\} \right) \\ &= \left[\sum_{k=1}^{n} \left[\overline{\mathbf{Q}}\right]_k (h_k - h_{k-1}) \right] \{\boldsymbol{\varepsilon}^0\} + \frac{1}{2} \left[\sum_{k=1}^{n} \left[\overline{\mathbf{Q}}\right]_k \left(h_k^2 - h_{k-1}^2\right) \right] \{\mathbf{k}\} \\ &= [\mathbf{A}]\{\boldsymbol{\varepsilon}^0\} + [\mathbf{B}]\{\mathbf{k}\} \end{aligned} \tag{3.24}$$

where

$$[\mathbf{A}] = \left[\sum_{k=1}^{n} \left[\overline{\mathbf{Q}}\right]_k (h_k - h_{k-1}) \right] \tag{3.25}$$

$$[\mathbf{B}] = \frac{1}{2} \left[\sum_{k=1}^{n} \left[\overline{\mathbf{Q}}\right]_k \left(h_k^2 - h_{k-1}^2\right) \right] \tag{3.26}$$

Please note that $(h_k - h_{k-1})$ is always positive (equal to the thickness of the lamina), but that the term $\left(h_k^2 - h_{k-1}^2\right)$ is positive for a lamina situated above the midplane and negative for a lamina situated below the midplane. In this way, $\mathbf{B} = \mathbf{0}$ for laminates where the laminae (plies) are placed symmetrically around the midplane, thus in that case there is **no coupling between curvatures and normal forces** which may occur in the general case.

Performing the same type of analysis for the moments, cf. e.g. Agarwal *et al.*, one obtains:

$$\{\mathbf{M}\} = \left\{ \begin{array}{c} M_x \\ M_y \\ M_{xy} \end{array} \right\} = [\mathbf{B}]\{\varepsilon^0\} + [\mathbf{D}]\{\mathbf{k}\} \tag{3.27}$$

where

$$[\mathbf{D}] = \frac{1}{3}\left[\sum_{k=1}^{n} \left[\overline{\mathbf{Q}}\right]_k \left(h_k^3 - h_{k-1}^3\right)\right] \tag{3.28}$$

To summarise, we can write the relation between **N**-**M** and ε^0-**k** as:

$$\left\{ \begin{array}{c} \mathbf{N} \\ \mathbf{M} \end{array} \right\} = \left[\begin{array}{cc} \mathbf{A} & \mathbf{B} \\ \mathbf{B} & \mathbf{D} \end{array} \right] \left\{ \begin{array}{c} \varepsilon^0 \\ \mathbf{k} \end{array} \right\} \tag{3.29}$$

3.4 Laminate orientation code

Each lamina in a laminate is normally defined by its rotation around the positive out-of-plane axis (positive z-axis) with respect to a global xyz coordinate system. Thus, referring to Figure 3.7 it is clear that a proper definition of the global coordinate system is required to avoid ambiguity in the definition of the lay-up sequence of the laminate.

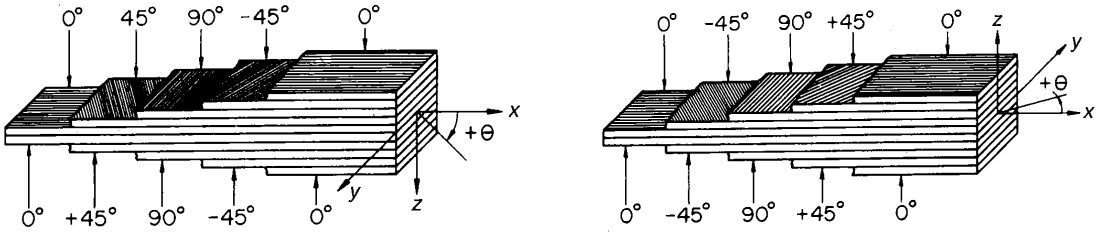

Figure 3.7: Sign convention for orientation of laminae in a laminate. Please note that in the figure, the laminate is identical in both the left and the right part. The only difference is the orientation of the coordinate axes (from Agarwal et al, figure A3-1).

With a given coordinate system at hand, the lay-up sequence of a laminate is easily defined according to the following:

- Each lamina is represented by a number representing the angle (in degrees) of rotation around the z-axis
- Individual laminae are separated by a slash sign (/)
- The laminae are listed in the sequence they are laid up.
- Adjacent laminae with the same orientation are denoted by a numerical subscript.
- Adjacent laminae with the same magnitude of orientation, but in the two different directions, are denoted by a 'plus-minus' ($\pm$) or 'minus-plus' ($\mp$) sign.
- For symmetric laminates, only half of the lay-up sequence needs to be defined followed by a subscript S denoting symmetry.
- For symmetric laminates, if the number of plies are uneven, the mid-lamina is denoted by an overbar.

For a couple of examples of laminate definitions, cf. Figure 3.8.

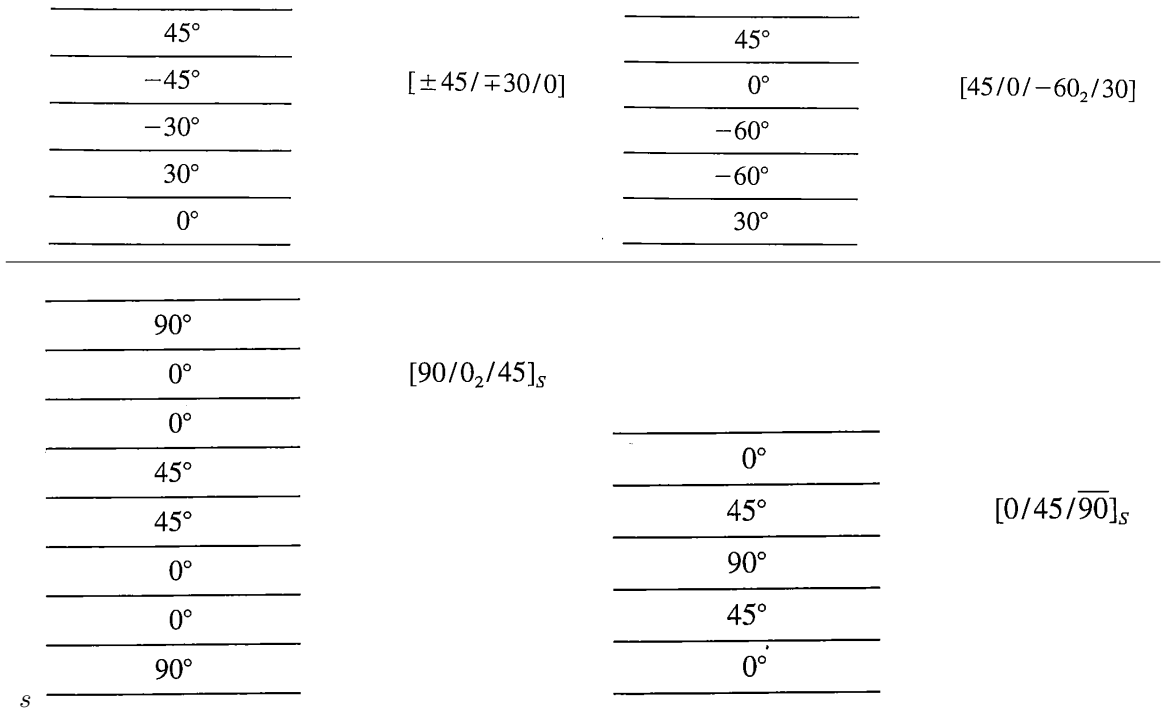

Figure 3.8: Four examples of lay-up sequences and their corresponding laminate orientation code (from Agarwal et al).

3.5 Read Subsection 6.6 on your own

3.6 Determining relevant stresses and strains in the laminae

It should be remembered that the interesting stresses (and strains) of a composite laminate (in terms of strength) are $(\sigma_L, \sigma_T, \tau_{LT})$ (and $(\varepsilon_L, \varepsilon_T, \gamma_{LT})$). Given the **A**, **B** and **D** matrices as well as the applied loads at a certain point (x_0, y_0), the procedure to determine these stresses (and strains) in each lamina of the laminate is as follows:

3.6.1 Calculate the strain distribution through the thickness

Invert the relation between $\boldsymbol{\varepsilon}^0, \mathbf{k}$ and $\mathbf{N}, \mathbf{M}$ to get the strain distribution:

$$\left\{ \begin{array}{c} \boldsymbol{\varepsilon}^0(x_0,y_0) \\ \mathbf{k}(x_0,y_0) \end{array} \right\} = \left[\begin{array}{cc} \mathbf{A}(x_0,y_0) & \mathbf{B}(x_0,y_0) \\ \mathbf{B}(x_0,y_0) & \mathbf{D}(x_0,y_0) \end{array} \right]^{-1} \left\{ \begin{array}{c} \mathbf{N}(x_0,y_0) \\ \mathbf{M}(x_0,y_0) \end{array} \right\} \Rightarrow \boldsymbol{\varepsilon}(x_0,y_0,z) = \boldsymbol{\varepsilon}^0(x_0,y_0) + z\mathbf{k}(x_0,y_0) \tag{3.30}$$

3.6.2 Transform strains into fibre oriented coordinate system

Transform the strains of each lamina from the global coordinate system to the fibre oriented coordinate system using the transformation matrix $[T_2]_k$ of each lamina as:

$$\left\{ \begin{array}{c} \varepsilon_L(x_0,y_0,z) \\ \varepsilon_T(x_0,y_0,z) \\ \gamma_{LT}(x_0,y_0,z) \end{array} \right\}_k = [T_2]_k \left\{ \begin{array}{c} \varepsilon_x(x_0,y_0,z) \\ \varepsilon_y(x_0,y_0,z) \\ \gamma_{xy}(x_0,y_0,z) \end{array} \right\}_k \tag{3.31}$$

where we remember $[T_2]_k$ from lecture 2 as:

$$[T_2]_k = \begin{bmatrix} \cos^2\theta_k & \sin^2\theta_k & \sin\theta_k\cos\theta_k \\ \sin^2\theta_k & \cos^2\theta_k & -\sin\theta_k\cos\theta_k \\ -2\sin\theta_k\cos\theta_k & 2\sin\theta_k\cos\theta_k & \cos^2\theta_k - \sin^2\theta_k \end{bmatrix} \tag{3.32}$$

3.6.3 Calculate stresses in global coordinate system for each lamina/ply

To compute the stress distribution through the thickness of each lamina, use the constitutive matrix $[\overline{\mathbf{Q}}]_k$ as

$$\{\boldsymbol{\sigma}_k(x_0,y_0,z)\}_k = \left\{ \begin{array}{c} \sigma_x(x_0,y_0,z) \\ \sigma_y(x_0,y_0,z) \\ \tau_{xy}(x_0,y_0,z) \end{array} \right\}_k = [\overline{\mathbf{Q}}]_k \left\{ \begin{array}{c} \varepsilon_x^0(x_0,y_0) + zk_x(x_0,y_0) \\ \varepsilon_y^0(x_0,y_0) + zk_y(x_0,y_0) \\ \gamma_{xy}^0(x_0,y_0) + zk_{xy}(x_0,y_0) \end{array} \right\} \tag{3.33}$$

Note that the stress varies linearly with z within the lamina!! Please also note that this is an unnecessary step if you want to assess the strength of the lamina since you then would need the stresses expressed in the fibre oriented coordinate system, obtained directly through

$$\left\{ \begin{array}{c} \sigma_L \\ \sigma_T \\ \tau_{LT} \end{array} \right\}_k = [\mathbf{Q}]_k \left\{ \begin{array}{c} \varepsilon_L(x_0,y_0,z) \\ \varepsilon_T(x_0,y_0,z) \\ \gamma_{LT}(x_0,y_0,z) \end{array} \right\}_k \tag{3.34}$$

3.6.4 Transform stresses into fibre oriented coordinate system

Transform the stresses of each lamina from the global coordinate system to the fibre oriented coordinate system using the transformation matrix $[T_1]_k$ of each lamina as:

$$\left\{ \begin{array}{c} \sigma_L \\ \sigma_T \\ \tau_{LT} \end{array} \right\}_k = [T_1]_k \left\{ \begin{array}{c} \sigma_x \\ \sigma_y \\ \tau_{xy} \end{array} \right\}_k \tag{3.35}$$

where we remember $[T_1]$ from lecture 2 as:

$$[T_1]_k = \begin{bmatrix} \cos^2\theta_k & \sin^2\theta_k & 2\sin\theta_k\cos\theta_k \\ \sin^2\theta_k & \cos^2\theta_k & -2\sin\theta_k\cos\theta_k \\ -\sin\theta_k\cos\theta_k & \sin\theta_k\cos\theta_k & \cos^2\theta_k - \sin^2\theta_k \end{bmatrix} \tag{3.36}$$

Note that the stress varies linearly with z within the lamina!!

3.7 Hygrothermal effects

There are two major sources of change of mechanical behaviour due to temperature (thermal effects) and moist absorption (hygroscopic effects) of polymer composites:

- Hygrothermal stresses and strains
- Hygrothermal degradation of properties (matrix dominated properties such as (transverse) stiffness and strength)

3.7.1 Hygrothermal stresses

Hygrothermal stresses are stresses induced by temperature change or moist absorption/desorption. Please note that hygrothermal stresses can occur within the different laminae (plies) even though the laminate itself is free to expand and can at the first glance appear to be stress-free (although the stress resultants are in fact left unchanged), cf. also Figure 3.9 for an explanatory sketch of a laminate consisting of isotropic laminae (the principle is the same also for transversely isotropic plies).

Temperature change and moist absorption/desortpion does not, as mentioned above, influence the stress resultants, but it introduces stresses and strains in each laminae and **may cause e.g. warping for *unsymmetric* composites**. The strains that produce stresses are the mechanical strains:

$$\boldsymbol{\varepsilon}^M = \boldsymbol{\varepsilon} - \boldsymbol{\varepsilon}^T - \boldsymbol{\varepsilon}^H. \tag{3.37}$$

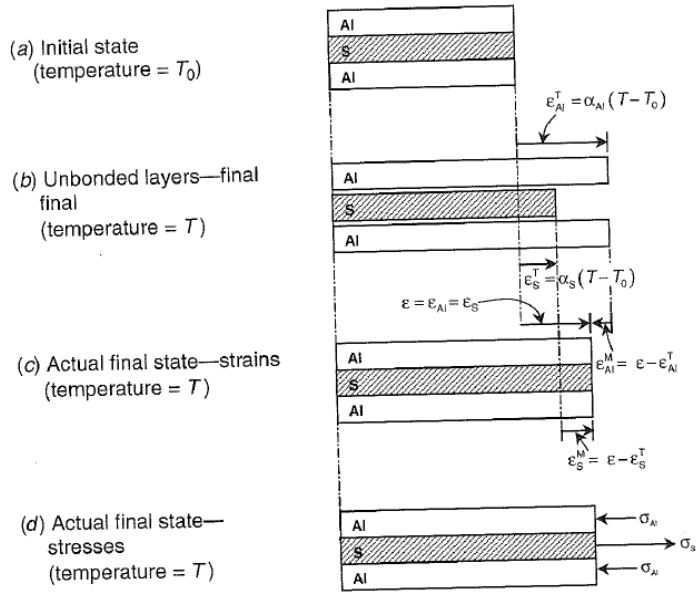

$$\sigma_{Al} = E_{Al}\varepsilon^M_{Al}$$
$$\sigma_S = E_S\varepsilon^M_S$$
$$\sigma_S = 2\sigma_{Al}$$

Figure 3.9: Concepts of thermal stresses and strains in a three-ply symmetric laminate (from Agarwal et al, figure 6-19.)

To study the thermal and hygroscopic strains, the 'hygrothermal' strains, we first consider the properties of an transversely isotropic material, such as an UD lamina. In this case, the coefficients of thermal and moisture expansion change with direction, cf. e.g. Subsection 3.7.1 and 3.7.3 in Agarwal *et al.*. Thus, changes in temperature and/or moist contents produce strains according to:

$$\varepsilon^T_L = \alpha_L \Delta T \tag{3.38}$$
$$\varepsilon^T_T = \alpha_T \Delta T \tag{3.39}$$
$$\varepsilon^H_L = \beta_L \Delta C = 0 \text{ (since } \beta_L \text{ is taken as} \approx 0\text{, cf. Subsection 3.7.2)} \tag{3.40}$$
$$\varepsilon^H_T = \beta_T \Delta C \tag{3.41}$$
$$\tag{3.42}$$

Since the thermal and hygroscopic strains transform in the same way as the total strain (using the transformation matrix T_2) it is clear that the coefficients of thermal and hygroscopic expansion transform in the same way, i.e. we obtain for each lamina:

$$\begin{Bmatrix} \alpha_x \\ \alpha_y \\ \alpha_{xy} \end{Bmatrix}_k = [T_2]_k^{-1} \begin{Bmatrix} \alpha_L \\ \alpha_T \\ 0 \end{Bmatrix}_k \tag{3.43}$$
$$\begin{Bmatrix} \beta_x \\ \beta_y \\ \beta_{xy} \end{Bmatrix}_k = [T_2]_k^{-1} \begin{Bmatrix} 0 \\ \beta_T \\ 0 \end{Bmatrix}_k \tag{3.44}$$

Thus, the thermal and hygroscopic strains may be expressed in the global coordinate system as:

$$\left\{ \begin{array}{c} \varepsilon_x^T \\ \varepsilon_y^T \\ \gamma_{xy}^T \end{array} \right\}_k = \left\{ \begin{array}{c} \alpha_x \\ \alpha_y \\ \alpha_{xy} \end{array} \right\} \Delta T \tag{3.45}$$

$$\left\{ \begin{array}{c} \varepsilon_x^H \\ \varepsilon_y^H \\ \gamma_{xy}^H \end{array} \right\}_k = \left\{ \begin{array}{c} \beta_x \\ \beta_y \\ \beta_{xy} \end{array} \right\} \Delta C \tag{3.46}$$

For clarity, due to the similarities between hygroscopic and thermal strains, we will only consider the thermal strains in the following. The derivations below can easily be extended to include also the hygroscopic effects, cf. the book, but it involves more terms.

Given the expressions for the thermal strains, and neglecting any moist absorption/desorption, one obtains the mechanical strains $\boldsymbol{\varepsilon}_M$ of each lamina as:

$$\left\{ \begin{array}{c} \varepsilon_x^M \\ \varepsilon_y^M \\ \gamma_{xy}^M \end{array} \right\}_k = \left\{ \begin{array}{c} \varepsilon_x^0 + zk_x \\ \varepsilon_y^0 + zk_y \\ \gamma_{xy}^0 + zk_{xy} \end{array} \right\} - \left\{ \begin{array}{c} \alpha_x \\ \alpha_y \\ \alpha_{xy} \end{array} \right\}_k \Delta T \tag{3.47}$$

Inserting this in the expression for the stresses in each lamina k, one obtains

$$\left\{ \begin{array}{c} \sigma_x \\ \sigma_y \\ \tau_{xy} \end{array} \right\}_k = \left[\overline{\mathbf{Q}}\right]_k \left\{ \begin{array}{c} \varepsilon_x^0 + zk_x \\ \varepsilon_y^0 + zk_y \\ \gamma_{xy}^0 + zk_{xy} \end{array} \right\} - \left[\overline{\mathbf{Q}}\right]_k \left\{ \begin{array}{c} \alpha_x \\ \alpha_y \\ \alpha_{xy} \end{array} \right\}_k \Delta T \tag{3.48}$$

Now, in order to obtain the relation between the 'total' midplane strains and curvatures and the forces produced by mechanical and thermal loads, we insert Eq. (3.48) in the expression for the stress resultants (normal forces and moments due to mechanical loading) one obtains:

$$\{\mathbf{N}^M\} = [\mathbf{A}]\{\boldsymbol{\varepsilon}^0\} + [\mathbf{B}]\{\mathbf{k}\} - \{\mathbf{N}^T\} \tag{3.49}$$

$$\{\mathbf{M}^M\} = [\mathbf{B}]\{\boldsymbol{\varepsilon}^0\} + [\mathbf{D}]\{\mathbf{k}\} - \{\mathbf{M}^T\} \tag{3.50}$$

or equivalently

$$\left[\begin{array}{cc} \mathbf{A} & \mathbf{B} \\ \mathbf{B} & \mathbf{D} \end{array} \right] \left\{ \begin{array}{c} \varepsilon_x^0 \\ \varepsilon_y^0 \\ \gamma_{xy}^0 \\ k_x^0 \\ k_y^0 \\ k_{xy}^0 \end{array} \right\} = \left\{ \begin{array}{c} N_x^M \\ N_Y^M \\ N_{xy}^M \\ M_x^M \\ M_y^M \\ M_{xy}^M \end{array} \right\} + \left\{ \begin{array}{c} N_x^T \\ N_y^T \\ N_{xy}^T \\ M_x^T \\ M_y^T \\ M_{xy}^T \end{array} \right\} \tag{3.51}$$

where, as stated above, $N_x^M, N_y^M, ..., M_{xy}^M$ are normal forces and moments due to mechanical loads and where the thermal loads are obtained as:

$$\{\mathbf{N}^T\} = \left\{ \begin{array}{c} N_x^T \\ N_y^T \\ N_{xy}^T \end{array} \right\} = \Delta T \sum_{k=1}^{n} \left[\overline{\mathbf{Q}}\right]_k \left\{ \begin{array}{c} \alpha_x \\ \alpha_y \\ \alpha_{xy} \end{array} \right\}_k (h_k - h_{k-1}) \tag{3.52}$$

$$\{\mathbf{M}^T\} = \left\{ \begin{array}{c} M_x^T \\ M_y^T \\ M_{xy}^T \end{array} \right\} = \frac{1}{2}\Delta T \sum_{k=1}^{n} \left[\overline{\mathbf{Q}}\right]_k \left\{ \begin{array}{c} \alpha_x \\ \alpha_y \\ \alpha_{xy} \end{array} \right\}_k \left(h_k^2 - h_{k-1}^2\right) \tag{3.53}$$

Remark. Please note that in Agarwal *et al.*, the authors refer to something called thermal stresses (denoted by a superscript T in e.g. Equation 6.62). This may be somewhat misleading since stresses are always cased by mechanical straining ($\boldsymbol{\sigma} = \boldsymbol{\sigma}(\boldsymbol{\varepsilon}^M)$ and nothing else. Stresses can not be anything but mechanical. A more proper description would be *thermally induced stresses*.

Chapter 4

Kirchhoff-Love plate theory for anisotropic laminated plates

4.1 Assumption in the Kirchhoff-Love plate theory

The Kirchhoff-Love plate theory is based the following assumptions (also discussed in Chapter 3 for the classical laminate theory)

- A line originally in the z-direction before deformation remains straight also after deformation.
- The deformation of a line in the z-direction follow the rotation of the middle surface during deformation, i.e. they remain perpendicular to the midsurface.
- There is no change of thickness of the plate.

.

4.2 Repetition of kinematics for the Kirchhoff-Love plate theory

We recall from Chapter 3 that the strains under the Kirchhoff assumptions become:

$$\begin{aligned}
\epsilon_x &= \frac{\partial u}{\partial x} = \frac{\partial u_0}{\partial x} - z\frac{\partial^2 w_0}{\partial x^2} \\
\varepsilon_y &= \frac{\partial v}{\partial y} = \frac{\partial v_0}{\partial y} - z\frac{\partial^2 w_0}{\partial y^2} \\
\gamma_{xy} &= \frac{\partial u}{\partial y} + \frac{\partial v}{\partial x} = \frac{\partial u_0}{\partial y} + \frac{\partial v_0}{\partial x} - 2\,z\frac{\partial^2 w_0}{\partial x\,\partial y}
\end{aligned}$$

It is worth pointing out the two contradiction that

1. the shear strains are assumed to be zero $\gamma_{xz} = \gamma_{yz} = 0$ although the corresponding shear stresses are not (cf. Section 4.3 below), e.g.

$$\gamma_{xz} = \frac{\partial u}{\partial z} + \frac{\partial w_0}{\partial x} = -\frac{\partial w_0}{\partial x} + \frac{\partial w_0}{\partial x} = 0$$

2. A simultaneous state of $\sigma_z = 0$ and a constant thickness (after deformation) of the laminate is assumed.

4.3 Equilibrium equations for a plate section

Consider an infinitesimally small element Δx-Δy of a rectangular plate shown in Figure 4.1. Stress resultants (per unit length) acting on this small plate element are:

- out-of-plane shear forces R_{yz} and R_{xz} (note that these are resultants from the shear stresses τ_{yz} and τ_{xz} respectively that previously have been neglected but now have to be considered to balance the applied surface load)
- in-plane normal and shear forces N_x, N_y and $N_{xy} = N_{yx}$ and
- moments M_x, M_y and $M_{xy} = M_{yx}$.

In addition, the outer vertical force acting on the element is the distributed load $p(x, y)$ (force per unit area and positive in the positive z-direction).

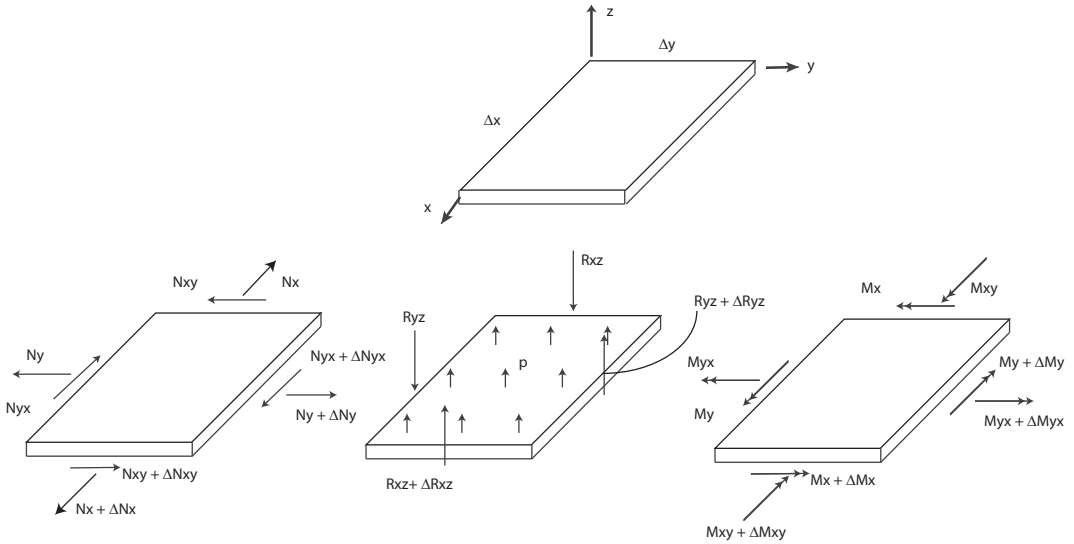

Figure 4.1: Definition of cross-sectional quantities in a rectangular plate.

As before, the in-plane forces and moments are resultants of the stresses σ_x, σ_y and τ_{xy} as follows:

$$\begin{aligned} N_x &= \int_{-h/2}^{h/2} \sigma_x \, \mathrm{d}z \, , \quad N_y = \int_{-h/2}^{h/2} \sigma_y \, \mathrm{d}z \, , \quad N_{xy} = \int_{-h/2}^{h/2} \tau_{xy} \, \mathrm{d}z = N_{yx} \\ M_x &= \int_{-h/2}^{h/2} z \, \sigma_x \, \mathrm{d}z \, , \quad M_y = \int_{-h/2}^{h/2} z \, \sigma_y \, \mathrm{d}z \, , \quad M_{xy} = \int_{-h/2}^{h/2} z \, \tau_{xy} \, \mathrm{d}z = M_{yx} \end{aligned}$$

Correspondingly, the internal shear forces per unit length are the resultants of the out-of-plane shear stresses

$$R_{xz} = \int_{-h/2}^{h/2} \tau_{xz} \, \mathrm{d}z, \quad R_{yz} = \int_{-h/2}^{h/2} \tau_{yz} \, \mathrm{d}z \tag{4.1}$$

We now study equilibrium of the small plate element

4.3.1 Force equilibrium in x-direction

$$\begin{aligned} &(N_x + \Delta N_x)\Delta y - N_x \Delta y + (N_{yx} + \Delta N_{yx})\Delta x - N_{yx}\Delta x = 0 \Rightarrow \\ &\{N_{xy} = N_{yx} + \text{ divide by } \Delta x \Delta y \text{ and let } \Delta x \to 0, \Delta y \to 0\} \Rightarrow \\ &\frac{\partial N_x}{\partial x} + \frac{\partial N_{xy}}{\partial y} = 0 \end{aligned} \tag{4.2}$$

4.3.2 Force equilibrium in y-direction

$$\begin{aligned} &(N_y + \Delta N_y)\Delta x - N_y \Delta x + (N_{xy} + \Delta N_{xy})\Delta y - N_{xy}\Delta y = 0 \Rightarrow \\ &\{\text{divide by } \Delta x \Delta y \text{ and let } \Delta x \to 0, \Delta y \to 0\} \Rightarrow \\ &\frac{\partial N_{xy}}{\partial x} + \frac{\partial N_y}{\partial y} = 0 \end{aligned} \tag{4.3}$$

4.3.3 Force squilibrium in z-direction

$$\begin{aligned}&(R_{xz}+\Delta R_{xz})\Delta y - R_{xz}\Delta y + (R_{yz}+\Delta R_{yz})\Delta x - R_{yz}\Delta x + p\Delta x\Delta y = 0 \Rightarrow\\ &\{\text{divide by } \Delta x\Delta y \text{ and let } \Delta x \to 0, \Delta y \to 0\} \Rightarrow\\ &\frac{\partial R_{xz}}{\partial x} + \frac{\partial R_{yz}}{\partial y} = -p\end{aligned} \tag{4.4}$$

4.3.4 Moment equilibrium around the x-axis

$$\begin{aligned}&-(M_y+\Delta M_y)\Delta x + M_y\Delta x - (M_{xy}+\Delta M_{xy})\Delta y + M_{xy}\Delta y + (R_{yz}+\Delta R_{yz})\,\Delta x\Delta y\\ &\quad + (R_{xz}+\Delta R_{xz})\,\Delta y\frac{\Delta y}{2} - R_{xz}\Delta y\frac{\Delta y}{2} + p\Delta x\Delta y\frac{\Delta y}{2} = 0 \Rightarrow\\ &\quad \{\text{divide by } \Delta x\Delta y \text{ and let } \Delta x \to 0, \Delta y \to 0\} \Rightarrow\\ &\quad \frac{\partial M_{xy}}{\partial x} + \frac{\partial M_y}{\partial y} = R_{yz}\end{aligned} \tag{4.5}$$

4.3.5 Moment equilibrium around the y-axis

$$\begin{aligned}&(M_x+\Delta M_x)\Delta y - M_x\Delta y + (M_{yx}+\Delta M_{yx})\Delta x - M_{yx}\Delta x - (R_{xz}+\Delta R_{xz})\,\Delta x\Delta y\\ &\quad - (R_{yz}+\Delta R_{yz})\,\frac{\Delta x}{2}\Delta y + R_{yz}\frac{\Delta x}{2}\Delta y + p\Delta x\Delta y\frac{\Delta x}{2} = 0 \Rightarrow\\ &\quad \{M_{xy} = M_{yx} + \text{divide by } \Delta x\Delta y \text{ and let } \Delta x \to 0, \Delta y \to 0\} \Rightarrow\\ &\quad \frac{\partial M_x}{\partial x} + \frac{\partial M_{xy}}{\partial y} = R_{xz}\end{aligned} \tag{4.6}$$

4.3.6 Governing equilibrium equations for the Kirchhoff-Love plate theory

Please note that the above five equations are valid for both plate theories to be considered in the course. However, since we in the Kirchhoff-Love plate theory only have three unknown fields (displacements of the midplane u_0, v_0 and w_0), only three equations are needed. This can be accomplished by utilising Eqs. (4.2) and (4.3) and inserting the results from Eqs. (4.5) and (4.6) into Eq. (4.4) leading to the three governing equilibrium equations for a Kirchhoff-Love plate as:

$$\frac{\partial N_x}{\partial x} + \frac{\partial N_{xy}}{\partial y} = 0 \tag{4.7}$$

$$\frac{\partial N_{xy}}{\partial x} + \frac{\partial N_y}{\partial y} = 0 \tag{4.8}$$

$$\frac{\partial^2 M_x}{\partial x^2} + 2\,\frac{\partial^2 M_{xy}}{\partial x\partial y} + \frac{\partial^2 M_y}{\partial y^2} = -p \tag{4.9}$$

For future purposes, we note that we also can write the equations above in a contracted way as:

$$\tilde{\boldsymbol{\nabla}}^T\mathbf{N} = \mathbf{0} \tag{4.10}$$

$$-\overset{*}{\boldsymbol{\nabla}}^T\mathbf{M} = p \tag{4.11}$$

with $\tilde{\boldsymbol{\nabla}}^T$ and $\overset{*}{\boldsymbol{\nabla}}^T$ defined as:

$$\tilde{\boldsymbol{\nabla}} = \begin{Bmatrix} \frac{\partial}{\partial x} & 0 \\ 0 & \frac{\partial}{\partial y} \\ \frac{\partial}{\partial y} & \frac{\partial}{\partial x} \end{Bmatrix},\ \overset{*}{\boldsymbol{\nabla}} = \begin{Bmatrix} \frac{\partial^2}{\partial x^2} \\ \frac{\partial^2}{\partial y^2} \\ 2\frac{\partial^2}{\partial x\partial y} \end{Bmatrix} = \tilde{\boldsymbol{\nabla}}\boldsymbol{\nabla} \text{ with } \boldsymbol{\nabla} = \begin{Bmatrix} \frac{\partial}{\partial x} \\ \frac{\partial}{\partial y} \end{Bmatrix} \tag{4.12}$$

Please note that it is the exact same equilibrium equations as for an isotropic plate. However, in that case there is no coupling between in-plane loading and bending due to the material symmetry (or rather isotropy).

4.4 Equilibrium equations in terms of displacements for the Kirchhoff-Love theory

The equilibrium equations can also be written in terms of displacements using the constitutive relations. Inserting the following expressions for the normal forces and moments from Chapter 3:

$$\{\mathbf{N}\} = [\mathbf{A}]\{\boldsymbol{\varepsilon}^0\} + [\mathbf{B}]\{\mathbf{k}\} \tag{4.13}$$

$$\{\mathbf{M}\} = [\mathbf{B}]\{\boldsymbol{\varepsilon}^0\} + [\mathbf{D}]\{\mathbf{k}\} \tag{4.14}$$

with

$$\{\boldsymbol{\varepsilon}^0\} = \tilde{\boldsymbol{\nabla}}\mathbf{u} = \begin{Bmatrix} \dfrac{\partial u_0}{\partial x} \\ \dfrac{\partial v_0}{\partial y} \\ \dfrac{\partial u_0}{\partial y} + \dfrac{\partial v_0}{\partial x} \end{Bmatrix}, \ \{\mathbf{k}\} = -\overset{*}{\boldsymbol{\nabla}} w_0 = - \begin{Bmatrix} \dfrac{\partial^2 w_0}{\partial x^2} \\ \dfrac{\partial^2 w_0}{\partial y^2} \\ 2\dfrac{\partial^2 w_0}{\partial x \partial y} \end{Bmatrix} \tag{4.15}$$

into the equilibrium equations Eqs. (4.7)-(4.9), one obtains the equilibrium equations in terms of the displacements as:

$$\begin{aligned} &A_{11}\frac{\partial^2 u_0}{\partial x^2} + 2A_{16}\frac{\partial^2 u_0}{\partial x \partial y} + A_{66}\frac{\partial^2 u_0}{\partial y^2} + A_{16}\frac{\partial^2 v_0}{\partial x^2} + (A_{12}+A_{66})\frac{\partial^2 v_0}{\partial x \partial y} + A_{26}\frac{\partial^2 v_0}{\partial y^2} \\ &- B_{11}\frac{\partial^3 w_0}{\partial x^3} - 3B_{16}\frac{\partial^3 w_0}{\partial x^2 \partial y} - (B_{12}+2B_{66})\frac{\partial^3 w_0}{\partial x \partial y^2} - B_{26}\frac{\partial^3 w_0}{\partial y^3} = 0 \end{aligned} \tag{4.16}$$

$$\begin{aligned} &A_{16}\frac{\partial^2 u_0}{\partial x^2} + (A_{12}+A_{66})\frac{\partial^2 u_0}{\partial x \partial y} + A_{26}\frac{\partial^2 u_0}{\partial y^2} + A_{66}\frac{\partial^2 v_0}{\partial x^2} + 2A_{26}\frac{\partial^2 v_0}{\partial x \partial y} + A_{22}\frac{\partial^2 v_0}{\partial y^2} \\ &- B_{16}\frac{\partial^3 w_0}{\partial x^3} - (B_{12}+2B_{66})\frac{\partial^3 w_0}{\partial x^2 \partial y} - 3B_{26}\frac{\partial^3 w_0}{\partial x \partial y^2} - B_{22}\frac{\partial^3 w_0}{\partial y^3} = 0 \end{aligned} \tag{4.17}$$

$$\begin{aligned} &D_{11}\frac{\partial^4 w_0}{\partial x^4} + 4D_{16}\frac{\partial^4 w_0}{\partial x^3 \partial y} + 2(D_{12}+2D_{66})\frac{\partial^4 w_0}{\partial x^2 \partial y^2} + 4D_{26}\frac{\partial^4 w_0}{\partial x \partial y^3} + D_{22}\frac{\partial^4 w_0}{\partial y^4} \\ &- B_{11}\frac{\partial^3 u_0}{\partial x^3} - 3B_{16}\frac{\partial^3 u_0}{\partial x^2 \partial y} - (B_{12}+2B_{66})\frac{\partial^3 u_0}{\partial x \partial y^2} - B_{26}\frac{\partial^3 u_0}{\partial y^3} - B_{16}\frac{\partial^3 v_0}{\partial x^3} \\ &- (B_{12}+2B_{66})\frac{\partial^3 v_0}{\partial x^2 \partial y} - 3B_{26}\frac{\partial^3 v_0}{\partial x \partial y^2} - B_{22}\frac{\partial^3 v_0}{\partial y^3} = p \end{aligned} \tag{4.18}$$

which are the general equilibrium equations for a laminated plate with any lay-up sequence.

4.4.1 Symmetric and specially orthotropic laminates

In the case of a symmetric laminate, i.e. $B_{ij} = 0$ the equilibrium equations are simplified to be:

$$A_{11}\frac{\partial^2 u_0}{\partial x^2} + 2A_{16}\frac{\partial^2 u_0}{\partial x \partial y} + A_{66}\frac{\partial^2 u_0}{\partial y^2} + A_{16}\frac{\partial^2 v_0}{\partial x^2} + (A_{12}+A_{66})\frac{\partial^2 v_0}{\partial x \partial y} + A_{26}\frac{\partial^2 v_0}{\partial y^2} = 0 \tag{4.19}$$

$$A_{16}\frac{\partial^2 u_0}{\partial x^2} + (A_{12}+A_{66})\frac{\partial^2 u_0}{\partial x \partial y} + A_{26}\frac{\partial^2 u_0}{\partial y^2} + A_{66}\frac{\partial^2 v_0}{\partial x^2} + 2A_{26}\frac{\partial^2 v_0}{\partial x \partial y} + A_{22}\frac{\partial^2 v_0}{\partial y^2} = 0 \tag{4.20}$$

$$D_{11}\frac{\partial^4 w_0}{\partial x^4} + 4D_{16}\frac{\partial^4 w_0}{\partial x^3 \partial y} + 2(D_{12}+2D_{66})\frac{\partial^4 w_0}{\partial x^2 \partial y^2} + 4D_{26}\frac{\partial^4 w_0}{\partial x \partial y^3} + D_{22}\frac{\partial^4 w_0}{\partial y^4} = p \tag{4.21}$$

Furthermore, specially orthotropic laminates (such as e.g. unidirectional laminates with all fibres oriented with an angle of 0° or 90° *or* symmetric cross-ply laminates) – the laminate that behave like a single layer of an orthotropic material – satisfy the following additional conditions:

$$A_{16} = A_{26} = 0 \tag{4.22}$$
$$D_{16} = D_{26} = 0 \tag{4.23}$$

whereby the equilibrium equations are further simplified to be:

$$A_{11}\frac{\partial^2 u_0}{\partial x^2} + A_{66}\frac{\partial^2 u_0}{\partial y^2} + (A_{12}+A_{66})\frac{\partial^2 v_0}{\partial x \partial y} = 0 \tag{4.24}$$
$$(A_{12}+A_{66})\frac{\partial^2 u_0}{\partial x \partial y} + A_{66}\frac{\partial^2 v_0}{\partial x^2} + A_{22}\frac{\partial^2 v_0}{\partial y^2} = 0 \tag{4.25}$$
$$D_{11}\frac{\partial^4 w_0}{\partial x^4} + 2(D_{12}+2D_{66})\frac{\partial^4 w_0}{\partial x^2 \partial y^2} + D_{22}\frac{\partial^4 w_0}{\partial y^4} = p \tag{4.26}$$

It should be remarked that since $B_{ij} = 0$ the in plane and transverse motions can be treated separately in this case. In the following, we will study a method for analytically solving the bending part for a simply supported specially orthotropic plate.

4.4.2 Analytical solutions - Simply supported specially orthotropic plates

Analytical approaches to solve the plate equation (bending part, i.e. Eq (4.26)) for simple boundary conditions exist. One example is the Navier's solutions for simply supported rectangular plates

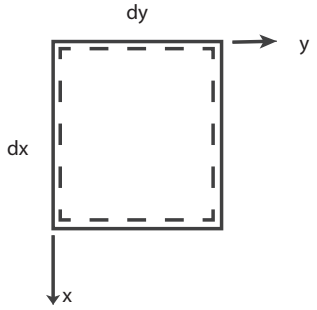

In this method, the deflection w_0 is proposed to be of the following form (Fourier series expansion):

$$w_0(x,y) = \sum_{m=1}^{\infty}\sum_{n=1}^{\infty} w_{mn} \sin\left(\frac{m\pi\, x}{a}\right) \sin\left(\frac{n\pi\, y}{b}\right) \tag{4.27}$$

where w_{mn} are unknown (Fourier) coefficients. The boundary conditions for a fully simply supported plate are

$$\begin{cases} w_0(0,y) = w_0(a,y) = 0\,, \quad w_0(x,0) = w_0(x,b) = 0 \\ M_x(0,y) = M_x(a,y) = 0\,, \quad M_y(x,0) = M_y(x,b) = 0 \end{cases} \tag{4.28}$$

The bending moments can, via (4.14) be expressed as

$$M_x = -D_{11}\frac{\partial^2 w_0}{\partial x^2} - D_{12}\frac{\partial^2 w_0}{\partial y^2} \tag{4.29}$$
$$M_y = -D_{12}\frac{\partial^2 w_0}{\partial x^2} - D_{22}\frac{\partial^2 w_0}{\partial y^2} \tag{4.30}$$

and with the assumed expression for w_0:

$$M_x = -\sum_{m=1}^{\infty}\sum_{n=1}^{\infty} w_{mn}\left(-D_{11}\left(\frac{m\pi}{a}\right)^2 - D_{12}\left(\frac{n\pi}{b}\right)^2\right) \sin\left(\frac{m\pi\, x}{a}\right) \sin\left(\frac{n\pi\, y}{b}\right) \tag{4.31}$$

$$M_y = -\sum_{m=1}^{\infty}\sum_{n=1}^{\infty} w_{mn}\left(-D_{12}\left(\frac{m\pi}{a}\right)^2 - D_{22}\left(\frac{n\pi}{b}\right)^2\right)\sin\left(\frac{m\pi\,x}{a}\right)\sin\left(\frac{n\pi\,y}{b}\right) \tag{4.32}$$

Clearly, the adopted expression for w_0 in (4.27) fulfills the boundary conditions since

$$\sin(n\,\pi) = 0\,, \quad \text{for } n = 0, 1, 2, \ldots$$

The loading p must also be expressed in a similar fashion as w_0

$$p(x,y) = \sum_{m=1}^{\infty}\sum_{n=1}^{\infty} p_{mn}\sin\left(\frac{m\pi\,x}{a}\right)\sin\left(\frac{n\pi\,y}{b}\right)$$

where the coefficients p_{mn} can be found from the following expression

$$p_{mn} = \frac{4}{ab}\int_0^b\int_0^a p(x,y)\sin\left(\frac{m\pi\,x}{a}\right)\sin\left(\frac{n\pi\,y}{b}\right)\mathrm{d}x\,\mathrm{d}y$$

To show this we insert $p(x,y)$ into the integral

$$\int_0^b\int_0^a\left(\sum_{i=1}^{\infty}\sum_{j=1}^{\infty} p_{ij}\sin\left(\frac{i\pi\,x}{a}\right)\sin\left(\frac{j\pi\,y}{b}\right)\right)\sin\left(\frac{m\pi\,x}{a}\right)\sin\left(\frac{n\pi\,y}{b}\right)\mathrm{d}x\,\mathrm{d}y$$

and use the orthogonality of sin functions, i.e.

$$\int_0^a \sin\left(\frac{i\pi\,x}{a}\right)\sin\left(\frac{m\pi\,x}{a}\right)\mathrm{d}x = \begin{cases} a/2 & \text{if } i = m \\ 0 & \text{else} \end{cases}$$

which proves the expression for p_{mn}.

The next step is now to insert the expressions for w_0 and p in the plate equation (4.26) and solve for the unknown coefficients w_{mn}. The result is

$$w_{mn} = \frac{p_{mn}}{\pi^4\left[D_{11}\left(\frac{m}{a}\right)^4 + 2(D_{12}+2D_{66})\left(\frac{m}{a}\right)^2\left(\frac{n}{b}\right)^2 + D_{22}\left(\frac{n}{b}\right)^4\right]} \tag{4.33}$$

Some examples of loading situations:

- Uniform loading $p(x,y) = p_0$:

$$\begin{aligned} p_{mn} &= \frac{4\,p_0}{ab}\int_0^b\int_0^a \sin\left(\frac{m\pi\,x}{a}\right)\sin\left(\frac{n\pi\,y}{b}\right)\mathrm{d}x\,\mathrm{d}y = \\ &= \frac{4\,p_0}{ab}\frac{a}{m\pi}\frac{b}{n\pi}\left[-\cos\left(\frac{m\pi\,x}{a}\right)\right]_0^a\left[-\cos\left(\frac{n\pi\,y}{b}\right)\right]_0^b \\ &= \frac{16\,p_0}{mn\,\pi^2}, \quad m,n = 1,3,\ldots \end{aligned}$$

  Please observe that, despite the fact that the sum in the Fourier series goes to infinity, it is often for practical reasons sufficient to truncate these series (i.e. use a finite value for the upper limit of the sum). It is generally the first modes (lowest values of m and n that have the most significant contributions). As an example, please consider Figure 4.2 where the uniform pressure load is approximated with truncated Fourier series with different maximum values.

- Hydrostatic loading $p(x,y) = p_0\,y/b$

$$\begin{aligned} p_{mn} &= \frac{4\,p_0}{ab^2}\int_0^b\int_0^a \sin\left(\frac{m\pi\,x}{a}\right)\,y\,\sin\left(\frac{n\pi\,y}{b}\right)\mathrm{d}x\,\mathrm{d}y = \\ &= \frac{8\,p_0}{\pi^2\,m\,n}(-1)^{n+1}, \quad m = 1,3,5,\ldots,\ n = 1,2,3,\ldots \end{aligned}$$

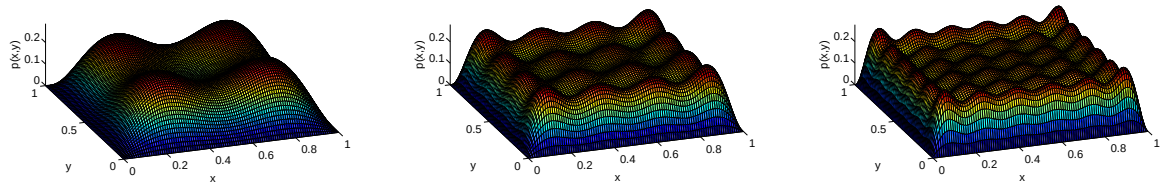

a) b) c)

Figure 4.2: Approximation of uniform pressure load $p(x, y) = 0.2$ using truncated Fourier series with maximum values according to a) $m = n = 3$, b) $m = n = 7$ and c) $m = n = 11$

- Point load Q_0 at x_0, y_0. The distributed force can be described by impulse function (Dirac-delta) $p = Q_0\,\delta(x - x_0, y - y_0)$. With the property

$$\int_0^b \int_0^a \delta(x - x_0, y - y_0)\, f(x, y)\, \mathrm{d}x\, \mathrm{d}y = f(x_0, y_0)$$

Thereby, p_{mn} become

$$\begin{aligned} p_{mn} &= \frac{4\,Q_0}{ab} \int_0^b \int_0^a \delta(x - x_0, y - y_0)\, \sin\left(\frac{m\pi\, x}{a}\right) \sin\left(\frac{n\pi\, y}{b}\right)\, \mathrm{d}x\, \mathrm{d}y = \\ &= \frac{4\,Q_0}{ab} \sin\left(\frac{m\pi\, x_0}{a}\right) \sin\left(\frac{n\pi\, y_0}{b}\right), \quad m, n = 1, 2, 3, \ldots \end{aligned}$$

4.5 Buckling of a Kirchhoff-Love plate

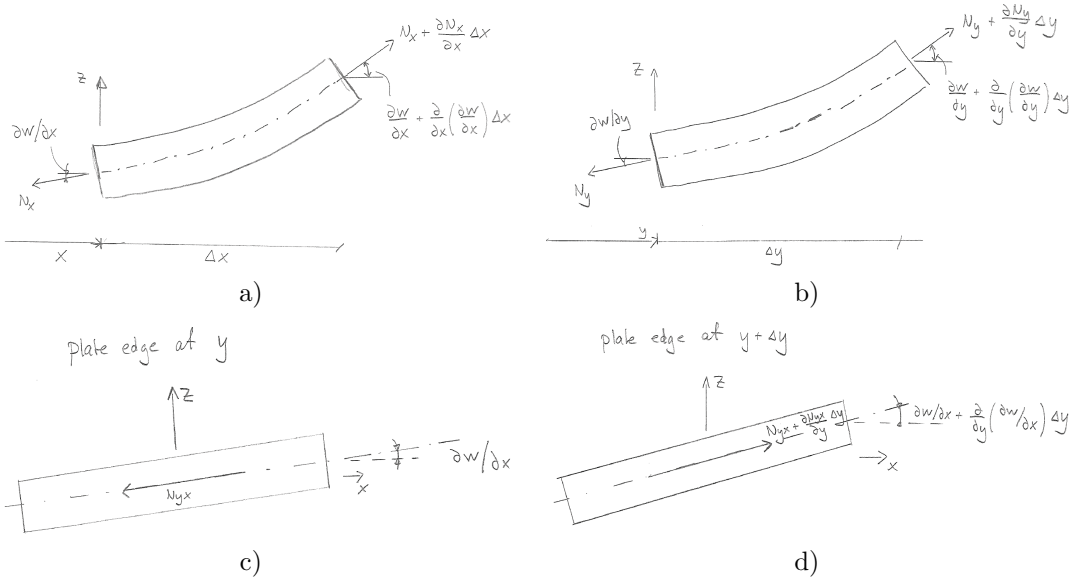

Figure 4.3: Views of the small plate element $\Delta x \Delta y$ showing the contributions from in-plane forces N_x, N_y, N_{xy} and N_{yx} to the vertical equilibrium equation. a) Contribution from N_x, b) contribution from N_y and c)-d) contribution from in N_{yx} (N_{xy} can be treated in the same way)

Moderate in-plane loads on a flat symmetric laminate cause in-plane displacements but no out-of-plane displacements. However, it is known that in-plane compressive loads, when high enough, cause

out-of-plane displacements (deflections) that may be excessive and lead to failure. This is called *elastic instability* or *buckling*. In buckling, out-of-plane displacements are caused by in-plane loads and, hence, the classical Kirchhoff-Love equilibrium equations cannot be used to predict this behaviour because interaction between in-plane loads and out-of-plane displacements were suppressed in the derivation (it was assumed that the out-of-plane displacements are so small that the in-plane force resultants N_x, N_y and N_{xy} act in their original direction in the xy-plane. Therefore, to study buckling, we need to modify the governing equations to take into account the out-of-plane displacements and thereby the vertical projection of the in-plane forces. To do so, we study the in-plane forces acting on the edges of the same small plate element in Figure 4.1, now accounting for the effects of the out-of-plane deformations as shown in Figure 4.3.

4.5.1 The vertical projection of N_x

Relate to Figure 4.3a:

$$\begin{aligned} -N_x\frac{\partial w}{\partial x}\Delta y + (N_x + \frac{\partial N_x}{\partial x}\Delta x)(\frac{\partial w}{\partial x} + \frac{\partial^2 w}{\partial x^2}\Delta x)\Delta y &= N_x\frac{\partial^2 w}{\partial x^2}\Delta x\Delta y + \frac{\partial N_x}{\partial x}\frac{\partial w}{\partial x}\Delta x\Delta y + \frac{\partial N_x}{\partial x}\frac{\partial^2 w}{\partial x^2}\Delta x^2\Delta y \\ &\approx N_x\frac{\partial^2 w}{\partial x^2}\Delta x\Delta y + \frac{\partial N_x}{\partial x}\frac{\partial w}{\partial x}\Delta x\Delta y \end{aligned} \tag{4.34}$$

where it was used that

$$\Delta x^2\Delta y \ll \Delta x\Delta y.$$

4.5.2 The vertical projection of N_y

Relate to Figure 4.3b:

$$\begin{aligned} -N_y\frac{\partial w}{\partial y}\Delta x + (N_y + \frac{\partial N_y}{\partial y}\Delta y)(\frac{\partial w}{\partial y} + \frac{\partial^2 w}{\partial y^2}\Delta y)\Delta x &= N_y\frac{\partial^2 w}{\partial y^2}\Delta x\Delta y + \frac{\partial N_y}{\partial y}\frac{\partial w}{\partial y}\Delta x\Delta y + \frac{\partial N_y}{\partial y}\frac{\partial^2 w}{\partial y^2}\Delta x\Delta y^2 \\ &\approx N_y\frac{\partial^2 w}{\partial y^2}\Delta x\Delta y + \frac{\partial N_y}{\partial y}\frac{\partial w}{\partial y}\Delta x\Delta y \end{aligned} \tag{4.35}$$

where it was used that

$$\Delta x\Delta y^2 \ll \Delta x\Delta y.$$

4.5.3 The vertical projection of N_{yx}

Relate to Figure 4.3c)-d):

$$\begin{aligned} -N_{yx}\frac{\partial w}{\partial x}\Delta x + (N_{yx} + \frac{\partial N_{yx}}{\partial y}\Delta y)(\frac{\partial w}{\partial x} + \frac{\partial^2 w}{\partial x\partial y}\Delta y)\Delta x &= N_{yx}\frac{\partial^2 w}{\partial x\partial y}\Delta x\Delta y + \frac{\partial N_{yx}}{\partial y}\frac{\partial w}{\partial x}\Delta x\Delta y + \frac{\partial N_{yx}}{\partial y}\frac{\partial^2 w}{\partial x\partial y}\Delta x\Delta y^2 \\ &\approx N_{yx}\frac{\partial^2 w}{\partial x\partial y}\Delta x\Delta y + \frac{\partial N_{yx}}{\partial y}\frac{\partial w}{\partial x}\Delta x\Delta y \end{aligned} \tag{4.36}$$

where it was used that

$$\Delta x\Delta y^2 \ll \Delta x\Delta y.$$

4.5.4 The vertical projection of N_{xy}

In the same way as for N_{yx} we can obtain the contribution from N_{xy} as:

$$\begin{aligned} -N_{xy}\frac{\partial w}{\partial y}\Delta y + (N_{xy} + \frac{\partial N_{xy}}{\partial x}\Delta x)(\frac{\partial w}{\partial y} + \frac{\partial^2 w}{\partial x\partial y}\Delta x)\Delta y &= N_{xy}\frac{\partial^2 w}{\partial x\partial y}\Delta x\Delta y + \frac{\partial N_{xy}}{\partial y}\frac{\partial w}{\partial y}\Delta x\Delta y + \frac{\partial N_{xy}}{\partial x}\frac{\partial^2 w}{\partial x\partial y}\Delta x^2\Delta y \\ &\approx N_{xy}\frac{\partial^2 w}{\partial x\partial y}\Delta x\Delta y + \frac{\partial N_{xy}}{\partial y}\frac{\partial w}{\partial y}\Delta x\Delta y \end{aligned} \tag{4.37}$$

where it was used that

$$\Delta x^2 \Delta y \ll \Delta x \Delta y.$$

4.5.5 Total equation

The total vertical contribution of the in-plane stress resultants becomes (via summation of Eqs. (4.34)-(4.37)):

$$\begin{aligned}
&N_x \frac{\partial^2 w}{\partial x^2}\Delta x\Delta y + \frac{\partial N_x}{\partial x}\frac{\partial w}{\partial x}\Delta x\Delta y + N_{yx}\frac{\partial^2 w}{\partial x \partial y}\Delta x\Delta y + \frac{\partial N_{yx}}{\partial y}\frac{\partial w}{\partial x}\Delta x\Delta y + N_{xy}\frac{\partial^2 w}{\partial x \partial y}\Delta x\Delta y \\
&+\frac{\partial N_{xy}}{\partial y}\frac{\partial w}{\partial y}\Delta x\Delta y + N_y \frac{\partial^2 w}{\partial y^2}\Delta x\Delta y + \frac{\partial N_y}{\partial y}\frac{\partial w}{\partial y}\Delta x\Delta y = \{N_{yx} = N_{xy}\} = \\
&= N_x \frac{\partial^2 w}{\partial x^2}\Delta x\Delta y + 2N_{xy}\frac{\partial^2 w}{\partial x \partial y}\Delta x\Delta y + N_y \frac{\partial^2 w}{\partial y^2}\Delta x\Delta y \\
&+ \underbrace{\left(\frac{\partial N_x}{\partial x} + \frac{\partial N_{yx}}{\partial y}\right)}_{=0\text{(in-plane equilib.)}}\frac{\partial w}{\partial x}\Delta x\Delta y + \underbrace{\left(\frac{\partial N_{xy}}{\partial y} + \frac{\partial N_y}{\partial y}\right)}_{=0\text{(in-plane equilib.)}}\frac{\partial w}{\partial y}\Delta x\Delta y
\end{aligned} \tag{4.38}$$

Adding the vertical contributions from in-plane force resultants to Eq. (4.4) yields (when $\Delta x \to 0$, $\Delta y \to 0$):

$$\frac{\partial R_{xz}}{\partial x} + \frac{\partial R_{yz}}{\partial y} + N_x \frac{\partial^2 w}{\partial x^2} + 2N_{xy}\frac{\partial^2 w}{\partial x \partial y} + N_y \frac{\partial^2 w}{\partial y^2} + p = 0 \Rightarrow \tag{4.39}$$

$$\frac{\partial^2 M_x}{\partial x^2} + 2\frac{\partial^2 M_{xy}}{\partial x \partial y} + \frac{\partial^2 M_y}{\partial y^2} + N_x \frac{\partial^2 w}{\partial x^2} + 2N_{xy}\frac{\partial^2 w}{\partial x \partial y} + N_y \frac{\partial^2 w}{\partial y^2} + p = 0 \tag{4.40}$$

4.5.6 Buckling equation for a symmetric laminate

Using that $B_{ij} = 0$ for a symmetric laminate, the buckling equation in terms of displacements can be obtained as:

$$\begin{aligned}
&-D_{11}\frac{\partial^4 w_0}{\partial x^4} - 4D_{16}\frac{\partial^4 w_0}{\partial x^3 \partial y} - 2(D_{12} + 2D_{66})\frac{\partial^4 w_0}{\partial x^2 \partial y^2} - 4D_{26}\frac{\partial^4 w_0}{\partial x \partial y^3} - D_{22}\frac{\partial^4 w_0}{\partial y^4} \\
&+ N_x \frac{\partial^2 w}{\partial x^2} + 2N_{xy}\frac{\partial^2 w}{\partial x \partial y} + N_y \frac{\partial^2 w}{\partial y^2} + p = 0
\end{aligned} \tag{4.41}$$

4.5.7 Buckling equation for a specially orthotropic laminate

As seen above, specially orthotropic laminates have apart from $B_{ij} = 0$ also the property that $D_{16} = D_{26} = 0$ which further reduces the buckling equation to:

$$\begin{aligned}
&-D_{11}\frac{\partial^4 w_0}{\partial x^4} - 2(D_{12} + 2D_{66})\frac{\partial^4 w_0}{\partial x^2 \partial y^2} - D_{22}\frac{\partial^4 w_0}{\partial y^4} \\
&+ N_x \frac{\partial^2 w}{\partial x^2} + 2N_{xy}\frac{\partial^2 w}{\partial x \partial y} + N_y \frac{\partial^2 w}{\partial y^2} + p = 0
\end{aligned} \tag{4.42}$$

By assuming the applied compressive loading according to $N_x = -N_{x0}$, $N_y = -N_{y0}$, $p = 0$ and $N_{xy} = 0$ one obtains:

$$D_{11}\frac{\partial^4 w_0}{\partial x^4} + 2(D_{12} + 2D_{66})\frac{\partial^4 w_0}{\partial x^2 \partial y^2} + D_{22}\frac{\partial^4 w_0}{\partial y^4} = -N_{x0}\frac{\partial^2 w}{\partial x^2} - N_{y0}\frac{\partial^2 w}{\partial y^2} \tag{4.43}$$

For the special case of simply supported specially orthotropic laminates we can again use Navier's solution. Hence, the deflection w_0 is once again given by:

$$w_0(x,y) = \sum_{m=1}^{\infty}\sum_{n=1}^{\infty} w_{mn} \sin\left(\frac{m\pi\, x}{a}\right) \sin\left(\frac{n\pi\, y}{b}\right) \Rightarrow$$

whereby the buckling equation can be rewritten as:

$$\begin{aligned}\sum_{m=1}^{\infty}\sum_{n=1}^{\infty} \pi^4 w_{mn} \left[D_{11}\left(\frac{m}{a}\right)^4 + 2(D_{12}+2D_{66})\left(\frac{mn}{ab}\right)^2 + D_{22}\left(\frac{n}{b}\right)^4\right] \sin\left(\frac{m\pi\, x}{a}\right) \sin\left(\frac{n\pi\, y}{b}\right) \\ = \sum_{m=1}^{\infty}\sum_{n=1}^{\infty} \pi^2 w_{mn} \left[N_{x0}\left(\frac{m}{a}\right)^2 + N_{y0}\left(\frac{n}{b}\right)^2\right] \sin\left(\frac{m\pi\, x}{a}\right) \sin\left(\frac{n\pi\, y}{b}\right)\end{aligned} \tag{4.44}$$

Finally, for non-trivial solutions $w_{mn} \neq 0$, we must have:

$$\pi^2 \left[D_{11}\left(\frac{m}{a}\right)^4 + 2(D_{12}+2D_{66})\left(\frac{mn}{ab}\right)^2 + D_{22}\left(\frac{n}{b}\right)^4\right] = \left[N_{x0}\left(\frac{m}{a}\right)^2 + N_{y0}\left(\frac{n}{b}\right)^2\right] \tag{4.45}$$

4.5.8 Example: Buckling under uniaxial compression

Let's consider the special case of a rectangular plate with side lengths a and b under uniaxial compression $N_{x0} = N_0$, $N_{y0} = 0$. We then obtain the following expression for the buckling load:

$$N_0(m,n) = \pi^2 \left[D_{11}\left(\frac{m}{a}\right)^2 + 2(D_{12}+2D_{66})\left(\frac{n}{b}\right)^2 + D_{22}\left(\frac{n}{b}\right)^4 \left(\frac{a}{m}\right)^2\right] \tag{4.46}$$

The critical buckling load is then the lowest value of N_0 for any combination of m and n which generally depends on the ratio a/b and the bending stiffness D_{ij}. Please note that m and n characterise the shape of the buckling modes in terms of half wavelengths in the x and y directions respectively. Thus, e.g. for a full sine-wave shape in x-direction we have $m = 2$.

In this particular case, the buckling load is obtained for $n = 1$. Furthermore, for a laminate with the properties $D_{11}/D_{22} = 10$ and $(D_{12} + 2D_{66})/D_{22} = 1$ this is reduced to:

$$N_0(m,1) = \frac{\pi^2 D_{22}}{b^2}\left[10m^2\left(\frac{b}{a}\right)^2 + 2 + \frac{1}{m^2}\left(\frac{a}{b}\right)^2\right] \tag{4.47}$$

or written on a non-dimensional form:

$$\overline{N} = \frac{N_0(m,1)b^2}{\pi^2 D_{22}} = \left[10m^2\left(\frac{b}{a}\right)^2 + 2 + \frac{1}{m^2}\left(\frac{a}{b}\right)^2\right] \tag{4.48}$$

cf. Figure 4.4. It can be seen that, depending on the geometry and lay-up sequence of the plate, the most critical load can be obtained also for $m > 1$. In addition, the corresponding buckling modes for the first three buckling modes are shown in Figure 4.5.

4.6 Free vibrations of a Kirchhoff-Love plate

4.6.1 Study Subsection 7.3.3 in the course book on your own

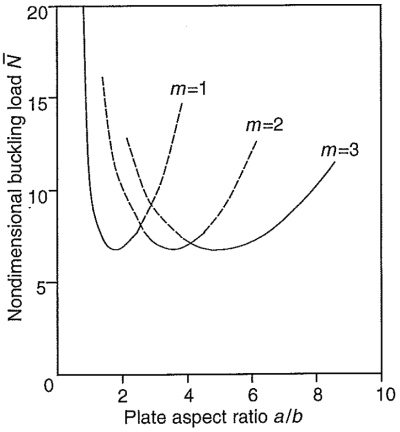

Figure 4.4: Non-dimensional buckling load $\overline{N} = (N_0[m,1]b^2)/(\pi^2 D_{22})$ for a rectangular laminate with properties $D_{11}/D_{22} = 10$ and $(D_{12} + 2D_{66})/D_{22} = 1$ subjected to uniaxial compression.

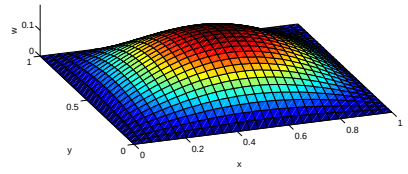

a)

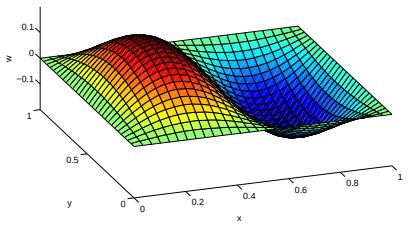

b)

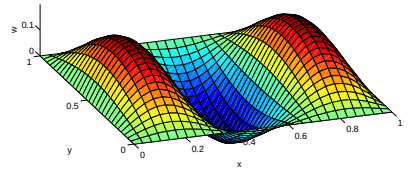

c)

Figure 4.5: Buckling modes for a quadratic laminate ($a = b$) subjected to uniaxial compression. The first three modes obtained for $n = 1$ and a) $m = 1$, b) $m = 2$ and c) $m = 3$.

Chapter 5

Mindlin - Reissner plate theory for anisotropic laminated plates

5.1 Extensions of the plate theory to account for out-of-plane shear: The Mindlin - Reissner theory

Experimental evidence exist in the literature that supports the Kirchhoff-Love plate theory, especially for thin plates with a high length-to-thickness ratio. Also numerical results where the plate is modelled as a 3D continuum (higher level of accuracy) agree well for thin plates. However, as the plate thickness increase in relation to other dimensions, experimental and 3D simulations generally show larger out-of-plane deflection than what is obtained by using Kirchhoff's plate theory. The discrepancy is largely dependent on the plate deformations induced by out-of-plane shear (which is neglected in Kirchhoff-Love plate theory). Thus, for moderately thick plates, the theory needs to take these shear strains into consideration.

5.2 First-order Mindlin-Reissner shear deformation theory

In order to account for the out-of-plane shear strains, the Kirchhoff-Love theory needs to be modified. This is done by relieving some of the restrictions imposed by the Kirchhoff-Love assumptions. Thus, we still assume that lines initially in the z-direction will remain straight after deformation **but they do no longer have to remain perpendicular to the midplane** (due to the shear strains).

5.2.1 Kinematics of the Mindlin-Reissner plate theory

To see how the assumptions influence the kinematics of the Mindlin-Reissner theory, we consider first the deformed plane in Figure 5.1. From this, we can conclude that the displacement in the direction of the x-axis of a point on the planar cross section can be written as:

$$u(x, y, z) = u_0(x, y) + z\phi_x(x, y) \tag{5.1}$$

where ϕ_x is the (positive) rotation around the y-axis $\neq \partial w/\partial x$. In the same way (if we would consider deformation in the yz-plane) one obtains the displacement in the y-direction as

$$v(x, y, z) = v_0(x, y) + z\phi_y(x, y) \tag{5.2}$$

with ϕ_y being the (negative!) rotation around the x-axis $\neq \partial w/\partial y$. Finally, the vertical displacement (in the z-direction) is as before given by

$$w(x, y, z) = w_0(x, y). \tag{5.3}$$

By definition, we obtain the strains as:

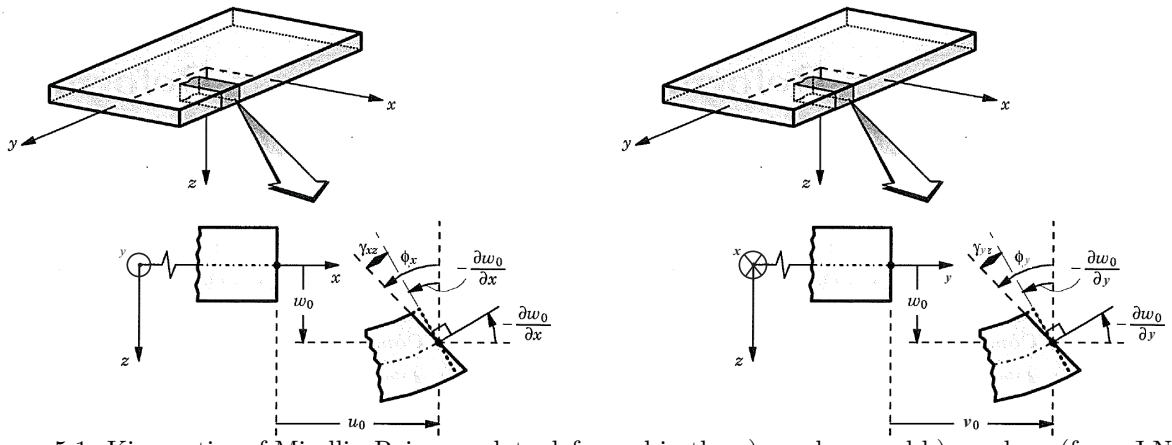

Figure 5.1: Kinematics of Mindlin-Reissner plate deformed in the a) xz plane and b) yz plane (from J.N. Reddy, *Theory and Analysis of Elastic Plates and Shells (2nd ed.)*, CRC Press, 2007).

$$\varepsilon_x = \frac{\partial u}{\partial x} = \frac{\partial u_0}{\partial x} + z\frac{\partial \phi_x}{\partial x} \tag{5.4}$$

$$\varepsilon_y = \frac{\partial v}{\partial y} = \frac{\partial v_0}{\partial y} + z\frac{\partial \phi_y}{\partial y} \tag{5.5}$$

$$\gamma_{xy} = \frac{\partial u}{\partial y} + \frac{\partial v}{\partial x} = \frac{\partial u_0}{\partial y} + \frac{\partial v_0}{\partial x} + z\left(\frac{\partial \phi_x}{\partial y} + \frac{\partial \phi_y}{\partial x}\right) \tag{5.6}$$

$$\gamma_{xz} = \frac{\partial u}{\partial z} + \frac{\partial w}{\partial x} = \phi_x + \frac{\partial w_0}{\partial x} \tag{5.7}$$

$$\gamma_{yz} = \frac{\partial v}{\partial z} + \frac{\partial w}{\partial y} = \phi_y + \frac{\partial w_0}{\partial y} \tag{5.8}$$

or

$$\{\varepsilon\} = \{\varepsilon^0\} + z\{\mathbf{k}\}_{Mindlin} \tag{5.9}$$

$$\{\boldsymbol{\gamma}_z\} = \left\{ \begin{array}{c} \phi_x + \dfrac{\partial w_0}{\partial x} \\ \phi_y + \dfrac{\partial w_0}{\partial y} \end{array} \right\} \tag{5.10}$$

with

$$\{\varepsilon^0\} = \left\{ \begin{array}{c} \dfrac{\partial u_0}{\partial x} \\ \dfrac{\partial v_0}{\partial y} \\ \dfrac{\partial u_0}{\partial y} + \dfrac{\partial v_0}{\partial x} \end{array} \right\}, \; \{\mathbf{k}\}_{Mindlin} = \left\{ \begin{array}{c} \dfrac{\partial \phi_x}{\partial x} \\ \dfrac{\partial \phi_y}{\partial y} \\ \dfrac{\partial \phi_x}{\partial y} + \dfrac{\partial \phi_y}{\partial x} \end{array} \right\} \tag{5.11}$$

As can be observed, the definition of the curvature is extended from the Kirchoff theory to the Mindlin-Reissner theory. However, it is clear that if we would neglect the shear strains, we would obtain the relation between the rotation angle and the derivative of the out-of-plane displacement w_0 as in the Kirchhoff-Love theory yielding the same curvature.

5.2.2 Transverse shear forces and stresses

Please note that the shear strains in the Mindlin-Reissner theory are assumed constant through the thickness which implies that constant shear stresses are predicted within each lamina k through

$$\left\{ \begin{array}{c} \tau_{yz} \\ \tau_{xz} \end{array} \right\} = \left[\begin{array}{cc} \overline{Q}_{44} & \overline{Q}_{45} \\ \overline{Q}_{45} & \overline{Q}_{55} \end{array} \right]_k \left\{ \begin{array}{c} \gamma_{yz} \\ \gamma_{xz} \end{array} \right\} \tag{5.12}$$

or equivalently

$$\left\{ \begin{array}{c} \tau_{xz} \\ \tau_{yz} \end{array} \right\} = \left[\begin{array}{cc} \overline{Q}_{55} & \overline{Q}_{45} \\ \overline{Q}_{45} & \overline{Q}_{44} \end{array} \right]_k \left\{ \begin{array}{c} \gamma_{xz} \\ \gamma_{yz} \end{array} \right\}. \tag{5.13}$$

Please note that in the last step, the order of the of the shear stresses and strains were reversed for reasons that will be more clear below (cf. the contracted notation of the equilibium equations, the weak formulation and in later sections also the FE formulation). Please note that this also means that elements of the stiffness matrix needs to change place, cf. Eq (5.13).

In order to obtain $\overline{Q}_{44}$, $\overline{Q}_{45}$ and $\overline{Q}_{55}$ we need to consider the coordinate transformation of the out-of-plane shear stresses and strains due to a fibre orientation $+\theta^\circ$ around the positive z-axis. For this case, the out-of-plane axis for the global coordinate system (the z-axis) and the out-of-plane axis for the fibre oriented local coordinate system (the so-called $T^{'}$-axis) coincide, whereby the relation between transverse stresses may be derived from either a standard change of basis or from equilibrium of forces in the vertical direction as:

$$\left\{ \begin{array}{c} \tau_{TT'} \\ \tau_{LT'} \end{array} \right\} = \underbrace{\left[\begin{array}{cc} \cos\theta & -\sin\theta \\ \sin\theta & \cos\theta \end{array} \right]}_{[\tilde{T}_1]} \left\{ \begin{array}{c} \tau_{yz} \\ \tau_{xz} \end{array} \right\}. \tag{5.14}$$

As a consequece, we can obtain $\overline{Q}_{44}$, $\overline{Q}_{45}$ and $\overline{Q}_{55}$, knowing that the shear strains $\boldsymbol{\gamma}_z$ transform in the same way

$$\left\{ \begin{array}{c} \gamma_{TT'} \\ \gamma_{LT'} \end{array} \right\} = \underbrace{\left[\begin{array}{cc} \cos\theta & -\sin\theta \\ \sin\theta & \cos\theta \end{array} \right]}_{[\tilde{T}_1]} \left\{ \begin{array}{c} \gamma_{yz} \\ \gamma_{xz} \end{array} \right\}, \tag{5.15}$$

as

$$\left[\begin{array}{cc} \overline{Q}_{44} & \overline{Q}_{45} \\ \overline{Q}_{45} & \overline{Q}_{55} \end{array} \right]_k = [\tilde{T}_1]_k^{-1} \left[\begin{array}{cc} Q_{44} & Q_{45} \\ Q_{45} & Q_{55} \end{array} \right] [\tilde{T}_1]_k \tag{5.16}$$

where

$$\left\{ \begin{array}{c} \tau_{TT'} \\ \tau_{LT'} \end{array} \right\} = \left[\begin{array}{cc} Q_{44} & Q_{45} \\ Q_{45} & Q_{55} \end{array} \right] \left\{ \begin{array}{c} \gamma_{TT'} \\ \gamma_{LT'} \end{array} \right\} \tag{5.17}$$

with

$$\left[\begin{array}{cc} Q_{44} & Q_{45} \\ Q_{45} & Q_{55} \end{array} \right] = \left[\begin{array}{cc} G_{TT'} & 0 \\ 0 & G_{LT'} \end{array} \right] = \left[\begin{array}{cc} G_{TT'} & 0 \\ 0 & G_{LT'} \end{array} \right]_k, \; G_{LT'} = G_{LT} \text{ (the } TT^{'} \text{ plane is a plane of isotropy)} \tag{5.18}$$

and where we need either experimental data or a model to predict $G_{TT'}$.

Micromechanical models to predict $G_{TT'}$ generally are rather complicated and thereby out of scope in this course[1]. However, interested readers are referred to *e.g.* the book by Christensen (*Mechanics of Composite Materials*, Krieger Publishing company, 1979). It should be known that $G_{TT'}$ depends on fibre volume fraction and the shear properties of the two constituents (fibre and matrix material) and is generally somewhat lower than the in-plane shear modulus G_{LT}, cf. also Figure 5.2 in which predictions of $G_{TT'}$ (denoted G_{23} in the figure) from a model developed at Swerea SICOMP denoted CCA (equivalent to the Christensen model for a pure fibre-matrix material) is compared to the derived upper and lower bounds by Hashin and the prediction of the in-plane shear modulus G_{LT} using the Halpin-Tsai equations with $\xi = 1$. Since the $TT^{'}$ plane is a plane of isotropy, we know for a fact that:

$$G_{TT'} = \frac{E_T}{2\left(1 + \nu_{TT'}\right).} \tag{5.19}$$

As a rule of thumb for carbon fibre/epoxy composites, $\nu_{TT'}$ normally lies in the interval 0.4-0.45.

[1] As an alternative, FEM can also be used to predict the transverse shear modulus based on an analysis of a representative volume element

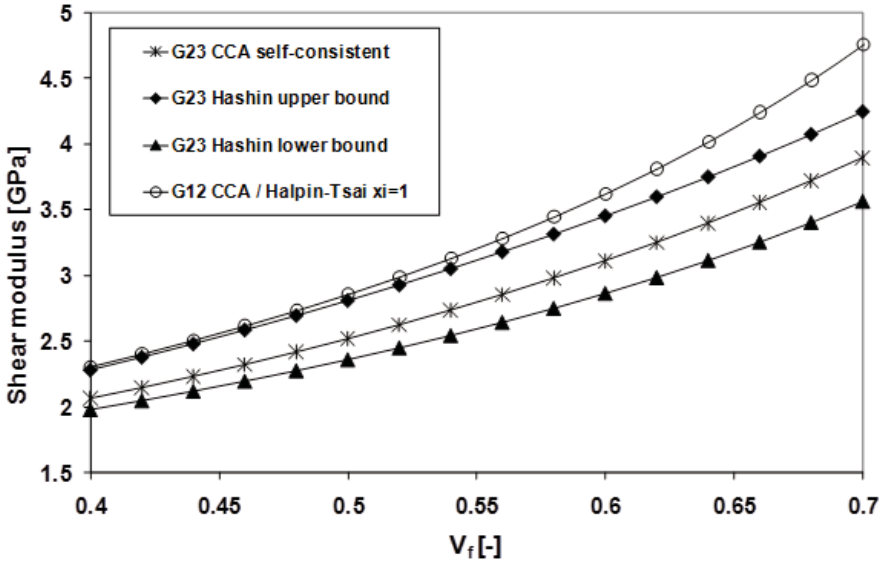

Figure 5.2: Predicted values (obtained by Erik Marklund, Swerea SICOMP) for the transverse shear modulus $G_{TT'} = G_{23}$ of a carbon fibre/epoxy composite based on the self-consistent model developed at Swerea SICOMP (for this case equivalent to the model by Christensen, *Mechanics of Composite Materials*, Krieger Publishing company, 1979) compared to the upper and lower bounds derived by Hashin and predictions of the in-plane shear modulus $G_{LT} = G_{12}$ by the Halpin-Tsai equations with $\xi = 1$. Parameters used in the predictions are: $E_m = 3$ GPa, $\nu_m = 0.38$, $E_{fL} = 230$ GPa, $E_{fT} = 23$ GPa, $G_{fLT} = 20$ GPa and $\nu_{fLT} = \nu_{fTT'} = 0.2$

5.2.2.1 The shear forces and the shear correction factor

Please note that the representation of shear stress through the thickness in unphysical in the sense that traction continuity no longer is preserved. This is generally accounted for in the laminate analysis by introducing a shear correction factor K such that the resulting out-of-plane shear forces are obtained as:

$$\left\{ \begin{array}{c} R_{xz} \\ R_{yz} \end{array} \right\} = K \underbrace{\int_{-h/2}^{h/2} \left[\begin{array}{cc} \overline{Q}_{55} & \overline{Q}_{45} \\ \overline{Q}_{45} & \overline{Q}_{44} \end{array} \right] dz}_{\left[\begin{array}{cc} A_{55} & A_{45} \\ A_{45} & A_{44} \end{array} \right]} \left\{ \begin{array}{c} \gamma_{xz} \\ \gamma_{yz} \end{array} \right\}. \tag{5.20}$$

Please note the slight modification compared to the course book in which the shear correction factor is included in the A_{ij} components!

By considering a homogeneous specially orthotropic plate and enforcing the condition that the work done by the external forces R_{xz} and R_{yz}

$$\frac{1}{2} \int_{A_{plate}} R_{xz}\gamma_{xz} + R_{yz}\gamma_{yz} dA = ... = \frac{1}{2K} \int_{A_{plate}} \frac{R_{xz}^2}{A_{55}} + \frac{R_{yz}^2}{A_{44}} dA \tag{5.21}$$

equals the internal strain energy produced by the shear stresses and strains

$$\frac{1}{2} \int_{-h/2}^{h/2} \int_{A_{plate}} \tau_{xz}\gamma_{xz} + \tau_{yz}\gamma_{yz} \, dA \, dz = ... = \frac{3}{5} \int_{A_{plate}} \frac{R_{xz}^2}{A_{55}} + \frac{R_{yz}^2}{A_{44}} dA \tag{5.22}$$

the shear correction factor gets the value $K = 5/6$. It should be noted that even thought the value of $5/6$ for K is derived only for a homogeneous orthotropic plate it generally provides good approximations also for other types of laminates (except for sandwich structures with a thick middle layer for which $K \to 1$).

5.3 Governing equations for the Mindlin-Reissner theory

The governing plate equations (forces and moments) for the Mindlin-Reissner theory are the same as for Kirchhoff-Love plate theory. But, since there are now five unknowns (u_0, v_0, w_0, ϕ_x and ϕ_y) the vertical equilibrium equation cannot be combined with the two moment equations. Thus, the governing equations for the Mindlin-Reissner (or first-order shear deformation) theory are:

$$\frac{\partial N_x}{\partial x} + \frac{\partial N_{xy}}{\partial y} = 0 \tag{5.23}$$

$$\frac{\partial N_{xy}}{\partial x} + \frac{\partial N_y}{\partial y} = 0 \tag{5.24}$$

$$\frac{\partial R_{xz}}{\partial x} + \frac{\partial R_{yz}}{\partial y} = -p \tag{5.25}$$

$$\frac{\partial M_x}{\partial x} + \frac{\partial M_{xy}}{\partial y} = R_{xz} \tag{5.26}$$

$$\frac{\partial M_{xy}}{\partial x} + \frac{\partial M_y}{\partial y} = R_{yz} \tag{5.27}$$

or on a contracted form:

$$\tilde{\boldsymbol{\nabla}}^T \mathbf{N} = \mathbf{0} \tag{5.28}$$

$$\boldsymbol{\nabla}^T \mathbf{R}_z = -p \tag{5.29}$$

$$\tilde{\boldsymbol{\nabla}}^T \mathbf{M} = \mathbf{R}_z \tag{5.30}$$

with

$$\mathbf{N} = \begin{Bmatrix} N_x \\ N_y \\ N_{xy} \end{Bmatrix}, \ \mathbf{R}_z = \begin{Bmatrix} R_{xz} \\ R_{yz} \end{Bmatrix}, \ \mathbf{M} = \begin{Bmatrix} M_x \\ M_y \\ M_{xy} \end{Bmatrix} \boldsymbol{\nabla} = \begin{Bmatrix} \frac{\partial}{\partial x} \\ \frac{\partial}{\partial y} \end{Bmatrix}, \ \tilde{\boldsymbol{\nabla}} = \begin{Bmatrix} \frac{\partial}{\partial x} & 0 \\ 0 & \frac{\partial}{\partial y} \\ \frac{\partial}{\partial y} & \frac{\partial}{\partial x} \end{Bmatrix} \tag{5.31}$$

5.4 Equilibrium equations in terms of displacements and rotations for the Mindlin-Reissner theory

Given the definition of strains and stress resultants, we obtain their inter-relationship as:

$$\mathbf{N} = [\mathbf{A}]\left\{\boldsymbol{\varepsilon}^0\right\} + [\mathbf{B}]\left\{\mathbf{k}\right\} = [\mathbf{A}]\tilde{\boldsymbol{\nabla}}\mathbf{u} + [\mathbf{B}]\tilde{\boldsymbol{\nabla}}\boldsymbol{\phi} \tag{5.32}$$

$$\mathbf{R}_z = K[\tilde{\mathbf{A}}]\left\{\boldsymbol{\gamma}_z\right\} = K[\tilde{\mathbf{A}}]\left(\boldsymbol{\phi} + \boldsymbol{\nabla} w_0\right) \tag{5.33}$$

$$\mathbf{M} = [\mathbf{B}]\left\{\boldsymbol{\varepsilon}^0\right\} + [\mathbf{D}]\left\{\mathbf{k}\right\} = [\mathbf{B}]\tilde{\boldsymbol{\nabla}}\mathbf{u} + [\mathbf{D}]\tilde{\boldsymbol{\nabla}}\boldsymbol{\phi} \tag{5.34}$$

with $\mathbf{N}$, $\mathbf{M}$, $\mathbf{A}$, $\mathbf{B}$ and $\mathbf{D}$ as before and

$$\tilde{\mathbf{A}} = \begin{bmatrix} A_{55} & A_{45} \\ A_{45} & A_{44} \end{bmatrix}, \ \mathbf{R}_z = \begin{Bmatrix} R_{xz} \\ R_{yz} \end{Bmatrix}, \ \mathbf{u} = \begin{Bmatrix} u_0 \\ v_0 \end{Bmatrix}, \ \boldsymbol{\phi} = \begin{Bmatrix} \phi_x \\ \phi_y \end{Bmatrix} \tag{5.35}$$

By insertion of Eqs. (5.32)-(5.35) into the governing equations, Eqs. (5.23)-(5.27), one obtains the equilibrium equations in terms of the displacement and rotation fields. However, this yields rather lengthy expressions that can be solved only for simple anisotropic conditions and boundary conditions (in analogy with Navier's solution for the Kirchhoff-Love plate). Instead, to allow for the solution of more general problems by FEM, we derive the weak (or variational) formulation of Eqs. (5.23)-(5.27).

5.5 Weak form of equilibrium for the Mindlin-Reissner theory

It is first noted that in order to obtain the weak form of the governing equations, each equation is multiplied by an arbitrary test functions ($\delta\mathbf{u} = \{\delta u \quad \delta v\}^T$, δw and $\delta\boldsymbol{\phi} = \{\delta\phi_x \quad \delta\phi_y\}^T$) (often also denoted virtual displacements) and integrated over the domain Ω. We treat the in-plane equations, the vertical equation and the moment equations separately to obtain:

$$\int_\Omega \delta\mathbf{u}^T \left(\tilde{\boldsymbol{\nabla}}^T \mathbf{N}\right) d\Omega = \int_\Gamma \delta\mathbf{u}^T \mathbf{P}\, d\Gamma - \int_\Omega \left(\tilde{\boldsymbol{\nabla}}\delta\mathbf{u}\right)^T \mathbf{N}\, d\Omega = \mathbf{0} \tag{5.36}$$

$$\int_\Omega \delta w \left(\boldsymbol{\nabla}^T \mathbf{R}_z\right) d\Omega = \int_\Gamma \delta w R_n\, d\Gamma - \int_\Omega \left(\boldsymbol{\nabla}\delta w\right)^T \mathbf{R}_z\, d\Omega = -\int_\Omega \delta w p\, d\Omega \tag{5.37}$$

$$\int_\Omega \delta\boldsymbol{\phi}^T \left(\tilde{\boldsymbol{\nabla}}^T \mathbf{M}\right) d\Omega = \int_\Gamma \delta\boldsymbol{\phi}^T \mathbf{M}_n\, d\Gamma - \int_\Omega \left(\tilde{\boldsymbol{\nabla}}\delta\boldsymbol{\phi}\right)^T \mathbf{M}\, d\Omega = \int_\Omega \delta\boldsymbol{\phi}^T \mathbf{R}_z\, d\Omega \tag{5.38}$$

where $\mathbf{P} = \{P_x \quad P_y\}^T$ is the external in-plane force (per unit length) acting on Γ, R_n is the external out-of-plane force (per unit length) and $\mathbf{M}_n = \{M_{nx} \quad M_{ny}\}^T$ is the external moment (per unit length).

Please note that $\mathbf{P}$ can be expressed in terms of the in-plane normal $\mathbf{n}$ and tangent $\mathbf{m}$ vectors as

$$\mathbf{P} = P_n\mathbf{n} + P_{nm}\mathbf{m},\ P_n = \int_{-h/2}^{h/2} \sigma_n\, dz,\ P_{nm} = \int_{-h/2}^{h/2} \tau_{nm}\, dz \tag{5.39}$$

where σ_n is the in-plane normal stress acting on the surface Γ and τ_{nm} is the corresponding in-plane shear stress (acting on Γ). In the same way, we have

$$R_n = \int_{-h/2}^{h/2} \tau_{nz}\, dz \tag{5.40}$$

$$\mathbf{M}_n = M_{nn}\mathbf{n} + M_{nm}\mathbf{m},\ M_{nn} = \int_{-h/2}^{h/2} \sigma_{nn} z\, dz,\ M_{nm} = \int_{-h/2}^{h/2} \tau_{nm} z\, dz \tag{5.41}$$

where τ_{nz} is the out-of-plane shear stress acting on Γ in the z-direction.

Please note that the weak formulation of the problem does not depend on if the plate is isotropic (also derived in the course *Finite Element Method - Structures*) or anisotropic since only stress resultants and displacements are involved. Please also note that there are a number of steps to be taken in order to arrive at the weak form of the governing equations (i.e. to derive Eqs. (5.36)-(5.38)) but that the steps are very similar for the three equations whereby we focus only on the first equation below.

5.5.1 Derivation of Eq. (5.36)

To derive Eq. (5.36), we follow the steps for 2D elasticity derived e.g. in the Chalmers courses *MHA021 - Finit elementmetod (FEM)* and *VSM167 - Finite element method - basics*, both given by the Department of Applied Mechanics. The procedure is also very nicely described (for 3D elasticity) in the book by Ottosen and Petersson (*Introduction to the Finite Element Method*, Prentice Hall, 1992.).

As a first step, Eqs. (5.23) and (5.24) are multiplied by arbitrary test functions u and v respectively which yields the following two equations:

$$\int_\Omega \delta u \left(\frac{\partial N_x}{\partial x} + \frac{\partial N_{xy}}{\partial y}\right) d\Omega = \int_\Omega \left(\frac{\partial}{\partial x}\left(\delta u N_x\right) + \frac{\partial}{\partial y}\left(\delta u N_{xy}\right)\right) d\Omega - \int_\Omega \left(\frac{\partial \delta u}{\partial x} N_x + \frac{\partial \delta u}{\partial y} N_{xy}\right) d\Omega = 0$$

$$\int_\Omega \delta v \left(\frac{\partial N_{xy}}{\partial x} + \frac{\partial N_y}{\partial y}\right) d\Omega = \int_\Omega \left(\frac{\partial}{\partial x}\left(\delta v N_{xy}\right) + \frac{\partial}{\partial y}\left(\delta v N_y\right)\right) d\Omega - \int_\Omega \left(\frac{\partial \delta v}{\partial x} N_{xy} + \frac{\partial \delta v}{\partial y} N_y\right) d\Omega = 0$$

Please also note that this corresponds to the multiplication of Eq. (5.28) with $\delta\mathbf{u} = \{\delta u \quad 0\}^T$ and $\delta\mathbf{u} = \{0 \quad \delta v\}^T$ respectively.

Utilising that

$$\int_\Omega \frac{\partial \psi}{\partial x}\, d\Omega = \int_\Gamma \psi n_x\, d\Gamma \tag{5.42}$$

$$\int_\Omega \frac{\partial \psi}{\partial y}\, d\Omega = \int_\Gamma \psi n_y\, d\Gamma \tag{5.43}$$

– where $n = \{n_x \;\; n_y\}^T$ is the in-plane normal of the boundary Γ of Ω – the expressions may be rewritten as

$$\int_\Gamma \delta u \left(N_x n_x + N_{xy} n_y\right)\, d\Gamma = \int_\Omega \left(\frac{\partial \delta u}{\partial x} N_x + \frac{\partial \delta u}{\partial y} N_{xy}\right)\, d\Omega \tag{5.44}$$

$$\int_\Gamma \delta v \left(N_{xy} n_x + N_y n_y\right)\, d\Gamma = \int_\Omega \left(\frac{\partial \delta v}{\partial x} N_{xy} + \frac{\partial \delta v}{\partial y} N_y\right)\, d\Omega \tag{5.45}$$

Taking the sum of Eqs. (5.44) and (5.45) yields

$$\int_\Gamma \left(\delta u \underbrace{\left(N_x n_x + N_{xy} n_y\right)}_{P_x} + \delta v \underbrace{\left(N_{xy} n_x + N_y n_y\right)}_{P_y} \right)\, d\Gamma = \int_\Omega \left(\frac{\partial \delta u}{\partial x} N_x + \frac{\partial \delta u}{\partial y} N_{xy} + \frac{\partial \delta v}{\partial x} N_{xy} + \frac{\partial \delta v}{\partial y} N_y\right)\, d\Omega$$

or equivalently

$$\int_\Gamma \delta \mathbf{u}^T \mathbf{P}\, d\Gamma = \int_\Omega \left(\tilde{\boldsymbol{\nabla}} \delta \mathbf{u}\right)^T \mathbf{N}\, d\Omega \tag{5.46}$$

By taking the sum of Eqs. (5.44) and (5.45), it appears as if we reduced the number of in-plane equations from two to one. However, as indicated in the beginning of this subsection, $\delta\mathbf{u}$ is arbitrary and by using both $\delta\mathbf{u} = \{\delta u \;\; 0\}^T$ and $\delta\mathbf{u} = \{0 \;\; \delta v\}^T$ we retain the two governing equations we started with. In fact, we can use any two arbitrary combinations of $\delta\mathbf{u}$ as long as they satisfy the condition $\delta\mathbf{u}_1^T \delta\mathbf{u}_2 = 0$ (vector multiplication).

In order to see

$$P_x = N_x n_x + N_{xy} n_y,\; P_y = N_{xy} n_x + N_y n_y$$

we utilise that $\mathbf{P}$ is the projection of the stress in the normal direction of the surface integrated over the thickness, i.e. in 2D we have

$$\mathbf{P} = \left\{ \begin{array}{c} P_x \\ P_y \end{array} \right\} = \int_{-h/2}^{h/2} \left[\begin{array}{cc} \sigma_x & \tau_{xy} \\ \tau_{xy} & \sigma_y \end{array} \right] \left\{ \begin{array}{c} n_x \\ n_y \end{array} \right\} dz = \int_{-h/2}^{h/2} \left\{ \begin{array}{c} \sigma_x n_x + \tau_{xy} n_y \\ \tau_{xy} n_x + \sigma_y n_y \end{array} \right\} dz = \left\{ \begin{array}{c} N_x n_x + N_{xy} n_y \\ N_{xy} n_x + N_y n_y \end{array} \right\}$$

5.5.2 Boundary conditions

By examining the surface integral (boundary terms) of Eqs. (5.36)-(5.38), we conclude that there are three pairs of boundary conditions:

5.5.2.1 Boundary conditions for the in-plane force equilibrium

The boundary term is

$$\int_\Gamma \delta \mathbf{u}^T \mathbf{P}\, d\Gamma \tag{5.47}$$

whereby we can conclude that we can subdivide the boundary Γ into two parts:

- $\Gamma_{D,u}$ on which the in-plane displacements are prescribed: ($\mathbf{u} = \{u_0 \;\; v_0\}^T = \{\overline{u}_0 \;\; \overline{v}_0\}^T = \overline{\mathbf{u}}$) where $\overline{u}_0$ and $\overline{v}_0$ are the prescribed displacement components in x- and y-direction respectively. Furthermore, for this part of the boundary, the corresponding test functions are set to zero.
- $\Gamma_{N,u}$ on which the external in-plane forces are prescribed: ($\mathbf{P} = \{P_x \;\; P_y\}^T = \{\overline{P}_x \;\; \overline{P}_y\}^T = \overline{\mathbf{P}}$) where $\overline{P}_x$ and $\overline{P}_y$ are the prescribed force components (per unit length) in the x- and y-direction respectively, acting on $\Gamma_{N,u}$.

Hence, the boundary term reduces to

$$\int_{\Gamma} \delta \mathbf{u}^T \mathbf{P} \, d\Gamma = \int_{\Gamma_{N,u}} \delta \mathbf{u}^T \overline{\mathbf{P}} \, d\Gamma \tag{5.48}$$

5.5.2.2 Boundary conditions for the out-of-plane force equilibrium

The boundary term is

$$\int_{\Gamma} \delta w R_n \, d\Gamma \tag{5.49}$$

whereby we can conclude that we can subdivide the boundary Γ into two parts:

- $\Gamma_{D,w}$ on which the out-of-plane displacements are prescribed: $(w = w_0 = \overline{w}_0)$ where $\overline{w}_0$ is the prescribed displacement component in z-direction. In analogy to the in-plane force balance equation, for this part of the boundary, the corresponding test functions is set to zero.

- $\Gamma_{N,w}$ on which the external out-of-plane force is prescribed: $(R_n = \overline{R}_n)$ where $\overline{R}_n$ is the prescribed vertical force (per unit length) in the z-direction acting on $\Gamma_{N,w}$.

Hence, the boundary term reduces to

$$\int_{\Gamma} \delta w R_n \, d\Gamma = \int_{\Gamma_{N,w}} \delta w \overline{R}_n \, d\Gamma \tag{5.50}$$

5.5.2.3 Boundary conditions for the moment equilibrium

The boundary term is

$$\int_{\Gamma} \delta \boldsymbol{\phi}^T \mathbf{M}_n \, d\Gamma \tag{5.51}$$

whereby we can conclude that we can subdivide the boundary Γ into two parts:

- $\Gamma_{D,\phi}$ on which the rotations are prescribed: $(\phi = \{\phi_x \;\; \phi_y\}^T = \{\overline{\phi}_x \;\; \overline{\phi}_y\}^T = \overline{\boldsymbol{\phi}})$ where $\overline{\phi}_x$ and $\overline{\phi}_y$ are the prescribed rotation components. As before, for this part of the boundary, the test functions are set to zero.

- $\Gamma_{N,\phi}$ on which the external moments are prescribed: $(\mathbf{M}_n = \{M_{nx} \;\; M_{ny}\}^T = \{\overline{M}_{nx} \;\; \overline{M}_{ny}\}^T = \overline{\mathbf{M}}_n)$ where $\overline{M}_{nx}$ and $\overline{M}_{ny}$ are the prescribed moment components (per unit length) acting on $\Gamma_{N,\phi}$.

Hence, the boundary term reduces to

$$\int_{\Gamma} \delta \boldsymbol{\phi}^T \mathbf{M}_n \, d\Gamma = \int_{\Gamma_{N,\phi}} \delta \boldsymbol{\phi}^T \overline{\mathbf{M}}_n \, d\Gamma \tag{5.52}$$

5.5.3 Final weak form

Rewriting the boundary terms and using the kinematical relations one obtains the weak form as:

Find $\mathbf{u} = \{u_0 \;\; v_0\}^T \in \mathbf{V}_u$, $w \in \mathbf{V}_w$ and $\boldsymbol{\phi} = \{\phi_x \;\; \phi_y\}^T \in \mathbf{V}_\phi$ where

$$\begin{aligned} \mathbf{V}_u &= \{\text{sufficiently regular}; \mathbf{u} = \overline{\mathbf{u}} \text{ on } \Gamma_{D,u}\} \\ \mathbf{V}_w &= \{\text{sufficiently regular}; w = \overline{w} \text{ on } \Gamma_{D,w}\} \\ \mathbf{V}_\phi &= \{\text{sufficiently regular}; \boldsymbol{\phi} = \overline{\boldsymbol{\phi}} \text{ on } \Gamma_{D,\phi}\} \end{aligned}$$

such that:

$$\begin{aligned} &\int_\Omega \left(\tilde{\boldsymbol{\nabla}}\delta\mathbf{u}\right)^T \left([\mathbf{A}]\tilde{\boldsymbol{\nabla}}\mathbf{u} + [\mathbf{B}]\tilde{\boldsymbol{\nabla}}\boldsymbol{\phi}\right) d\Omega = \int_{\Gamma_{N,u}} \delta\mathbf{u}^T \overline{\mathbf{P}}\, d\Gamma, \;\; \forall \delta\mathbf{u} \in \mathbf{V}_{\delta u} \\ &\int_\Omega K \left(\boldsymbol{\nabla}\delta w\right)^T [\tilde{\mathbf{A}}] \left(\boldsymbol{\phi} + \boldsymbol{\nabla} w\right) d\Omega = \int_\Omega \delta w p \, d\Omega + \int_{\Gamma_{N,w}} \delta w \overline{R}_n \, d\Gamma, \;\; \forall \delta w \in \mathbf{V}_{\delta w} \\ &\int_\Omega \left(\tilde{\boldsymbol{\nabla}}\delta\boldsymbol{\phi}\right)^T \left([\mathbf{B}]\tilde{\boldsymbol{\nabla}}\mathbf{u} + [\mathbf{D}]\tilde{\boldsymbol{\nabla}}\boldsymbol{\phi}\right) d\Omega + \int_\Omega \delta\boldsymbol{\phi}^T K [\tilde{\mathbf{A}}] \left(\boldsymbol{\phi} + \boldsymbol{\nabla} w\right) d\Omega = \int_{\Gamma_{N,\phi}} \delta\boldsymbol{\phi}^T \mathbf{M}_n \, d\Gamma, \;\; \forall \delta\boldsymbol{\phi} \in \mathbf{V}_{\delta\phi} \\ &\mathbf{u} = \overline{\mathbf{u}} \text{ on } \Gamma_{D,u} \\ &w = \overline{w} \text{ on } \Gamma_{D,w} \\ &\boldsymbol{\phi} = \overline{\boldsymbol{\phi}} \text{ on } \Gamma_{D,\phi} \end{aligned} \tag{5.53}$$

where

$$\begin{aligned} \mathbf{V}_{\delta u} &= \{\text{sufficiently regular}; \delta\mathbf{u} = \mathbf{0} \text{ on } \Gamma_{D,u}\} \\ \mathbf{V}_{\delta w} &= \{\text{sufficiently regular}; \delta w = 0 \text{ on } \Gamma_{D,w}\} \\ \mathbf{V}_{\delta\phi} &= \{\text{sufficiently regular}; \delta\boldsymbol{\phi} = \mathbf{0} \text{ on } \Gamma_{D,\phi}\} \end{aligned}$$

which is the starting point for the FE formulation of the problem.

Chapter 6

FEM formulation of laminated composite plates

6.1 Preliminaries

The point of departure is the weak (or variational formulation) of the governing equations for the Mindlin plate as:

Find $\mathbf{u} = \{u_0 \;\; v_0\}^T \in \mathbf{V}_u$, $w \in \mathbf{V}_w$ and $\boldsymbol{\phi} = \{\phi_x \;\; \phi_y\}^T \in \mathbf{V}_\phi$ where

$$\begin{aligned} \mathbf{V}_u &= \{\text{sufficiently regular}; \mathbf{u} = \overline{\mathbf{u}} \text{ on } \Gamma_{D,u}\} \\ \mathbf{V}_w &= \{\text{sufficiently regular}; w = \overline{w} \text{ on } \Gamma_{D,w}\} \\ \mathbf{V}_\phi &= \{\text{sufficiently regular}; \boldsymbol{\phi} = \overline{\boldsymbol{\phi}} \text{ on } \Gamma_{D,\phi}\} \end{aligned}$$

such that:

$$\begin{aligned} &\int_\Omega \left(\tilde{\boldsymbol{\nabla}}\delta\mathbf{u}\right)^T \left([\mathbf{A}]\tilde{\boldsymbol{\nabla}}\mathbf{u} + [\mathbf{B}]\tilde{\boldsymbol{\nabla}}\boldsymbol{\phi}\right) d\Omega = \int_{\Gamma_{N,u}} \delta\mathbf{u}^T \overline{\mathbf{P}}\, d\Gamma, \;\; \forall \delta\mathbf{u} \in \mathbf{V}_{\delta u} \\ &\int_\Omega K \left(\boldsymbol{\nabla}\delta w\right)^T [\tilde{\mathbf{A}}] \left(\boldsymbol{\phi} + \boldsymbol{\nabla} w\right) d\Omega = \int_\Omega \delta w p \, d\Omega + \int_{\Gamma_{N,w}} \delta w \overline{R}_n \, d\Gamma, \;\; \forall \delta w \in \mathbf{V}_{\delta w} \\ &\int_\Omega \left(\tilde{\boldsymbol{\nabla}}\delta\boldsymbol{\phi}\right)^T \left([\mathbf{B}]\tilde{\boldsymbol{\nabla}}\mathbf{u} + [\mathbf{D}]\tilde{\boldsymbol{\nabla}}\boldsymbol{\phi}\right) d\Omega + \int_\Omega \delta\boldsymbol{\phi}^T K [\tilde{\mathbf{A}}] \left(\boldsymbol{\phi} + \boldsymbol{\nabla} w\right) d\Omega = \int_{\Gamma_{N,\phi}} \delta\boldsymbol{\phi}^T \overline{\mathbf{M}}_n \, d\Gamma, \;\; \forall \delta\boldsymbol{\phi} \in \mathbf{V}_{\delta\phi} \\ &\mathbf{u} = \overline{\mathbf{u}} \text{ on } \Gamma_{D,u} \\ &w = \overline{w} \text{ on } \Gamma_{D,w} \\ &\boldsymbol{\phi} = \overline{\boldsymbol{\phi}} \text{ on } \Gamma_{D,\phi} \end{aligned}$$

where

$$\begin{aligned} \mathbf{V}_{\delta u} &= \{\text{sufficiently regular}; \delta\mathbf{u} = \mathbf{0} \text{ on } \Gamma_{D,u}\} \\ \mathbf{V}_{\delta w} &= \{\text{sufficiently regular}; \delta w = 0 \text{ on } \Gamma_{D,w}\} \\ \mathbf{V}_{\delta\phi} &= \{\text{sufficiently regular}; \delta\boldsymbol{\phi} = \mathbf{0} \text{ on } \Gamma_{D,\phi}\} \end{aligned}$$

and where we recall that

$$\boldsymbol{\nabla} = \begin{bmatrix} \dfrac{\partial}{\partial x} \\ \dfrac{\partial}{\partial y} \end{bmatrix}, \; \tilde{\boldsymbol{\nabla}} = \begin{bmatrix} \dfrac{\partial}{\partial x} & 0 \\ 0 & \dfrac{\partial}{\partial y} \\ \dfrac{\partial}{\partial y} & \dfrac{\partial}{\partial x} \end{bmatrix} \tag{6.1}$$

6.2 FE-approximations of fields

So far, we have considered only planar problems such that everything is just a function of x and y since the xy-plane is placed in the plane of the plate. Proceeding in this way, are now in the position of introducing the FE approximation of the different fields in terms of unknown node variables so-called *degrees-of-freedom* (e.g. $\hat{w}_i$ for the out-of-plane displacement) and shape functions $N_i(x,y)$ as:

$$\mathbf{u}(x,y) = \left\{ \begin{array}{c} u_0(x,y) \\ v_0(x,y) \end{array} \right\} = \sum_{i=1}^{nno} N_i(x,y)\hat{\mathbf{u}}_i, \quad \text{where } \hat{\mathbf{u}}_i = \left\{ \begin{array}{c} u_i \\ v_i \end{array} \right\} \tag{6.2}$$

$$w(x,y) = w_0(x,y) = \sum_{i=1}^{nno} N_i(x,y)\hat{w}_i \tag{6.3}$$

$$\boldsymbol{\phi}(x,y) = \left\{ \begin{array}{c} \phi_x(x,y) \\ \phi_y(x,y) \end{array} \right\} = \sum_{i=1}^{nno} N_i(x,y)\hat{\boldsymbol{\phi}}_i, \quad \text{where } \hat{\boldsymbol{\phi}}_i = \left\{ \begin{array}{c} \phi_{x,i} \\ \phi_{y,i} \end{array} \right\} \tag{6.4}$$

or equivalently

$$\mathbf{u} = \mathbf{N}\hat{\mathbf{u}} \tag{6.5}$$

$$w = \bar{\mathbf{N}}\hat{\mathbf{w}} \tag{6.6}$$

$$\boldsymbol{\phi} = \mathbf{N}\hat{\boldsymbol{\phi}} \tag{6.7}$$

with

$$\begin{array}{l} \mathbf{N} = \left[\begin{array}{cccccccc} N_1 & 0 & N_2 & 0 & ... & N_{nno} & 0 \\ 0 & N_1 & 0 & N_2 & ... & 0 & N_{nno} \end{array} \right], \; \bar{\mathbf{N}} = \left[\begin{array}{cccc} N_1 & N_2 & ... & N_{nno} \end{array} \right] \\ \hat{\mathbf{u}} = \left[\begin{array}{cccccccc} \hat{u}_1 & \hat{v}_1 & \hat{u}_2 & \hat{v}_2 & ... & \hat{u}_{nno} & \hat{v}_{nno} \end{array} \right]^T, \; \hat{w} = \left[\begin{array}{cccc} \hat{w}_1 & \hat{w}_2 & ... & \hat{w}_{nno} \end{array} \right]^T \\ \hat{\boldsymbol{\phi}} = \left[\begin{array}{cccccccc} \hat{\phi}_{x,1} & \hat{\phi}_{y,1} & \hat{\phi}_{x,2} & \hat{\phi}_{y,2} & ... & \hat{\phi}_{x,nno} & \hat{\phi}_{y,nno} \end{array} \right]^T \end{array} \tag{6.8}$$

where we dropped (x,y) for brevity. Please note that the sum $\sum_{i=1}^{nno}$ is defined over all nodes (nno) in the domain and that the shape functions have the properties

$$N_i = \left\{ \begin{array}{c} 1 \text{ in node } i \\ 0 \text{ in all other nodes } j \neq i \end{array} \right. , \; \sum_{i=1}^{nno} N_i = 1 \text{ in any point of the domain} \tag{6.9}$$

Furthermore, from the weak form, we know that we also need $\tilde{\boldsymbol{\nabla}}\mathbf{u}$, $\boldsymbol{\nabla} w$ and $\tilde{\boldsymbol{\nabla}}\boldsymbol{\phi}$ which we, via the approximation above, obtain as:

$$\tilde{\boldsymbol{\nabla}}\mathbf{u} = \tilde{\boldsymbol{\nabla}}\left(\mathbf{N}\hat{\mathbf{u}}\right) = \mathbf{B}\hat{\mathbf{u}}, \; \mathbf{B} = \tilde{\boldsymbol{\nabla}}\mathbf{N} \tag{6.10}$$

$$\boldsymbol{\nabla} w = \boldsymbol{\nabla}\left(\bar{\mathbf{N}}\hat{\mathbf{w}}\right) = \bar{\mathbf{B}}\hat{\mathbf{w}}, \; \bar{\mathbf{B}} = \boldsymbol{\nabla}\bar{\mathbf{N}} \tag{6.11}$$

$$\tilde{\boldsymbol{\nabla}}\boldsymbol{\phi} = \tilde{\boldsymbol{\nabla}}\left(\mathbf{N}\hat{\boldsymbol{\phi}}\right) = \mathbf{B}\hat{\boldsymbol{\phi}}, \; \mathbf{B} = \tilde{\boldsymbol{\nabla}}\mathbf{N} \tag{6.12}$$

since all degrees-of-freedom are constant nodal values and not functions of x or y.

6.3 FE-formulation of laminated plates

On order to end up with the FE formulation of the laminated Mindlin plate, we start of by considering each equation separately.

6.3.1 FE formulation of in-plane equilibrium

Before we insert the FE approximation of the unknown displacement field into the weak form of the in-plane equilibrium

$$\int_\Omega \left(\tilde{\boldsymbol{\nabla}}\delta\mathbf{u}\right)^T \left([\mathbf{A}]\tilde{\boldsymbol{\nabla}}\mathbf{u} + [\mathbf{B}]\tilde{\boldsymbol{\nabla}}\boldsymbol{\phi}\right) d\Omega = \int_{\Gamma_{N,u}} \delta\mathbf{u}^T\overline{\mathbf{P}}\, d\Gamma, \quad \forall\delta\mathbf{u} \in \mathbf{V}_{\delta u} \tag{6.13}$$

we first note this should hold for all arbitrary test functions $\delta\mathbf{u} \in \mathbf{V}_{\delta u}$. By using the so-called Galerkin's method, and choosing $\delta\mathbf{u}_1 = \{\delta u \;\; 0\}^T$ *and* $\delta\mathbf{u}_2 = \{0 \;\; \delta v\}^T$ (where u and v can be arbitrary, given that they satisfy the necessary restrictions in terms of *e.g.* boundary conditions) we will obtain two coupled equations for the in-plane displacements. Furthermore, according to Galerkin's method we use the shape functions N_i to represent also the arbitrary test functions

$$\delta\mathbf{u}_1 = \left\{ \begin{array}{c} \delta u \\ 0 \end{array} \right\} = \mathbf{N}\mathbf{c}_1,\ \mathbf{c}_1 = \left[\begin{array}{cccccc} c_{1,1} & 0 & c_{1,2} & 0 & ... & c_{1,nno} \quad 0 \end{array} \right]^T \tag{6.14}$$

$$\delta\mathbf{u}_2 = \left\{ \begin{array}{c} 0 \\ \delta v \end{array} \right\} = \mathbf{N}\mathbf{c}_2,\ \mathbf{c}_2 = \left[\begin{array}{cccccc} 0 & c_{2,1} & 0 & c_{2,2} & ... & 0 \quad c_{2,nno} \end{array} \right]^T \tag{6.15}$$

whereby

$$\tilde{\boldsymbol{\nabla}}\delta\mathbf{u}_1 = \tilde{\boldsymbol{\nabla}}\left(\mathbf{N}\mathbf{c}_1\right) = \mathbf{B}\mathbf{c}_1,\ \mathbf{B} = \tilde{\boldsymbol{\nabla}}\mathbf{N} \tag{6.16}$$

$$\tilde{\boldsymbol{\nabla}}\delta\mathbf{u}_2 = \tilde{\boldsymbol{\nabla}}\left(\mathbf{N}\mathbf{c}_2\right) = \mathbf{B}\mathbf{c}_2,\ \mathbf{B} = \tilde{\boldsymbol{\nabla}}\mathbf{N} \tag{6.17}$$

If we start by choosing $\delta\mathbf{u} = \delta\mathbf{u}_1$ (with arbitrary non-zero coefficients in $\mathbf{c}_1$) and inserting the FE approximations of $\mathbf{u}$, $\boldsymbol{\phi}$ and $\delta\mathbf{u}_1$ we obtain:

$$\mathbf{c}_1^T \left(\int_\Omega \mathbf{B}^T[\mathbf{A}]\mathbf{B}\, d\Omega\hat{\mathbf{u}} + \int_\Omega \mathbf{B}^T[\mathbf{B}]\mathbf{B}\, d\Omega\hat{\boldsymbol{\phi}} - \int_{\Gamma_{N,u}} \mathbf{N}^T\overline{\mathbf{P}}\, d\Gamma \right) = 0. \tag{6.18}$$

In the same way, if we choose $\delta\mathbf{u} = \delta\mathbf{u}_2$ (with arbitrary non-zero coefficients in $\mathbf{c}_2$) we obtain:

$$\mathbf{c}_2^T \left(\int_\Omega \mathbf{B}^T[\mathbf{A}]\mathbf{B}\, d\Omega\hat{\mathbf{u}} + \int_\Omega \mathbf{B}^T[\mathbf{B}]\mathbf{B}\, d\Omega\hat{\boldsymbol{\phi}} - \int_{\Gamma_{N,u}} \mathbf{N}^T\overline{\mathbf{P}}\, d\Gamma \right) = 0 \tag{6.19}$$

which if combined can be written as:

$$\mathbf{c}^T \left(\int_\Omega \mathbf{B}^T[\mathbf{A}]\mathbf{B}\, d\Omega\hat{\mathbf{u}} + \int_\Omega \mathbf{B}^T[\mathbf{B}]\mathbf{B}\, d\Omega\hat{\boldsymbol{\phi}} - \int_{\Gamma_{N,u}} \mathbf{N}^T\overline{\mathbf{P}}\, d\Gamma \right) = 0 \text{ with } \mathbf{c}^T = \left[\begin{array}{c} \mathbf{c}_1^T \\ \mathbf{c}_2^T \end{array} \right] \tag{6.20}$$

Now, since we know that this should hold for arbitrary test functions, i.e. for any choice of $\mathbf{c}$ we must have

$$\underbrace{\int_\Omega \mathbf{B}^T[\mathbf{A}]\mathbf{B}\, d\Omega}_{\mathbf{K}_{uu}}\hat{\mathbf{u}} + \underbrace{\int_\Omega \mathbf{B}^T[\mathbf{B}]\mathbf{B}\, d\Omega}_{\mathbf{K}_{u\phi}}\hat{\boldsymbol{\phi}} - \underbrace{\int_{\Gamma_{N,u}} \mathbf{N}^T\overline{\mathbf{P}}\, d\Gamma}_{\mathbf{f}_{b,u}} = \mathbf{0} \tag{6.21}$$

or

$$\mathbf{K}_{uu}\hat{\mathbf{u}} + \mathbf{K}_{u\phi}\hat{\boldsymbol{\phi}} = \mathbf{f}_{b,u} \tag{6.22}$$

6.3.2 FE formulation of out-of-plane equilibrium

Following the procedure above, now simply by using $\delta w = \bar{\mathbf{N}}\mathbf{c}$, $\boldsymbol{\nabla}\delta w = \bar{\mathbf{B}}\mathbf{c}$ and $\boldsymbol{\phi} = \mathbf{N}\hat{\boldsymbol{\phi}}$ we obtain the FE-formulation of the out-of-plane equation as:

$$\mathbf{c}^T \left(\int_\Omega K\bar{\mathbf{B}}^T[\tilde{\mathbf{A}}]\mathbf{N}\, d\Omega\hat{\boldsymbol{\phi}} + \int_\Omega K\bar{\mathbf{B}}^T[\tilde{\mathbf{A}}]\bar{\mathbf{B}}\, d\Omega\hat{\mathbf{w}} - \int_\Omega \bar{\mathbf{N}}^T p\, d\Omega - \int_{\Gamma_{N,w}} \bar{\mathbf{N}}^T\overline{R}_n\, d\Gamma \right) = 0 \tag{6.23}$$

Again, since this should hold for arbitrary $\mathbf{c}^T$, we obtain the FE-formulation of the out-of-plane equilibrium as

$$\mathbf{K}_{ww}\hat{\mathbf{w}} + \mathbf{K}_{w\phi}\hat{\boldsymbol{\phi}} = \mathbf{f}_{b,w} + \mathbf{f}_{l,w} \tag{6.24}$$

with

$$\mathbf{K}_{ww} = \int_\Omega K\bar{\mathbf{B}}^T[\tilde{\mathbf{A}}]\bar{\mathbf{B}}\, d\Omega,\ \mathbf{K}_{w\phi} = \int_\Omega K\bar{\mathbf{B}}^T[\tilde{\mathbf{A}}]\mathbf{N}\, d\Omega,\ \mathbf{f}_{b,w} = \int_{\Gamma_{N,w}} \bar{\mathbf{N}}^T\overline{R}_n\, d\Gamma,\ \mathbf{f}_{l,w} = \int_\Omega \bar{\mathbf{N}}^T p\, d\Omega \tag{6.25}$$

6.3.3 FE formulation of moment equilibrium

Again, we choose the arbitrary test function in two ways ($\delta\boldsymbol{\phi}_1 = \{\delta\phi_x \;\; 0\}^T$ and $\delta\boldsymbol{\phi}_2 = \{0 \;\; \delta\phi_y\}^T$) which results in

$$\mathbf{c}^T \left(\int_\Omega \mathbf{B}^T[\mathbf{B}]\mathbf{B}\, d\Omega\hat{\mathbf{u}} + \int_\Omega K\mathbf{N}^T[\tilde{\mathbf{A}}]\bar{\mathbf{B}}\, d\Omega\hat{\mathbf{w}} + \int_\Omega \left(\mathbf{B}^T[\mathbf{D}]\mathbf{B} + K\mathbf{N}^T[\tilde{\mathbf{A}}]\mathbf{N}\right) d\Omega\hat{\boldsymbol{\phi}} - \int_{\Gamma_{N,\phi}} \mathbf{N}^T\overline{\mathbf{M}}_n\, d\Gamma \right) = 0 \tag{6.26}$$

again with

$$\text{with } \mathbf{c}^T = \begin{bmatrix} \mathbf{c}_1^T \\ \mathbf{c}_2^T \end{bmatrix}. \tag{6.27}$$

Now, since we know that this should hold for arbitrary test functions, *i.e.* for any choice of $\mathbf{c}$, we must have:

$$\mathbf{K}_{\phi u}\hat{\mathbf{u}} + \mathbf{K}_{\phi w}\hat{\mathbf{w}} + \mathbf{K}_{\phi\phi}\hat{\boldsymbol{\phi}} = \mathbf{f}_{b,\phi} \tag{6.28}$$

with:

$$\begin{aligned} &\mathbf{K}_{\phi u} = \mathbf{K}_{u\phi} = \int_\Omega \mathbf{B}^T[\mathbf{B}]\mathbf{B}\, d\Omega,\; \mathbf{K}_{\phi w} = \mathbf{K}_{w\phi}^T = \int_\Omega K\mathbf{N}^T[\tilde{\mathbf{A}}]\bar{\mathbf{B}}\, d\Omega \\ &\mathbf{K}_{\phi\phi} = \int_\Omega \left(\mathbf{B}^T[\mathbf{D}]\mathbf{B} + K\mathbf{N}^T[\tilde{\mathbf{A}}]\mathbf{N}\right) d\Omega \text{ and } \mathbf{f}_{b,\phi} = \int_{\Gamma_{N,\phi}} \mathbf{N}^T\overline{\mathbf{M}}_n\, d\Gamma \end{aligned} \tag{6.29}$$

6.3.4 Total formulation

By collecting the unknowns in one vector $\mathbf{a} = \{\hat{\mathbf{u}}^T\mathbf{w}^T\hat{\boldsymbol{\phi}}^T\}^T$ we can write the total system of equations as:

$$\underbrace{\begin{bmatrix} \mathbf{K}_{uu} & \mathbf{0} & \mathbf{K}_{u\phi} \\ \mathbf{0} & \mathbf{K}_{ww} & \mathbf{K}_{w\phi} \\ \mathbf{K}_{\phi u} & \mathbf{K}_{w\phi}^T & \mathbf{K}_{\phi\phi} \end{bmatrix}}_{\mathbf{K}} \underbrace{\begin{Bmatrix} \hat{\mathbf{u}} \\ \hat{\mathbf{w}} \\ \hat{\boldsymbol{\phi}} \end{Bmatrix}}_{\mathbf{a}} = \underbrace{\begin{Bmatrix} \mathbf{f}_{b,u} \\ \mathbf{f}_{b,w} + \mathbf{f}_{l,w} \\ \mathbf{f}_{b,\phi} \end{Bmatrix}}_{\mathbf{f}} \tag{6.30}$$

Please note that $\mathbf{K}$ is symmetric since $\mathbf{K}_{u\phi} = \mathbf{K}_{u\phi}^T = \mathbf{K}_{\phi u}$. Please also note that for symmetric laminates, $B_{ij} = 0$ which implies that $\mathbf{K}_{u\phi} = \mathbf{0}$ leading to that $\hat{\mathbf{u}}$ can be solved for **independently of** w **and** $\boldsymbol{\phi}$.

6.4 Element-wise approximation

In the derivations so far, we have assumed that the support of the shape functions N_i span over the entire domain Ω. However, in practice, these shape functions only have local support in the elements surrounding the node j to which the shape function N_j is associated. This means that the shape functions are only defined locally in the domain. Often, we speak of element shape functions N_i^e which is the part of N_i with support in the element e. Thereby, we can write the approximation of our unknown variables as a local approximation on each element as:

$$\mathbf{u}^e = \sum_{i=1}^{neno} N_i\hat{\mathbf{u}}_i^e = \mathbf{N}^e\hat{\mathbf{u}}^e \Rightarrow \tilde{\boldsymbol{\nabla}}\mathbf{u}^e = \mathbf{B}^e\hat{\mathbf{u}}^e \tag{6.31}$$

$$w^e = \sum_{i=1}^{neno} N_i\hat{w}_i^e = \bar{\mathbf{N}}^e\hat{\mathbf{w}} \Rightarrow \boldsymbol{\nabla}w^e = \bar{\mathbf{B}}^e\hat{\mathbf{w}} \tag{6.32}$$

$$\boldsymbol{\phi}^e = \sum_{i=1}^{neno} N_i\hat{\boldsymbol{\phi}}_i^e = \mathbf{N}^e\hat{\boldsymbol{\phi}}^e \Rightarrow \tilde{\boldsymbol{\nabla}}\boldsymbol{\phi}^e = \mathbf{B}^e\hat{\boldsymbol{\phi}}^e \tag{6.33}$$

where *neno* is the number of nodes associated with the element and $\hat{\mathbf{u}}_i^e$, $\hat{w}_i^e$ and $\hat{\boldsymbol{\phi}}_i^e$ are the associated degrees-of-freedom in node i. Considering the special case of a four node quadrilateral element, $\hat{\mathbf{u}}^e$, $\hat{\mathbf{w}}^e$,

$\hat{\boldsymbol{\phi}}^e$, $\mathbf{N}^e$ and $\bar{\mathbf{N}}^e$ take on the form shown in Figure 6.1 (one example):

$$\hat{\mathbf{u}}^e = \left\{ \begin{array}{c} u_1 \\ v_1 \\ u_2 \\ v_2 \\ u_3 \\ v_3 \\ u_4 \\ v_4 \end{array} \right\}, \ \hat{\mathbf{w}}^e = \left\{ \begin{array}{c} w_1 \\ w_2 \\ w_3 \\ w_4 \end{array} \right\} \ \hat{\boldsymbol{\phi}}^e = \left\{ \begin{array}{c} \phi_{x1} \\ \phi_{y1} \\ \phi_{x2} \\ \phi_{y2} \\ \phi_{x3} \\ \phi_{y3} \\ \phi_{x4} \\ \phi_{y4} \end{array} \right\} \tag{6.34}$$

$$\mathbf{N}^e = \left[\begin{array}{cccccccc} N_1 & 0 & N_2 & 0 & N_3 & 0 & N_4 & 0 \\ 0 & N_1 & 0 & N_2 & 0 & N_3 & 0 & N_4 \end{array} \right], \ \bar{\mathbf{N}}^e = \left[\begin{array}{cccc} N_1 & N_2 & N_3 & N_4 \end{array} \right]$$

and we have

$$\mathbf{B}^e = \tilde{\boldsymbol{\nabla}} \mathbf{N}^e, \ \bar{\mathbf{B}}^e = \boldsymbol{\nabla} \bar{\mathbf{N}}^e \tag{6.35}$$

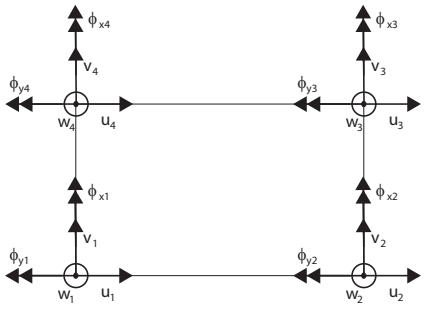

Figure 6.1: Ordering of the degrees of freedom for the prototype element according to Eq. (6.36)

This means that we can obtain the FE equations on one element as:

$$\underbrace{\left[\begin{array}{ccc} \mathbf{K}^e_{uu} & \mathbf{0} & \mathbf{K}^e_{u\phi} \\ \mathbf{0} & \mathbf{K}^e_{ww} & \mathbf{K}^e_{w\phi} \\ \mathbf{K}^e_{\phi u} & \mathbf{K}^{e\ T}_{w\phi} & \mathbf{K}^e_{\phi\phi} \end{array} \right]}_{\mathbf{K}^e} \underbrace{\left\{ \begin{array}{c} \hat{\mathbf{u}}^e \\ \hat{\mathbf{w}}^e \\ \hat{\boldsymbol{\phi}}^e \end{array} \right\}}_{\mathbf{a}^e} = \underbrace{\left\{ \begin{array}{c} \mathbf{f}^e_{b,u} \\ \mathbf{f}^e_{b,w} + \mathbf{f}^e_{l,w} \\ \mathbf{f}^e_{b,\phi} \end{array} \right\}}_{\mathbf{f}^e} \tag{6.36}$$

where $\mathbf{K}^e_{uu}$ is obtained by replacing $\mathbf{B}$ by $\mathbf{B}^e$ and so on in the equations above. Finally, the global stiffness matrix and force vector are obtained by assembling the element contributions into the global system, i.e. by adding the contributions of each element stiffness matrix and element force vector to the corresponding positions in the global matrices, cf. any basic course in FEM.

6.4.1 Prototype example: The four node isoparametric quadrilateral element

6.4.1.1 Preliminaries

The isoparametric quadrilateral (bilinear) element fulfil both requirements for convergence:

- Compatibility: The approximation of all fields is continuous across the common boundary of two neighbouring elements
- Completeness: The approximation over the element is able to represent both an arbitrary constant gradient as well as an arbitrary constant value of any of the fields.

6.4.1.2 Parent and global domain

If we consider a four-noded finite element in the xy-plane as part of the discretisation (or mesh) of a plate, cf. Figure 6.2 (right), the basics of the isoparametric mapping is that this element in the so-called

global domain (xy-plane) corresponds to an element in the so-called *parent domain* ($\xi\eta$-plane) with edges parallel with the coordinate axes $\xi = \pm 1$ and $\eta = \pm 1$, cf. Figure 6.2 (right). Furthermore, there exist a *one-to-one* mapping from the parent domain to the global domain such that any point (x, y) can be found as:

$$x = x(\xi, \eta),\ y = y(\xi, \eta) \tag{6.37}$$

Furthermore, if we differentiate x and y we obtain:

$$\mathrm{d}x = \frac{\partial x}{\partial \xi}\mathrm{d}\xi + \frac{\partial x}{\partial \eta}\mathrm{d}\eta,\ \mathrm{d}y = \frac{\partial y}{\partial \xi}\mathrm{d}\xi + \frac{\partial y}{\partial \eta}\mathrm{d}\eta \tag{6.38}$$

or

$$\left\{ \begin{array}{c} \mathrm{d}x \\ \mathrm{d}y \end{array} \right\} = \underbrace{\left[\begin{array}{cc} \dfrac{\partial x}{\partial \xi} & \dfrac{\partial x}{\partial \eta} \\ \dfrac{\partial y}{\partial \xi} & \dfrac{\partial y}{\partial \eta} \end{array} \right]}_{\mathbf{J}} \left\{ \begin{array}{c} \mathrm{d}\xi \\ \mathrm{d}\eta \end{array} \right\} \tag{6.39}$$

In order for the mapping to be one-to-one, we need to be able to invert the *Jacobian* $\mathbf{J}$ in Eq. (6.39). Thus we have the requirement that

$$\det \mathbf{J} > \mathbf{0}$$

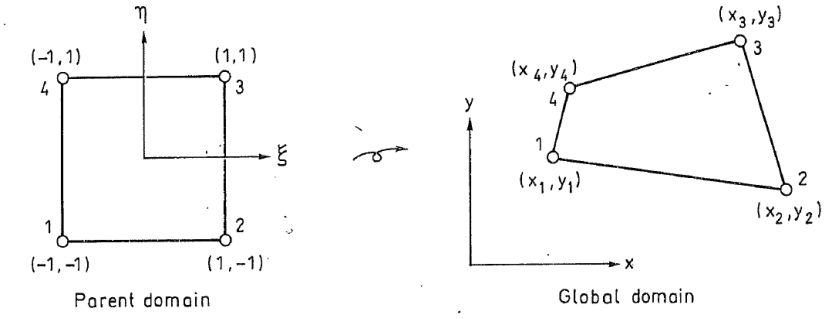

Figure 6.2: Mapping of four-node isoparametric quadrilateral element from the parent domain to the global (FE) domain. (from Ottosen and Petersson, *Introduction to the Finite Element Method*, Prentice Hall, 1992)

6.4.1.3 Element shape functions and their derivatives

The basics of the isoparametric mapping is that the mapping of a point (x, y) is represented via the element shape functions N_i^e such that:

$$x(\xi, \eta) = N_1^e(\xi, \eta)x_1 + N_2^e(\xi, \eta)x_2 + N_3^e(\xi, \eta)x_3 + N_4^e(\xi, \eta)x_4 \tag{6.40}$$

$$y(\xi, \eta) = N_1^e(\xi, \eta)y_1 + N_2^e(\xi, \eta)y_2 + N_3^e(\xi, \eta)y_3 + N_4^e(\xi, \eta)y_4 \tag{6.41}$$

or

$$x(\xi, \eta) = \bar{\mathbf{N}}^e(\xi, \eta)\mathbf{x}^e,\ y(\xi, \eta) = \bar{\mathbf{N}}^e(\xi, \eta)\mathbf{y}^e \tag{6.42}$$

with

$$\bar{\mathbf{N}}^e = \left[\begin{array}{cccc} N_1(\xi, \eta) & N_2(\xi, \eta) & N_3(\xi, \eta) & N_4(\xi, \eta) \end{array} \right],\ \mathbf{x}^e = \left[\begin{array}{c} x_1 \\ x_2 \\ x_3 \\ x_4 \end{array} \right],\ \mathbf{y}^e = \left[\begin{array}{c} y_1 \\ y_2 \\ y_3 \\ y_4 \end{array} \right] \tag{6.43}$$

where x_i, y_i are the coordinates of node i numbered counter-clockwise and where the shape functions are (considering the numbering according to Figure 6.2):

$$N_1^e = \frac{1}{4}(\xi - 1)(\eta - 1) \tag{6.44}$$

$$N_2^e = -\frac{1}{4}(\xi + 1)(\eta - 1) \tag{6.45}$$

$$N_3^e = \frac{1}{4}(\xi + 1)(\eta + 1) \tag{6.46}$$

$$N_4^e = -\frac{1}{4}(\xi - 1)(\eta + 1) \tag{6.47}$$

In the FE-formulation above, it is clear that we need the derivatives of the shape functions with respect to x and y. By noting that

$$\begin{bmatrix} \frac{\partial \bar{\mathbf{N}}^e}{\partial \xi} \\ \frac{\partial \bar{\mathbf{N}}^e}{\partial \eta} \end{bmatrix} = \begin{bmatrix} \frac{\partial \bar{\mathbf{N}}^e}{\partial x}\frac{\partial x}{\partial \xi} + \frac{\partial \bar{\mathbf{N}}^e}{\partial y}\frac{\partial y}{\partial \xi} \\ \frac{\partial \bar{\mathbf{N}}^e}{\partial x}\frac{\partial x}{\partial \eta} + \frac{\partial \bar{\mathbf{N}}^e}{\partial y}\frac{\partial y}{\partial \eta} \end{bmatrix} = \underbrace{\begin{bmatrix} \frac{\partial x}{\partial \xi} & \frac{\partial y}{\partial \xi} \\ \frac{\partial x}{\partial \eta} & \frac{\partial y}{\partial \eta} \end{bmatrix}}_{\mathbf{J}^T} \begin{bmatrix} \frac{\partial \bar{\mathbf{N}}^e}{\partial x} \\ \frac{\partial \bar{\mathbf{N}}^e}{\partial y} \end{bmatrix} \tag{6.48}$$

the derivatives with respect to x and y may be obtained as

$$\begin{bmatrix} \frac{\partial \bar{\mathbf{N}}^e}{\partial x} \\ \frac{\partial \bar{\mathbf{N}}^e}{\partial y} \end{bmatrix} = \begin{bmatrix} \frac{\partial N_1^e}{\partial x} & \frac{\partial N_2^e}{\partial x} & \frac{\partial N_3^e}{\partial x} & \frac{\partial N_4^e}{\partial x} \\ \frac{\partial N_1^e}{\partial y} & \frac{\partial N_2^e}{\partial y} & \frac{\partial N_3^e}{\partial y} & \frac{\partial N_4^e}{\partial y} \end{bmatrix} = \left(\mathbf{J}^T\right)^{-1} \begin{bmatrix} \frac{\partial \bar{\mathbf{N}}^e}{\partial \xi} \\ \frac{\partial \bar{\mathbf{N}}^e}{\partial \eta} \end{bmatrix} \tag{6.49}$$

Finally, $\mathbf{J}^T$ can be found as

$$\mathbf{J}^T = \begin{bmatrix} \frac{\partial \bar{\mathbf{N}}^e}{\partial \xi} \\ \frac{\partial \bar{\mathbf{N}}^e}{\partial \eta} \end{bmatrix} \begin{bmatrix} \mathbf{x}^e & \mathbf{y}^e \end{bmatrix} = \begin{bmatrix} \frac{\partial N_1^e}{\partial \xi} & \frac{\partial N_2^e}{\partial \xi} & \frac{\partial N_3^e}{\partial \xi} & \frac{\partial N_4^e}{\partial \xi} \\ \frac{\partial N_1^e}{\partial \eta} & \frac{\partial N_2^e}{\partial \eta} & \frac{\partial N_3^e}{\partial \eta} & \frac{\partial N_4^e}{\partial \eta} \end{bmatrix} \begin{bmatrix} x_1 & y_1 \\ x_2 & y_2 \\ x_3 & y_3 \\ x_4 & y_4 \end{bmatrix} \tag{6.50}$$

6.4.1.4 Numerical integration

We start by considering that the integral over an element Ω^e can be written as:

$$\int_\Omega^e \bullet \, d\Omega = \int\int \bullet(x, y)\, \mathrm{d}x\mathrm{d}y \tag{6.51}$$

It can be shown that by using the isoparametric mapping ($x = x(\xi, \eta)$ and $y = y(\xi, \eta)$) the integral can be rewritten as:

$$\int\int \bullet(x, y)\, \mathrm{d}x\mathrm{d}y = \int_{-1}^{1}\int_{-1}^{1} \bullet(\xi, \eta) \det \mathbf{J} \mathrm{d}\xi\mathrm{d}\eta \tag{6.52}$$

Furthermore, in any textbook containing numerical integration, it is shown that the integral in one dimension

$$\int_{-1}^{1} f(\xi)\, \mathrm{d}\xi \tag{6.53}$$

may be approximated, with close accuracy as:

$$\int_{-1}^{1} f(\xi)\, \mathrm{d}\xi \approx \sum_{i=1}^{n} f(\xi_i) H_i \tag{6.54}$$

where a finite number (n) of so-called *integration points* ξ_i (in which the function to be integrated is evaluated) is used, and where H_i is the integration weight associated with that point. This can be expanded to two dimensions as:

$$\int_{-1}^{1}\int_{-1}^{1} f(\xi,\eta)\,\mathrm{d}\xi\mathrm{d}\eta \approx \sum_{i=1}^{n}\sum_{j=1}^{m} f(\xi_i,\eta_j)H_iH_j \tag{6.55}$$

where each integration point ij now has the coordinates (ξ_i, η_j).

There exists several ways of choosing the positions of the integration points and the corresponding weights. A common (and the most accurate) scheme is the so-called Gauss integration scheme for which it can be proven that in one dimension, the Gauss integration using n integration points exactly integrates a polynomial of order $2n-1$.

In our case, if we want to integrate the stiffness matrix contributions $\mathbf{K}_{uu}, \mathbf{K}_{u\phi}, ...$ and the force vector contribution $\mathbf{f}_{l,w}$ as accurately as possible, we start by noting that the highest order of accuracy necessary is for a polynomial of order 3 (since that is approximately what get by multiplying $\mathbf{N}$ (bilinear) with $\mathbf{B}$ (linear)). Thus, if the integration should be performed in one dimension we would need two integration points, Now, since it is an area integral performed in two dimensions, we need 2x2 integration points, cf. Figure 6.3.

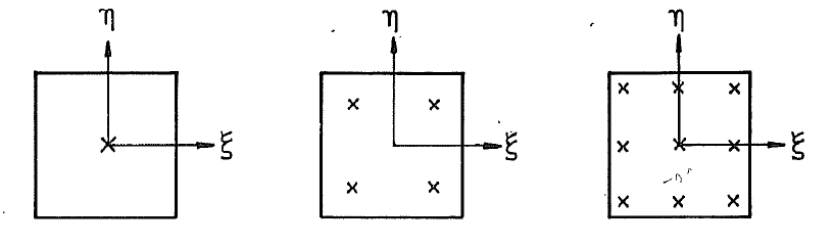

Figure 6.3: Location of integration points of the Gauss scheme for 1 x 1, 2 x 2 and 3 x 3 point integration in the parent domain (ξ, η). (from Ottosen and Petersson, *Introduction to the Finite Element Method*, Prentice Hall, 1992)

For the Gauss integration scheme, it can be shown that for a 2D integration with $n \,\mathrm{x}\, n$ integration points, we have the positioning of the integration points and the corresponding weights as:

For $n = 1$

Point 1 $(n=1, m=1)$: $\quad \xi_1 = 0,\ \eta_1 = 0,\ H_1 = 2,\ H_1 = 2$

For $n = 2$

Point 1 $(n=1, m=1)$: $\quad (\xi,\eta) = \left(\frac{-1}{\sqrt{3}}, \frac{-1}{\sqrt{3}}\right),\ H_1 = 1,\ H_1 = 1$

Point 2 $(n=1, m=2)$: $\quad (\xi,\eta) = \left(\frac{-1}{\sqrt{3}}, \frac{1}{\sqrt{3}}\right),\ H_1 = 1,\ H_2 = 1$

Point 3 $(n=2, m=1)$: $\quad (\xi,\eta) = \left(\frac{1}{\sqrt{3}}, \frac{-1}{\sqrt{3}}\right),\ H_1 = 1,\ H_2 = 1$

Point 4 $(n=2, m=2)$: $\quad (\xi,\eta) = \left(\frac{1}{\sqrt{3}}, \frac{1}{\sqrt{3}}\right),\ H_2 = 1,\ H_2 = 1$

6.4.1.5 Reordering the degrees-of-freedom before assembly

In order to derive the expression for the stiffness matrix and force vector for the laminate element, it was convenient to arrange the degrees-of-freedom in the element degree-of-freedom vector (cf. also Figure 6.1)

$\mathbf{a}^e$ as

$$\mathbf{a}^e = \left\{ \begin{array}{c} \hat{\mathbf{u}}^e \\ \hat{\mathbf{w}}^e \\ \hat{\boldsymbol{\phi}}^e \end{array} \right\} \text{ with } \hat{\mathbf{u}}^e = \left\{ \begin{array}{c} u_1 \\ v_1 \\ u_2 \\ v_2 \\ u_3 \\ v_3 \\ u_4 \\ v_4 \end{array} \right\}, \ \hat{\mathbf{w}}^e = \left\{ \begin{array}{c} w_1 \\ w_2 \\ w_3 \\ w_4 \end{array} \right\} \ \hat{\boldsymbol{\phi}}^e = \left\{ \begin{array}{c} \phi_{x1} \\ \phi_{y1} \\ \phi_{x2} \\ \phi_{y2} \\ \phi_{x3} \\ \phi_{y3} \\ \phi_{x4} \\ \phi_{y4} \end{array} \right\}$$

which yields the format of the element stiffness matrix $\mathbf{K}^e$ and element force vector $\mathbf{f}^e$ as in Eq. (6.36). However, for computational reasons, it is more convenient to number the degrees of freedom as for the element in Figure 6.4. Please note that we keep the $\boldsymbol{\phi}_y$ **degrees-of-freedom defined as positive around the negative x-axis**.

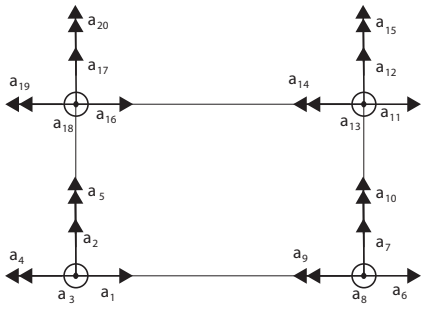

Figure 6.4: Ordering of the degrees of freedom for the prototype element according to the global numbering.

Therefore, first determine the element contributions according to Eq. (6.36) and then reorder the rows of the force vector and rows and columns of the stiffness matrix to meet the numbering in Figure 6.4. This final step can in MATLAB be accomplished e.g. by:

```
Ke = Ke([1 2 9 14 13 3 4 10 16 15 5 6 11 18 17 7 8 12 20 19],...
         [1 2 9 14 13 3 4 10 16 15 5 6 11 18 17 7 8 12 20 19])


fe = fe([1 2 9 14 13 3 4 10 16 15 5 6 11 18 17 7 8 12 20 19]')
```

6.4.2 Reduced integration of out-of-plane shear parts

It can be shown that the current formulation with linear (bi-linear) approximations of $\mathbf{u}$, w and $\boldsymbol{\phi}$ experience locking (i.e. the element become too stiff) when fully integrated. This can be seen by considering a plate in pure bending, cf. Figure 6.5 for a view in the xz-plane, for which the out-of-plane shear stresses and strains should be zero. However, if we use a linear (or bi-linear) approximation of the out-of-plane displacement, as indicated by red piecewise linear curves (one for each element) in Figure 6.5a, and the same approximation for the rotation angles, zero shear strains $\gamma_{xz} = \phi_x + \partial w/\partial x$ can only be accomplished over the whole element in the case of both ϕ_x and $\partial w/\partial x$ being constant over the element. This means that the plate can not have any curvature. Hence, locking occurs for this case, cf. the sketch in Figure 6.5b.

The locking effect can be avoided by so-called selective integration where parts of the stiffness matrix are integrated by reduced integration (1 x 1 integration point in the plane of a plate). This means that if the terms involving e.g. γ_{xz} are integrated using just one integration point in each element, cf. the cross in Figure 6.5b, it is possible to achieve $\gamma_{xz} = 0$ (in this point) for these elements. The rest of the terms (not involving out-of-plane shear strains) can still be fully integrated (2 x 2 integration points in the plane).

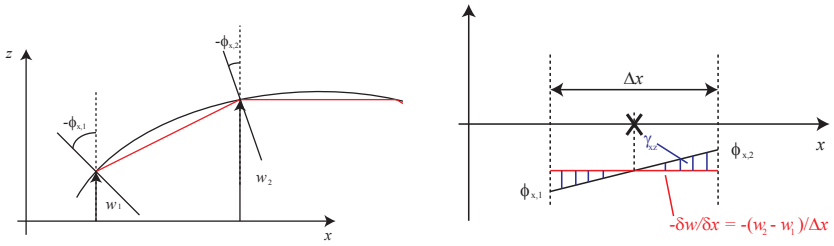

a) b)

Figure 6.5: Sketch explaining the cause of locking for bilinear quadrilateral Mindlin plate elements with full integration. In a), the red curves indicate the linear approximation of the out-of-plane displacement w for the plate which is sketched in black. Also the resulting rotations in the nodes are indicated by $\phi_{x,1}$ and $\phi_{x,2}$. In b), the resulting ϕ_x variation (black), $-\partial w/\partial x$ variation (red) and the resulting shear strain γ_{xz} are indicated together with the point in which $\gamma_{xz} = 0$ can be obtained (black cross).

To generalise this discussion, it can be shown that in order to avoid locking, all parts of $\mathbf{K}$ involving the out-of-plane shear stiffness ($[\tilde{\mathbf{A}}]$) need to be integrated with a reduced order. Thus, if we subdivide $\mathbf{K}_{\phi\phi}$ as:

$$\mathbf{K}_{\phi\phi} = \int_\Omega \mathbf{B}^T[\mathbf{D}]\mathbf{B}\, d\Omega + \int_\Omega K\mathbf{N}^T[\tilde{\mathbf{A}}]\mathbf{N}\, d\Omega = \mathbf{K}_{\phi\phi,1} + \mathbf{K}_{\phi\phi,2} \tag{6.56}$$

the order of integration should be like:

1 x 1 integration of:

$$\mathbf{K}_{\phi\phi,2},\ \mathbf{K}_{w\phi},\ \mathbf{K}_{\phi w},\ \mathbf{K}_{ww}$$

2 x 2 integration of:

$$\mathbf{K}_{\phi\phi,1},\ \mathbf{K}_{uu},\ \mathbf{K}_{u\phi},\ \mathbf{K}_{\phi u}$$

Please note that selective (under) integration of the stiffness matrix may lead to spurious zero energy modes under certain conditions. Therefore, one should always carefully investigate the results obtained. The treatment (or stabilisation) of such behaviour is however considered as outside the scope of this course.

Chapter 7

Failure in composites

The definition of failure depend on the application. This means that a component can be considered as failing long before it breaks. As an example, if a laminated composite component's main purpose is to ensure a certain stiffness, it has failed already when the first ply breaks since this will have a direct impact on the stiffness, cf. the first kink in the load-displacement curve in Figure 7.1. However, the component may still be able to carry an increase in load, meaning that the function is lost whereas collapse or catastrophic failure still can be avoided. On the other hand, some components, such as crash boxes or other components intended for energy absorption during a car crash, are designed to fail in a reliable way. In this case, 'failure' is considered first when the component looses all load carrying capacity.

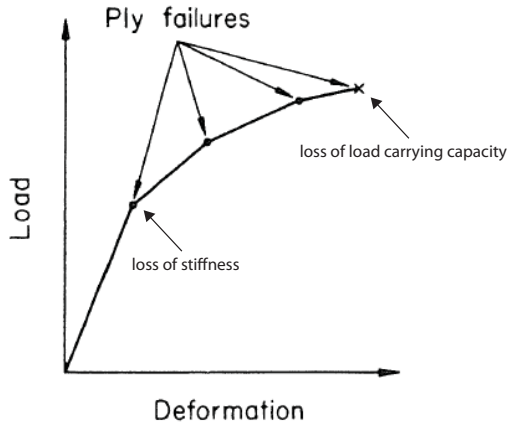

Figure 7.1: Load-displacement behaviour of a hypothetical laminate (from Agarwal *et al.*, Figure 6-13).

In addition, in the case of composite materials, internal material failure occurs much before any change in macroscopic behaviour can be observed. Examples of types of internal failure are:

- Breakage of fibres (but not causing total ply-failure)
- Microcracking of the matrix
- Separation of fibres from the matrix (debonding)
- Local separation of plies (local delamination)

The effects of such internal material failure is however only observable if it occurs to a large extent.

7.1 Intralaminar failure - failure *within* a lamina

7.1.1 Lamina failure modes

Most unidirectional materials (including UD fibre reinforced plies) exhibit a linear elastic behaviour up to failure. Thus, for a single lamina the decrease (loss) of stiffness and loss of all load carrying capacity

	Loading type	Possible failure modes
σ_{LU}	Longitudinal tension	Brittle (concentrated fibre breakage) Brittle + fibre pullout (stress concentration at fibre ends) Brittle + interface shear failure or debonding
$\sigma_{LU}^{'}$	Longitudinal compression	Micro-buckling Shear failure Fibre crushing Splitting
σ_{TU}	Transverse tension	Matrix tensile failure Constituent debonding and/or fibre splitting
$\sigma_{TU}^{'}$	Transverse compression	Shear failure of the matrix -In combination with constituent debonding -In combination with fibre crushing
τ_{LTU}	In-plane shear	Matrix shear failure Matrix shear failure + constituent debonding Pure constituent debonding

Table 7.1: Possible lamina failure modes

occurs simultaneously. In the presentation material for this lecture, a number of different failure modes (depending on loading type) is presented, cf. also a summary of these failure modes in Table 7.1.

7.1.2 Multi-axial lamina failure criteria

There exist a number of failure criteria to predict failure of a composite ply subjected to multi-axial loading, some of them being presented below. All these criteria require a number of material parameters to characterise failure under certain one-dimensional loading conditions, cf. the failure modes of a ply. These material strength parameters, summarised in Table 7.1, can either be predicted by micromechanical models (such as the rule of mixtures for predicting the longitudinal tensile failure stress, cf. the lecture notes for lecture 3) or determined experimentally (interested readers are referred to Chapter 10 in the course book).

7.1.2.1 The maximum-stress criterion

This criterion states that fracture will occur if the in-plane shear stress or any of the normal stresses in the direction of the principal material axes (the L, T and $T^{'}$ axes of a ply) exceed the corresponding allowable stress. Thus, in order to avoid failure, the following inequalities need to be satisfied:

$$-\sigma'_{LU} < \quad \sigma_L \quad < \sigma_{LU} \tag{7.1}$$

$$-\sigma'_{TU} < \quad \sigma_T \quad < \sigma_{TU} \tag{7.2}$$

$$\text{abs}(\tau_{LT}) < \quad \tau_{LTU} \tag{7.3}$$

Please note that, of course, the sign of the shear stress does not have an influence. According to this theory, failure occurs when any of the inequalities are violated. Thereby, it is not really one fracture criterion but five subcriteria not taking into consideration the effects of coinciding loads. Thereby, it becomes non-conservative under certain conditions, e.g. combined tensile and shear loading.

7.1.2.2 The maximum-strain criterion

This criterion states that fracture will occur if the in-plane shear strain or any of the normal strains in the direction of the principal material axes (the L, T and $T^{'}$ axes of a ply) exceed the corresponding allowable strains. Thus, in order to avoid failure, the following inequalities need to be satisfied:

$$-\varepsilon'_{LU} < \quad \varepsilon_L \quad < \varepsilon_{LU} \tag{7.4}$$

$$-\varepsilon'_{TU} < \quad \varepsilon_T \quad < \varepsilon_{TU} \tag{7.5}$$

$$\text{abs}(\gamma_{LT}) < \quad \gamma_{LTU} \tag{7.6}$$

According to this theory, failure occurs when any of the inequalities are violated. Thereby, it is neither in this case really one fracture criterion but five subcriteria without consideration of interaction. This criterion is indeed very similar to the maximum stress criterion, especially if we assume linear elastic behaviour of the composite up to failure. Thereby, only minor differences can be noted that are attribute to Poisson effects, cf Figure 7.2.

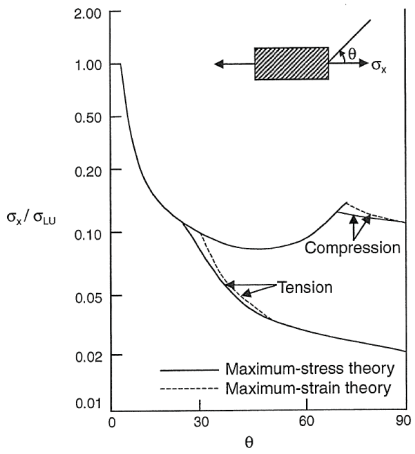

Figure 7.2: Off-axis strength predicted my maximum stress and maximum-strain theories of failure (from Agarwal *et al.*, Figure 5-13).

7.1.2.3 The maximum-work criterion (Tsai-Hill)

The maximum-work criterion, also denoted the *Tsai-Hill* criterion, states that a lamina in the state of plain stress ($\sigma_{T'} = \tau_{LT'} = \tau_{TT'} = 0$ where T' is the coordinate axis pointing out of the lamina plane) fails when the following criterion is violated:

$$\left(\frac{\sigma_L}{\sigma_{LU}}\right)^2 + \left(\frac{\sigma_T}{\sigma_{TU}}\right)^2 + \left(\frac{\tau_{LT}}{\tau_{LTU}}\right)^2 - \left(\frac{\sigma_L}{\sigma_{LU}}\right)\left(\frac{\sigma_T}{\sigma_{LU}}\right) < 1 \tag{7.7}$$

The criterion is derived on the basis of the theory for anisotropic plasticity according to Hill:

$$H\left(\sigma_L - \sigma_T\right)^2 + F\left(\sigma_T - \sigma_{T'}\right)^2 + G\left(\sigma_{T'} - \sigma_L\right)^2 + L\tau_{LT}^2 + M\tau_{TT'}^2 + N\tau_{LT'}^2 = 1 \tag{7.8}$$

where $F - N$ are material constants. By adding the restrictions that

- Failure in pure shear occurs when the shear stress reaches the maximum strength value (for all three directions) $\Rightarrow L = \left(\tau_{LTU}\right)^{-2}, M = \left(\tau_{TT'U}\right)^{-2}, N = \left(\tau_{LT'U}\right)^{-2}$
- Failure under uniaxial loading occurs when the normal stress reaches the maximum strength value (for all three directions) $\Rightarrow H + G = \left(\sigma_{LU}\right)^{-2}, H + F = \left(\sigma_{TU}\right)^{-2}$
- The ply is transversely isotropic $\Rightarrow H = G$
- The out of plane normal stress $\sigma_{T'}$ is zero

the parameters $F - N$ can be expressed in the material strength parameters as

$$\left(\frac{\sigma_L}{\sigma_{LU}}\right)^2 + \left(\frac{\sigma_T}{\sigma_{TU}}\right)^2 + \left(\frac{\tau_{LT}}{\tau_{LTU}}\right)^2 + \left(\frac{\tau_{TT'}}{\tau_{TT'U}}\right)^2 + \left(\frac{\tau_{LT'}}{\tau_{LT'U}}\right)^2 - \left(\frac{\sigma_L}{\sigma_{LU}}\right)\left(\frac{\sigma_T}{\sigma_{LU}}\right) < 1 \tag{7.9}$$

which is further reduced to Eq. (7.7) if we assume that also the transverse shear stresses are zero. For a visualisation of the Tsai-Hill criterion, refer to Figure 7.3 where the failure envelope is plotted under the condition $\tau_{LT} = 0$.

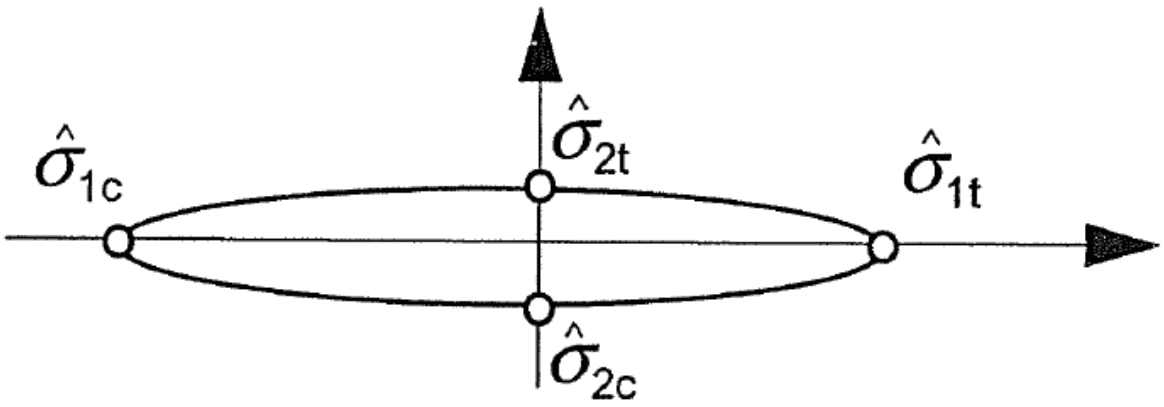

Figure 7.3: Visualisation of the Tsai-Hill criterion for zero shear stresses (from Zenkert and Battley, *Foundations of Fibre composites*, Figure 4-10). $\hat{\sigma}_{1c} = \sigma'_{LU}$, $\hat{\sigma}_{1t} = \sigma_{LU}$, $\hat{\sigma}_{2c} = \sigma'_{TU}$, $\hat{\sigma}_{2t} = \sigma_{TU}$

It should be realised that this criterion in its original form does not distinguish between the tensile and compressive strength in longitudinal and transverse direction. Therefore, it cannot in this form adequately model materials with different strength in tension and compression (as is the case for many polymer composite materials). However, to improve the performance of the criterion, one should carefully **take into consideration the sign of $\boldsymbol{\sigma}_L$ and $\boldsymbol{\sigma}_T$** meaning that **if any of these are negative, the corresponding compressive strength should be used**.

As an example, if the stress state is such that $\sigma_L > 0$ and $\sigma_T < 0$, the Tsai-Hill criterion should take the form:

$$\left(\frac{\sigma_L}{\sigma_{LU}}\right)^2 + \left(\frac{\sigma_T}{\sigma'_{TU}}\right)^2 + \left(\frac{\tau_{LT}}{\tau_{LTU}}\right)^2 - \left(\frac{\sigma_L}{\sigma_{LU}}\right)\left(\frac{\sigma_T}{\sigma_{LU}}\right) < 1 \tag{7.10}$$

It should be remarked that the Tsai-Hill criterion indeed takes the interaction between different stress components into account, but really without any micromechanical motivation to support the actual interaction. Thereby, this criterion can be considered more in the form of a 'curve-fitting' criterion which matches the single-mode conditions. Generally, this criterion is more conservative than the maximum-stress criterion (important in industrial applications) except in small regions in the third and fourth quadrant (when σ_T is negative (depending on the strength values).

7.1.2.4 The Tsai-Wu failure criterion

Another common criterion used for evaluating possible failure of composite plies is the Tsai-Wu criterion. It states that a lamina in the state of plain stress ($\sigma_{T'} = \tau_{LT'} = \tau_{TT'} = 0$) fails when the following criterion is violated:

$$\frac{\sigma_L^2}{\sigma_{LU}\sigma'_{LU}} + \frac{\sigma_T^2}{\sigma_{TU}\sigma'_{TU}} + \frac{\tau_{LT}^2}{\tau_{LTU}^2} + 2F_{12}\sigma_L\sigma_T + \frac{\sigma_L}{\sigma_{LU}} - \frac{\sigma_L}{\sigma'_{LU}} + \frac{\sigma_T}{\sigma_{TU}} - \frac{\sigma_T}{\sigma'_{TU}} < 1 \tag{7.11}$$

where F_{12} is another material parameter that needs to be determined experimentally in addition to the separate strength parameters. In order for the criterion to represent a closed ellipse (and not parallel lines or a hyperbola) we need the restriction

$$-1 < F_{12}\sqrt{\sigma_{LU}\sigma'_{LU}\sigma_{TU}\sigma'_{TU}} < 1$$

It is very difficult to perform specific experiments to determine F_{12} and it is thereby often necessary to combine several experiments to calibrate the most suitable value. It should however be remarked that the parameter F_{12} influence both the slenderness ratio and the inclination of the major axis of the failure ellipse described by the Tsai-Wu criterion, cf. Figure 7.4 for a visualisation of the Tsai-Wu criterion when $\tau_{LT} = 0$.

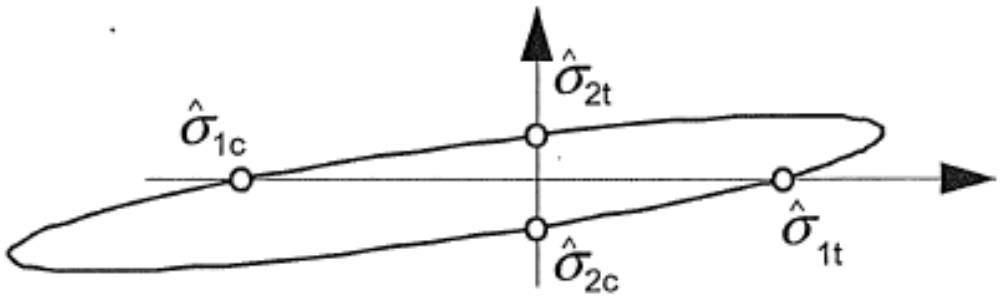

Figure 7.4: Visualisation of the Tsai-Wu criterion for zero shear stresses (from Zenkert and Battely, *Foundations of Fibre composites*, Figure 4-11). $\hat{\sigma}_{1c} = \sigma'_{LU}$, $\hat{\sigma}_{1t} = \sigma_{LU}$, $\hat{\sigma}_{2c} = \sigma'_{TU}$, $\hat{\sigma}_{2t} = \sigma_{TU}$

As for the Tsai-Hill criterion, the Tsai-Wu criterion also takes multi-axial loading effects into account, but also in this case without any real motivation for the interaction. Instead, it is a mathematically easy-to-use criterion adapted for a limited number of measure points. This criterion is widely used, it has however some significant limitations. Most important, if the transverse compressive strength is decreased, the predicted strength in compressive-compressive loading is actually increased (unphysical!).

7.1.2.5 The Hashin criterion

In an attempt to account for load interaction and at the same time having a physical basis (failure mode basis) for the criterion, Hashin (*Journal of Applied Mechanics*, 47:329–334, 1980) developed a set of equations to predict failure based on four failure modes (details are omitted here but can be found in the reference):

Fibre direction tensile failure (combined effect from shear and tensile loading):

$$\left(\frac{\sigma_L}{\sigma_{LU}}\right)^2 + \alpha\left(\frac{\tau_{LT}}{\tau_{LTU}}\right)^2 < 1 \text{ when } \sigma_L > 0 \tag{7.12}$$

Fibre direction compressive failure (not considering the failure mode of matrix shear failure):

$$\left(\frac{\sigma_L}{\sigma'_{LU}}\right)^2 < 1 \text{ when } \sigma_L < 0 \tag{7.13}$$

Transverse direction matrix tensile failure:

$$\left(\frac{\sigma_T}{\sigma_{TU}}\right)^2 + \left(\frac{\tau_{LT}}{\tau_{LTU}}\right)^2 < 1 \tag{7.14}$$

Transverse direction matrix compressive failure

$$\left(\frac{\sigma_T}{2\tau_{LT'U}}\right)^2 + \left(\left(\frac{\sigma'_{TU}}{2\tau_{LT'U}}\right)^2 - 1\right)\frac{\sigma_T}{\sigma'_{TU}} + \left(\frac{\tau_{LT}}{\tau_{LTU}}\right)^2 < 1 \tag{7.15}$$

where $\tau_{LT'U}$ in the last criterion is the out-of-plane shear strength and where α is an additional material parameter (representing the effect of shear on the longitudinal tensile failure) that needs to be calibrated against experimental data. Often, however, α is chosen as 1. I should also be pointed out that the two matrix failure modes also comprise the loading case of pure shear, for which we set $\sigma_T = 0$ such that failure in pure shear occurs when the in-plane shear stress reaches the critical shear stress value τ_{LTU}.

7.1.2.6 The LaRC set of criteria

To further consider the physical mechanisms behind failure initiation in a laminate, a set of failure criteria denoted the LaRC criteria have been proposed in the literature, cf. Pinho *et al.* (Pinho *et al.*, Failure

Models and Criteria for FRP Under In-Plane or Three-Dimensional Stress States Including Shear Non-Linearity. *NASA/TM-2005-213530*. NASA Langley Research Center. Hampton, VA 23681, 2005). The criteria are based on physical models for each failure mode and also take into consideration non-linear matrix shear behaviour. Furthermore, the model for matrix compressive failure is based on the so-called Mohr-Coulomb criterion and it predicts the fracture angle. Fiber kinking is triggered by an initial fiber misalignment angle and by the rotation of the fibers during compressive loading. The plane of fiber kinking is also predicted by the model. LaRC consists of 6 expressions that can be used directly for design purposes. This set of criteria are however quite advanced and considered out-of-scope in the current course. Interested readers are referred to the reference mentioned above (also available on the course homepage).

7.2 Progressive failure of a laminate - The analysis of laminates after initial intralaminar failure

7.2.1 Preliminaries

Given the failure criteria presented in Section 7.1.2, it is rather straightforward to predict whether any of the plies will fail under certain loading conditions. This means that the load when the first ply will fail can be computed. However, since the strength of a ply is directly related to its orientation, not all plies will fail at the same time. Instead, one will see progressive ply failure as indicated in Figure 7.1.

Failure will most likely first occur in plies oriented perpendicular to the loading (due to the lower strength). This may in fact occur at rather low loads meaning that the laminate at this point is in no real danger of complete failure. Sometimes even, the effect of the failure of the first couple of plies may be difficult to observe from the macroscopic viewpoint. However, as the number of failed plies increase, the macroscopic behaviour will change (e.g. manifested as a decrease in stiffness). Finally, when enough plies have failed, a critical point will be reached after which no further increase in the load can be made without total failure and fracture of the component. To analyse the ultimate strength of a laminate and to be able to follow the entire load-displacement history, a procedure where progressive failure is taken into account is thereby necessary.

7.2.2 Simplified approach to handle progressive failure

One approach to invoke the progressive failure in the modelling of laminates is to update the lamina properties whenever failure is detected. For instance, if longitudinal tensile failure occurs, it is very likely that the stiffness in this direction is reduced (or vanishes completely). This can be modelled by modification of the $[\mathbf{Q}]$-matrix of the current ply in such a way that E_L is set to zero (or rather a 'very low' number to avoid numerical difficulties) whereas the other properties, such as the transverse modulus E_T and the in-plane shear modulus G_{LT} can be considered as unaffected by the failure mode. In a general sense, the modification of particular material parameters should be made considering the associated failure mode. One such procedure, could be as described in Table 7.2 (from Zenkert and Battley (Zenkert and Battley, *Foundations of Fibre Composites*, Paper 96-10, KTH, 2003)).

It should be remarked that in order for such a failure assessment procedure to work well, it is essential to involve a physically based intralaminar failure criterion (or set of criteria) such that the associated failure mode in each ply is indicated. If instead a more pragmatic curve-fitting failure criterion (such as Tsai-Hill and Tsai-Wu) is used, the only option is to reduce all stiffness properties (since the mode of failure is NOT indicated) following the so-called *ply discount method*. This ply discount method however, provides a more conservative estimation of the total load carrying capacity of the laminate.

Please note that whenever any of the material parameters for a ply is updated, new $[\mathbf{A}]$, $[\mathbf{B}]$, and $[\mathbf{D}]$ matrices need to be generated, cf. the work flow described in Figure 7.5. Please also note that, due to failure, an initially symmetric ply will most probably become un-symmetric whereby a coupling is introduced between membrane and bending action (i.e. $[\mathbf{B}] \neq \mathbf{0}$)

It should also be remarked that by applying such a stiffness modification approach in a finite element analysis, based on a stress (or strain) based failure criterion, the results may be mesh dependent. Therefore, the mesh convergence of the results should always be carefully considered.

Material state	Material constants to be reduced (or set to zero)
No failure	–
Transverse matrix failure	E_T
Fibre failure (tension)	E_L
Fibre/matrix shear failure	ν_{LT}, G_{LT}
Shear failure	G_{LT}
Matrix failure + fibre/matrix shear failure	E_T, ν_{LT}, G_{LT}
Fibre/matrix shear + shear failure	E_T, ν_{LT}, G_{LT}
Total failure	E_L, E_T, ν_{LT}, G_{LT}

Table 7.2: Stiffness reduction scheme for progressive failure analysis (Reproduced from Zenkert and Battley (*Foundations of Fibre Composites*, Paper 96-10, KTH, 2003).

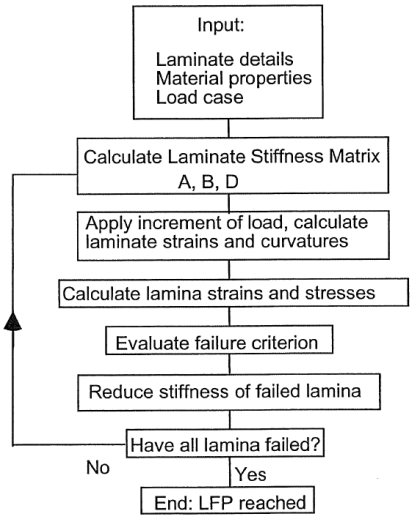

Figure 7.5: Work flow for progressive failure analysis for laminated fibre composites (From Zenkert and Battley (*Foundations of Fibre Composites*, Paper 96-10, KTH, 2003).

7.2.3 Application to in-plane loading of cross-ply laminates

Consider a cross-ply laminate made up of n equal plies of which l have the fibres oriented in the direction of the load, here equal to the x-direction, and m have the fibres oriented perpendicular to the load ($l + m = n$). If we set the longitudinal and transverse stiffnesses (moduli) to E_L and E_T respectively, we have by the rule of mixtures that the composite modulus E (in the loading direction x) is

$$E = \frac{l}{n}E_L + \frac{m}{n}E_T \tag{7.16}$$

which sometimes is denoted the *primary modulus*. Adopting the maximum-strain criterion, failure in the plies will occur when the composite strain is equal to ε_{TU} at which stage the composite stress σ_C, defined as the stress resultant force N_x divided by the laminate thickness h as

$$\sigma_C = \frac{N_x}{h}, \tag{7.17}$$

becomes

$$\sigma_C = \sigma_A = E\varepsilon_{TU}. \tag{7.18}$$

Let us now first assume that there is no stress relaxation in the failing plies. Then, when the load increase further, the transverse plies will fail and the remaining *secondary modulus* E_S becomes (by setting $E_T = 0$)

$$E_S = \frac{l}{n}E_L. \tag{7.19}$$

Final fracture will then occur when the load is such that the composite fracture strain is reached ($\varepsilon = \varepsilon_{LU}$) resulting in the composite failure stress σ_F as:

$$\sigma_F = \sigma_A + E_S \left(\varepsilon_{LU} - \varepsilon_{TU}\right) \tag{7.20}$$

The total response can be illustrated by studying Figure 7.6. Based on the stress-strain curve in Figure 7.6, we can also write the composite strain as:

$$\varepsilon = \begin{cases} \dfrac{\sigma_C}{E} & \sigma_C \leq \sigma_A \\ \dfrac{\sigma_A}{E} + \dfrac{\sigma_C - \sigma_A}{E_S} & \sigma_A < \sigma_C < \sigma_F \end{cases} \tag{7.21}$$

or in the latter stage using an effective stiffness E_e as

$$\varepsilon = \begin{cases} \dfrac{\sigma_C}{E} & \sigma_C \leq \sigma_A \\ \dfrac{\sigma_C}{E_e} & \sigma_A < \sigma_C < \sigma_F \end{cases} \tag{7.22}$$

where

$$E_e(\sigma_C) = \frac{E}{1 + \left[(E/E_S) - 1\right]\left[1 - (\sigma_C/\sigma_A)\right]} \tag{7.23}$$

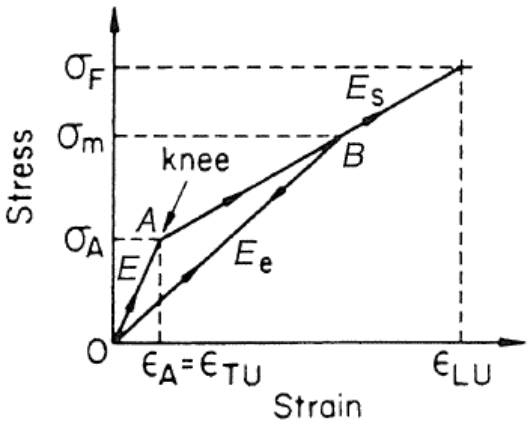

Figure 7.6: Stress-strain diagram for a cross-ply laminate up to failure (from Agarwal et al, Figure 6-14).

It should be remarked that, due to the assumption made above that there is no stress relaxation in the failing plies, the resulting composite stress-strain (or load-displacement) curve is continuous, cf. Figure 7.6. However, in many relevant cases, (partial) stress relaxation *will* occur in the failing plies which will yield a sudden change in the magnitude of the stress in the case of displacement (or strain) controlled loading (path C) or the magnitude of the strain for load controlled loading (path B), cf. Figure 7.7. Please also note that the intermediate path (path D) is possible.

The level of discontinuity in the laminate response will depend how pronounced the stress relaxation in the failed plies is. If the plies were to be considered more or less independent of each other, full stress relaxation would be expected. But in most real applications, when the interlaminar bond is strong the adjoining 0° plies will restrain the failure in the 90° plies. As a result, the failure of a 90° ply is localised, and only partial stress relaxation is to be expected.

Read the remaining part of Chapter 6.8 on your own! Pay special attention to the experiments by Hahn and Tsai that better explains the true stress relaxation in failing plies

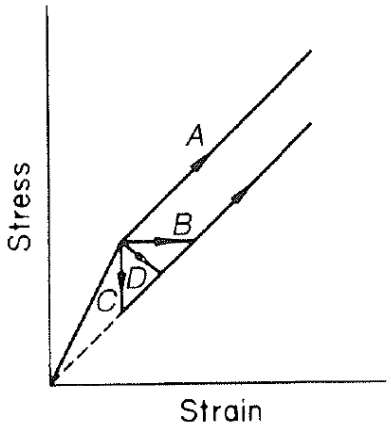

Figure 7.7: Stress-strain diagram for a cross-ply laminate with (partial) stress relaxation in the plies that have failed. (from Agarwal et al, Figure 6-15).

7.3 Fracture mechanics of fibre composites

7.3.1 Preliminaries

Up until now we have treated the composites as more or less free of defects, flaws, microcracks etc. whereby a continuum approach has been valid. However, in order to account for both defects and stress concentrations, e.g. holes, we need to resort to the theory of fracture mechanics with emphasis on anisotropic material. This theory can be used to determine the criticality of an existing crack and thereby also maximum allowable crack size within a component (normally to be related to the size of detectable cracks during inspection).

Generally, failure within composites (just as in metals) will emanate from existing flaws or microcracks such as broken fibres, matrix cracks and debonded interfaces between fibres and matrix. From there, cracks will propagate very much like in the schematic in Figure 7.8. Hence, at some distance in front of the crack, the fibres remain intact. Closer to the vicinity of the crack tip, fibres will break due to the high stresses, although not necessarily in the plane of the crack. As a consequence, fibre pullout will occur *behind* the crack tip. In the case of strong bonding between the matrix and the fibres, it is more likely that the fibres break in the crack plane in front to the crack tip, leaving a pure matrix dominated zone which will break in a ductile (plastic deformation) manner.

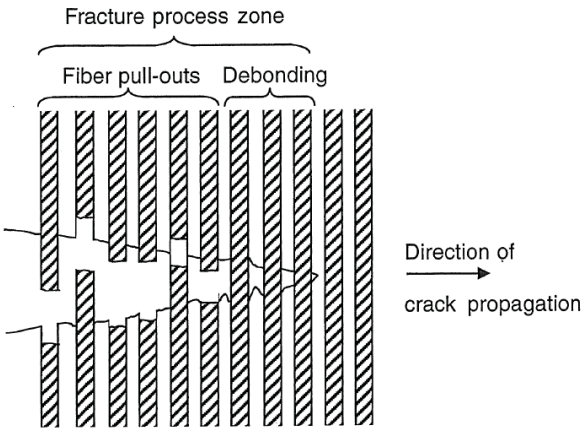

Figure 7.8: A model of the fracture-process zone (from Agarwal et al, Figure 8-11).

It should be remarked that for laminated composites, the direction of crack propagation will be strongly affected by the fibre orientation (as opposed to metals where the crack propagation direction is more or less entirely governed by the stress state in the vicinity of the crack tip). In fact, **cracks may very well propagate in different directions in different plies with alternating fibre**

orientation. Another conclusion that can be made is that practically all laminates are highly notch sensitive and that several of the following parameters may affect this notch sensitivity:

- Fibre volume fraction
- Fibre properties
- Manufacturing conditions
- Environmental conditions

There exists several methods to assess the notch sensitivity and strength of a notched composite of which the approach proposed by Whitney and Nuismer is one of the more commonly used, partly because it is simple to operate.

7.3.2 Whitney-Nuismer criteria for holes

The basic motivation for the Whitney-Nuismer failure criteria for notched laminates (with holes) is the so-called *hole-size effect* which means that larger holes causes a greater strength reduction of the laminate. This can be explained by the fact that even though the stress concentration factor (and thereby the maximum stress) is independent of the size of the hole, a larger hole will produce large stresses over a larger area with higher chance for the existence of flaws that will initiate failure, cf. Figure 7.9 for a sketch of the hole-size effect for isotropic plates.

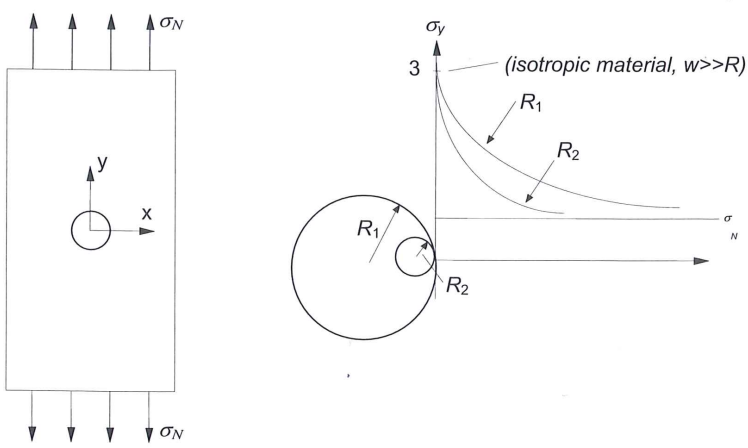

Figure 7.9: Sketch of the motivation behind the so-called hole-size effect, i.e. that larger holes causes a greater strength reduction of the laminate (from Zenkert and Battley, *Foundations of Fibre composites*, Figure 6-8).

As a starting point for the derivation of these criteria, let us consider an infinite orthotropic plate with a hole with radius R subjected to a uniform load σ 'far away' from the hole, as shown in Figure 7.10. If the axes x and y are assumed to be normal to the planes of elastic symmetry (the laminate is specially orthotropic with respect to in-plane loading, cf. Chapter 6.6.2 in the course book), the normal stress σ_y acting along the line $y = 0$ can be approximated by

$$\sigma_y(x,0) = \frac{\sigma}{2}\left\{2 + \left(\frac{R}{x}\right)^2 + 3\left(\frac{R}{x}\right)^4 - (k_T - 3)\left[5\left(\frac{R}{x}\right)^6 - 7\left(\frac{R}{x}\right)^8\right]\right\} \tag{7.24}$$

where k_T is the orthotropic stress concentration factor

$$k_T = 1 + \sqrt{\frac{2}{A_{11}}\left(\sqrt{A_{11}A_{22}} - A_{12} + \frac{A_{11}A_{22} - A_{12}^2}{2A_{66}}\right)} \tag{7.25}$$

where index 2 relates to the loading (y) direction **opposed to the way it is written in the book where, in that case, 1 denotes the direction of the applied load**. Please note that for a uni-directional ply loaded in the longitudinal direction (in this case $L = 2$), the expression for the stress

concentration factor takes the form

$$k_T = 1 + \sqrt{2\left(\sqrt{\frac{E_L}{E_T}} - \nu_{LT}\right) + \frac{E_L}{G_{LT}}} \quad \textbf{(Note the error in the course book!)} \tag{7.26}$$

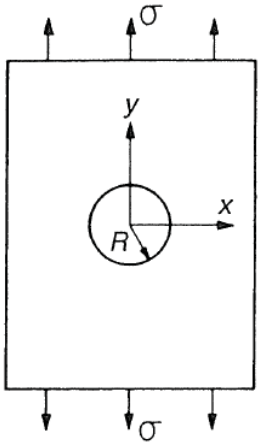

Figure 7.10: An orthotropic plate with a circular hole of radius R (from Agarwal et al, Figure 8-17).

Now, Whitney and Nuismer propose two ways to predict failure:

1. The *point-stress criterion* saying that failure will occur when the stress at a distance d_0 from the notch (hole edge or crack tip) reach the unnotched strength σ_0 of the material

2. The *average stress criterion* saying that failure will occur when the average value of the stress over some fixed distance a_0 from the notch (hole edge or crack tip) reach the unnotched strength σ_0 of the material

For both cases, the underlying assumption is that d_0 and/or a_0 are laminate strength parameters which are constant and applicable to any type of notch for a given material system, volume fraction of fibres and lay-up sequence. Please note that, thereby, the in-plane strength of the laminate σ_0 will depend on the material system as well as the orientation of the fibres.

7.3.2.1 Point-stress criterion for a hole

According to the statement above, the point-stress criterion for holes states that failure occurs when the stress at a distance d_0 from the hole edge reach the unnotched strength σ_0 such that

$$\sigma_y(R + d_0, 0) = \sigma_0, \tag{7.27}$$

cf. also Figure 7.11 for an illustration.

Inserting Eq. (7.27) in Eq. (7.24) yields the relation between the notched (σ_N) and unnotched (σ_0) strength (corresponding to the critical stress applied far away from the hole) as

$$\frac{\sigma_N}{\sigma_0} = \frac{2}{2 + p_1^2 + 3p_1^4 - (k_T - 3)(5p_1^6 - 7p_1^8)} \tag{7.28}$$

where

$$p_1 = \frac{R}{R + d_0}. \tag{7.29}$$

Interesting to note is that, for very large holes $p_1 \to 1$ and consequently $\sigma_N/\sigma_0 \to (1/k_T)$ whereas for vanishingly small holes $p_1 \to 0$ and consequently $\sigma_N/\sigma_0 \to 1$.

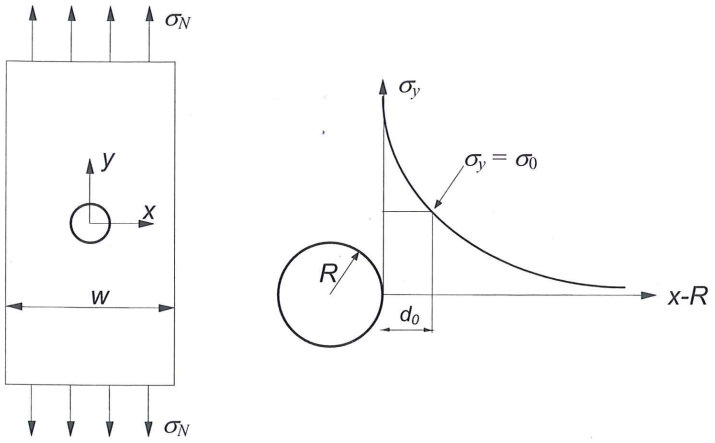

Figure 7.11: Illustration of the Whitney-Nuismer point-stress criterion for laminates with a hole (from Zenkert and Battley, *Foundations of Fibre composites*, Figure 6-28).

7.3.2.2 Average-stress criterion for a hole

The average-stress criterion for holes states that failure occurs when the averaged stress over a distance a_0 from the hole edge reach the unnotched strength σ_0 such that

$$\frac{1}{a_0}\int_R^{R+a_0} \sigma_y(x,0)\,dx = \sigma_0, \tag{7.30}$$

cf. also Figure 7.12 for an illustration (where $\overline{\sigma}_y$ is the averaged σ_y-stress over the distance a_0 and $\hat{\sigma}_{1t} = \sigma_0$).

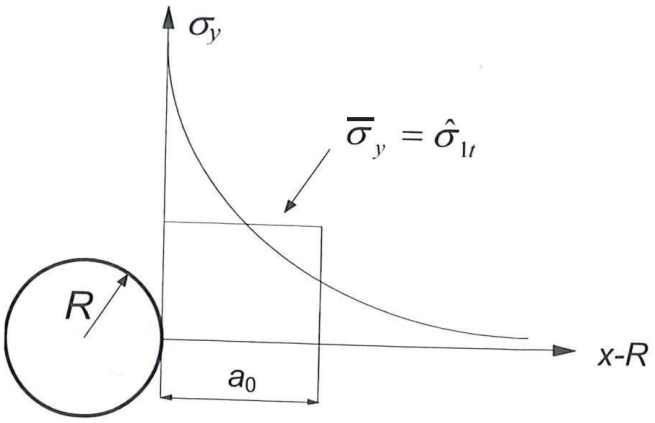

Figure 7.12: Illustration of the Whitney-Nuismer average-stress criterion for laminates with a hole (from Zenkert and Battley, *Foundations of Fibre composites*, Figure 6-28).

Inserting this condition in Eq. (7.24) yields the relation between the notched (σ_N) and unnotched (σ_0) strength as

$$\frac{\sigma_N}{\sigma_0} = \frac{2(1-p_2)}{2-p_2^2-p_2^4+(k_T-3)(p_2^6-p_2^8)} \tag{7.31}$$

where

$$p_2 = \frac{R}{R+a_0}. \tag{7.32}$$

Interesting to note is that also in this case, for very large holes $p_2 \to 1$ and consequently $\sigma_N/\sigma_0 \to (1/k_T)$ whereas for vanishingly small holes $p_2 \to 0$ and consequently $\sigma_N/\sigma_0 \to 1$.

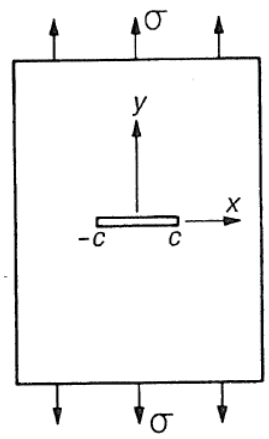

Figure 7.13: An orthotropic plate with a sharp crack of length $2c$ (from Agarwal et al, Figure 8-18).

7.3.3 Whitney-Nuismer criteria for cracks

In order to derive similar criteria for the case of a cracked laminate, let us now instead consider an infinite orthotropic plate with a sharp crack of length $2c$ subjected to a uniform load σ_y 'far away' from the crack, as shown in Figure 7.13. If the axes x and y are assumed to be normal to the planes of elastic symmetry (of the laminate), the normal stress σ_y acting along the line $y = 0$ can be approximated by

$$\sigma_y(x,0) = \frac{\sigma x}{\sqrt{x^2 - c^2}} = \frac{k_1 x}{\sqrt{\pi c\,(x^2 - c^2)}} \quad x > c \tag{7.33}$$

where, in the latter stage, the orthotropic stress intensity factor k_1 was introduced as

$$k_1 = \sigma\sqrt{\pi c}. \tag{7.34}$$

By applying the two failure criteria to the case of a sharp crack, we get the following:

7.3.3.1 Point-stress criterion for a crack

The point-stress criterion for cracks in a laminate which is specially orthotropic with respect to in-plane loading states that failure occurs when the stress at a distance d_0 from the crack tip reach the unnotched strength σ_0 such that

$$\sigma_y(c + d_0, 0) = \sigma_0 \tag{7.35}$$

which yields the relation between the notched (σ_N) and unnotched strength (σ_0) as

$$\frac{\sigma_N}{\sigma_0} = \sqrt{1 - p_3^2} \tag{7.36}$$

where

$$p_3 = \frac{c}{c + d_0}. \tag{7.37}$$

Interesting to note is that, for very large cracks $(\sigma_N/\sigma_0) \to \sqrt{2d_0/c}$ whereas for vanishingly small cracks $p_3 \to 0$ and consequently $\sigma_N/\sigma_0 \to 1$.

7.3.3.2 Average-stress criterion for a crack

The average-stress criterion for cracks in a laminate which is specially orthotropic with respect to in-plane loading states that failure occurs when the averaged stress over a distance a_0 from the hole edge reach the unnotched strength σ_0 such that

$$\frac{1}{a_0}\int_c^{c+a_0} \sigma_y(x,0)\,dx = \sigma_0 \tag{7.38}$$

which yields the relation between the notched and unnotched strength (σ_N) as

$$\frac{\sigma_N}{\sigma_0} = \sqrt{\frac{1-p_4}{1+p_4}} \tag{7.39}$$

where

$$p_4 = \frac{c}{c+a_0} \tag{7.40}$$

Interesting to note is that, for very large cracks $(\sigma_N/\sigma_0) \rightarrow \sqrt{0.5a_0/c}$ whereas for vanishingly small cracks $p_4 \rightarrow 0$ and consequently $\sigma_N/\sigma_0 \rightarrow 1$.

7.3.4 Concluding remarks regarding the Whitney-Nuismer criteria

It should be remarked that the benefit and usefulness of the Whitney-Nuismer approach to both holes and cracks is that the characteristic distances **remains constant for all hole or crack sizes in at least a particular laminate of a particular material system**. In this case, only two test are necessary (one for σ_0 and one for a_0/d_0) to characterise the notch strength. This does not of course hold in the general case but there are some experimental evidence that it holds for fibre dominated laminates in glass-epoxy, boron-epoxy and graphite-epoxy, cf. e.g. Figure 7.14 and Figure 7.15. Consequently, these criteria appears to a suitable rough estimate of the strength of notched laminates. For further reading on the validity of the Whitney-Nusimer criteria, interested readers can consult e.g. the paper by Eriksson and Aronsson (Eriksson and Aronsson, *Journal of Composite Materials*, Vol 24, pp 456–482, 1990). However, in real applications the appearance of e.g. cracks that penetrate the entire laminate, as in the idealised cases above, is in fact limited. Most often, crack initiate and propagate differently in the different plies depending on the fibre orientation.

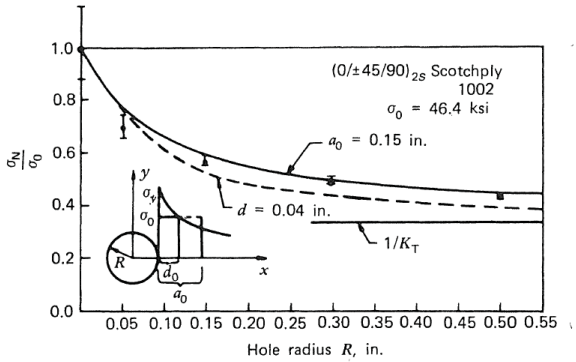

Figure 7.14: Comparison of experimentally measured and theoretically predicted strengths of $[0/\pm 45/90]_{2S}$ glass-epoxy laminates containing holes (from Agarwal et al, Figure 8-19).

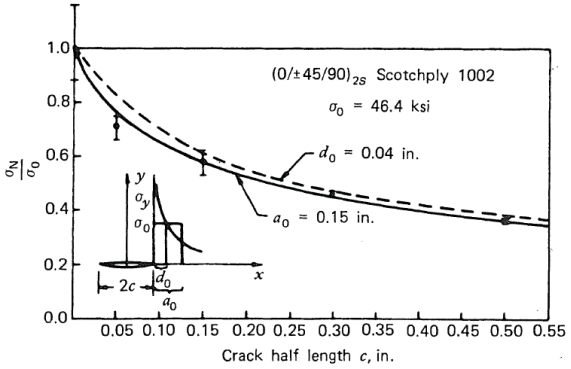

Figure 7.15: Comparison of experimentally measured and theoretically predicted strengths of $[0/\pm 45/90]_{2S}$ glass-epoxy laminates containing holes (from Agarwal et al, Figure 8-20).

Chapter 8

Viscoelasticity and damping

8.1 Introduction to viscoelasticity

In general, polymers behave viscoelastically. This will have a direct impact on fibre composites with the matrix material being a polymer. Viscoelastic materials are capable of storing elastic energy, while at the same time dissipating a certain amount of energy, especially when loaded at high rates or during a long time interval. Being elastic means that, opposed to energy dissipating *plastic* materials, the viscoelastic material will return to the original form (after some time) when all load is relieved. Furthermore, viscoelastic materials have a 'fading memory' which means that the current stress state depends on the total strain history, but with a larger emphasis on the most recent part. Thus, what happened 'long time ago' fades away.

Generally, viscoelasticity has (at least) the following four characteristics:

- When applying a constant stress, the strain will vary over time. This is denoted creep and a representative creep curve can be seen in Figure 8.1a. Of interest is that an initial elastic strain is obtained at the time the stress is applied. Thereafter, the strain will gradually increase up to a limiting value at 'infinite time'.

- When applying a constant strain, the stress will vary over time. This is denoted relaxation and a representative relaxation curve can be seen in Figure 8.1b. Of interest is that an initial elastic stress response is obtained at the time the constant strain is applied. Thereafter, the stress will gradually decrease (relax) down to a limiting value at 'infinite time'.

- A viscoelastic material will dissipate energy when subjected to cyclic loading, characterised by the hysteresis loop as shown in Figure 8.1c.

- A viscoelastic material is strain-rate dependent such that a stiffer (and sometimes more brittle) response is obtained when the strain-rate is increased, cf Figure 8.1d.

8.1.1 Creep compliance

In the case of creep where the stress is constant $\sigma = \sigma_0$, the strain will vary over time $\varepsilon = \varepsilon(t)$. Consequently, we can define the relation between the stress and strain by the *time-dependent* creep compliance $S(t)$:

$$\varepsilon(t) = S(t)\sigma_0 \Rightarrow S(t) = \frac{\varepsilon(t)}{\sigma_0} \tag{8.1}$$

The shape of the creep compliance as function of time will be the same as for the strain history shown in Figure 8.1a (the scale factor σ_0 relates the two).

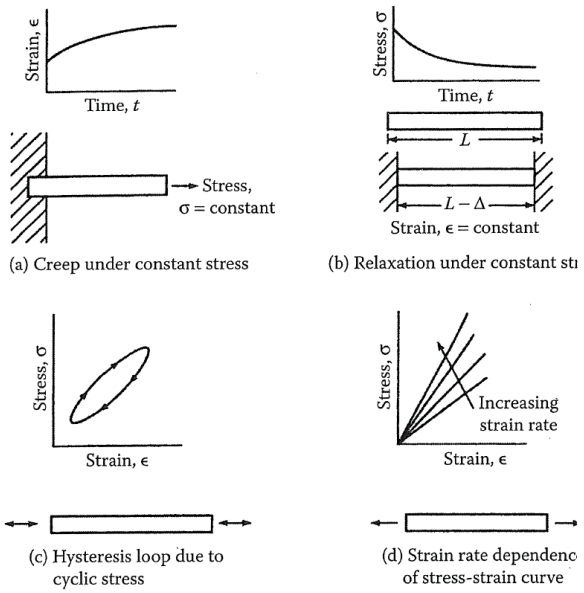

Figure 8.1: Characteristic behaviour of a viscoelastic material (from Gibson, *Principles of Composite Material Mechanics (2nd ed.)*, CRC Press, 2007, Figure 8.1).

8.1.2 Relaxation stiffness

In a similar fashion, we define the relaxation stiffness (or modulus) as the relation between the constant strain $\varepsilon = \varepsilon_0$ and time-varying stress $\sigma = \sigma(t)$ as

$$\sigma(t) = C(t)\varepsilon_0 \Rightarrow C(t) = \frac{\sigma(t)}{\varepsilon_0} \tag{8.2}$$

Please note that the shape of the creep compliance as function of time normally takes the same form as the stress history curve shown in Figure 8.1b (the scale factor ε_0 relates the two).

8.1.3 Boltzman superposition principle

It can be shown that, by knowing the creep compliance $S(t)$ (and the relaxation stiffness $C(t)$) and a given stress (strain) history, the corresponding time-varying strain (stress) can be computed as

$$\varepsilon(t) = \int_{-\infty}^{t} S(t-\tau)\frac{d\sigma(\tau)}{d\tau}d\tau \tag{8.3}$$

$$\sigma(t) = \int_{-\infty}^{t} C(t-\tau)\frac{d\varepsilon(\tau)}{d\tau}d\tau \tag{8.4}$$

The above equations are denoted as the *Boltzman superposition principle* and can easily be generalised to

$$\varepsilon_i(t) = \int_{-\infty}^{t} S_{ij}(t-\tau)\frac{d\sigma_j(\tau)}{d\tau}d\tau \tag{8.5}$$

$$\sigma_i(t) = \int_{-\infty}^{t} C_{ij}(t-\tau)\frac{d\varepsilon_j(\tau)}{d\tau}d\tau \tag{8.6}$$

where $S_{ij}(t)$ and $C_{ij}(t)$ are the creep compliance tensor and the relaxation stiffness tensor respectively.

8.1.4 Basic models for viscoelasticity

A normal way to visualise the models for viscoelasticity is by a system of springs (to represent the elastic response) and dashpots (for the rate-dependence causing energy dissipation). Below, three of the most basic models for viscoelasticity will be presented and discussed.

8.1.4.1 The Maxwell model

The simple model by Maxwell can be visualised by one spring with stiffness k $[N/m^2]$ and one dashpot with viscosity μ $[N\,s/m^2]$ in series, as shown in Figure 8.2a. In order to find a way to describe the relation between stresses, strains and their mutual rates, we start of by noting that the total strain over the system ε will be split into one part over the spring ε_1 and one part over the dashpot ε_2 as:

$$\varepsilon = \varepsilon_1 + \varepsilon_2 \tag{8.7}$$

Taking the rate of this equation:

$$\frac{\mathrm{d}\,\varepsilon}{\mathrm{d}\,t} = \frac{\mathrm{d}\,\varepsilon_1}{\mathrm{d}\,t} + \frac{\mathrm{d}\,\varepsilon_2}{\mathrm{d}\,t} \tag{8.8}$$

and realising that we, by equilibrium, have the same stress in both components such that:

$$\frac{\mathrm{d}\,\varepsilon_1}{\mathrm{d}\,t} = \frac{1}{k}\frac{\mathrm{d}\,\sigma}{\mathrm{d}\,t} \tag{8.9}$$

$$\frac{\mathrm{d}\,\varepsilon_2}{\mathrm{d}\,t} = \frac{\sigma}{\mu} \tag{8.10}$$

we end up with the following differential equation to describe the stress-strain relation:

$$\frac{\mathrm{d}\,\varepsilon}{\mathrm{d}\,t} = \frac{1}{k}\frac{\mathrm{d}\,\sigma}{\mathrm{d}\,t} + \frac{\sigma}{\mu} \tag{8.11}$$

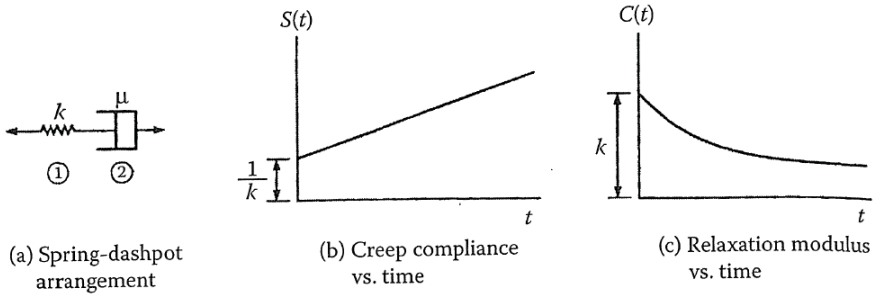

(a) Spring-dashpot arrangement

(b) Creep compliance vs. time

(c) Relaxation modulus vs. time

Figure 8.2: The Maxwell model for viscoelasticity (from Gibson, *Principles of Composite Material Mechanics (2nd ed.)*, CRC Press, 2007, Figure 8.8).

Creep compliance of the Maxwell model

To study the response of the Maxwell model in creep, we set $\sigma = \sigma_0$ (constant) and $\varepsilon = \varepsilon(t)$. Thereby, the differential equation reduces to:

$$\frac{\mathrm{d}\,\varepsilon}{\mathrm{d}\,t} = \frac{\sigma_0}{\mu} \tag{8.12}$$

which integrated gives the following form for the strain

$$\varepsilon(t) = \frac{\sigma_0}{\mu}t + C_1 \tag{8.13}$$

In order to determine the constant C_1 we make use of the initial condition $\varepsilon(0) = \frac{\sigma_0}{k}$ (the stress is applied so quickly that the dashpot 'has no chance to react'). Thus, we obtain the strain as

$$\frac{\sigma_0}{k} = C_1 \Rightarrow \varepsilon(t) = \frac{\sigma_0}{\mu}t + \frac{\sigma_0}{k} \tag{8.14}$$

and, consequently, the creep compliance as

$$S(t) = \frac{\varepsilon(t)}{\sigma_0} = \frac{t}{\mu} + \frac{1}{k} \tag{8.15}$$

which has the shape as shown in Figure 8.2b. Note that this does not match what is generally observed in experiments, cf. Figure 8.1a, which leads to the conclusion that the Maxwell model is *not adequate to describe creep in a realistic way.*

Relaxation stiffness of the Maxwell model

To study the response of the Maxwell model in relaxation, we set $\varepsilon = \varepsilon_0$ (constant) and $\sigma = \sigma(t)$. Thereby, the differential equation reduces to:

$$0 = \frac{1}{k}\frac{\mathrm{d}\,\sigma}{\mathrm{d}\,t} + \frac{\sigma}{\mu}. \tag{8.16}$$

Integration and utilisation of the initial value $\sigma(0) = k\,\varepsilon_0$ (cf. motivation above) we end up with the relaxation stiffness $C(t)$ as:

$$C(t) = \frac{\sigma(t)}{\varepsilon_0} = k\,\mathrm{e}^{-t/\lambda} \tag{8.17}$$

where $\lambda = \mu/k$ is the so-called relaxation time. The resulting shape of $C(t)$ can be seen in Figure 8.2c and it is clear that it corresponds to what is generally observed in experiments, cf Figure 8.1b. Thus, it can be concluded that *the Maxwell model can represent relaxation in a physically realistic way.*

8.1.4.2 The Kelvin-Voight model

The simple model by Kelvin and Voight can be visualised by one spring with stiffness k $[N/m^2]$ and one dashpot with viscosity μ $[N\,s/m^2]$ in parallel, as shown in Figure 8.3a. In order to find a way to describe the relation between stresses, strains and their mutual rates, we start of by noting that the strain over the individual components will be the same:

$$\varepsilon = \varepsilon_1 = \varepsilon_2 \tag{8.18}$$

and that the total stress σ will be the sum of the contributions from the spring and the dashpot. Thereby, we directly obtain the differential equation to describe the Kelvin-Voight model as:

$$\sigma = k\,\varepsilon + \mu\frac{\mathrm{d}\,\varepsilon}{\mathrm{d}\,t} \tag{8.19}$$

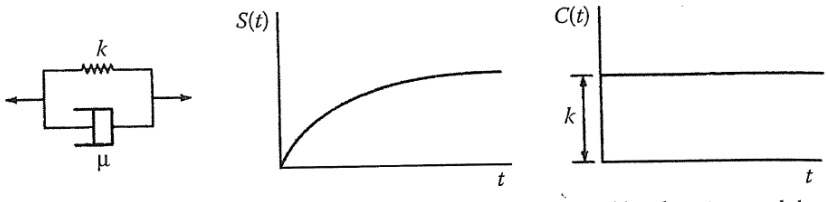

(a) Spring-dashpot arrangement

(b) Creep compliance vs. time

(c) Relaxation modulus vs. time

Figure 8.3: The Kelvin-Voight model for viscoelasticity (from Gibson, *Principles of Composite Material Mechanics (2nd ed.)*, CRC Press, 2007, Figure 8.9).

Creep compliance of the Kelvin-Voight model

It is rather straightforward to prove the expression of the creep compliance to be:

$$S(t) = \frac{1}{k}\left(1 - \mathrm{e}^{-t/\rho}\right) \tag{8.20}$$

where $\rho = \mu/k$ is the retardation time. Show this on your own! (use the same argumentation for the dashpot as in the description of the Maxwell model). It can from Figure 8.3b be concluded that the shape of the creep compliance is reasonable, cf. Figure 8.1a, except for the lack of an initial elastic response.

Relaxation stiffness of the Kelvin-Voight model

It is straightforward to prove the expression of the relaxation stiffness to be:

$$C(t) = k. \tag{8.21}$$

It can from Figure 8.3c be concluded that the shape of the relaxation stiffness is unphysical (should decrease and reach an asymptotic value), cf. Figure 8.1b. Thus, it can be concluded that *the Kelvin-Voight cannot represent creep in a physically realistic way.*

8.1.4.3 The Zener model (or three parameter model)

As can be realised from the analysis of the two most basic models for viscoelasticity above, there is a need for a somewhat more advanced model in order to have a model that can represent both limiting cases (creep and relaxation) in a physically acceptable way. One such model is the Zener single relaxation model (sometimes denoted the three-parameter model) as shown in Figure 8.4a. Thus, this model can be described by the parallel coupling between one spring with stiffness k_0 and one spring (k_1) and one dashpot (μ_1) in series. Furthermore, it can be shown that the differential equation for this model can be written as:

$$\sigma + \frac{\mu_1}{k_1}\frac{\mathrm{d}\,\sigma}{\mathrm{d}\,t} = k_0\,\varepsilon + \frac{\mu_1}{k_1}\,(k_0 + k_1)\,\frac{\mathrm{d}\,\varepsilon}{\mathrm{d}\,t} \tag{8.22}$$

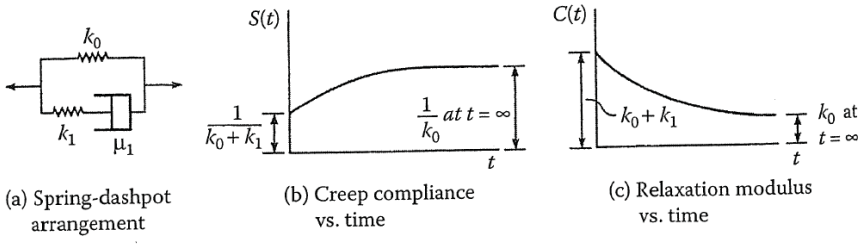

(a) Spring-dashpot arrangement

(b) Creep compliance vs. time

(c) Relaxation modulus vs. time

Figure 8.4: The Zener model for viscoelasticity (from Gibson, *Principles of Composite Material Mechanics (2nd ed.)*, CRC Press, 2007, Figure 8.10).

Creep compliance of the Zener model

It can be shown (cf. the tutorial session) that the creep compliance for the Zener model can be written as

$$S(t) = \frac{1}{k_0}\left(1 - \frac{k_1}{k_0 + k_1}\mathrm{e}^{-t/\rho_1}\right) \tag{8.23}$$

where the retardation time is given by $\rho_1 = \frac{\mu_1}{k_0 k_1}\,(k_0 + k_1)$. From the shape of this curve, cf. Figure 8.4b, it can be concluded that *the Zener model can represent creep in a physically realistic way.*

Relaxation stiffness of the Zener model

It can be shown (cf. the tutorial session) that the relaxation stiffness for the Zener model can be written as

$$C(t) = \left(k_0 + k_1\mathrm{e}^{-t/\lambda_1}\right) \tag{8.24}$$

where the relaxation time is $\lambda_1 = \mu_1/k_1$. From the shape of this curve, cf. Figure 8.4c, it can be conclude that *the Zener model can represent also relaxation in a physically realistic way.*

8.1.5 Viscoelastic material subjected to sinusoidal loading

In many practical structural applications, the response under oscillatory loading is of major importance. Therefore, we will in the following section investigate the response of a viscoelastic material under sinusoidal loading $\tilde{\sigma}(t) = \sigma_0 \sin(\omega t)$ (in the following we use $\tilde{\sigma}(t)$ and $\tilde{\varepsilon}(t)$ to denote sinusoidal variations in time). We will use the Zener model as a representative of the viscoelastic response since it is the simplest possible model with physically acceptable behaviour.

We start by noting that we can, by making use of complex numbers, write the time-varying stress as[1]:

$$\tilde{\sigma}(t) = \text{Imag}\left[\sigma_0 \mathrm{e}^{i\omega t}\right] \tag{8.25}$$

where Imag $[\bullet]$ represents the imaginary part of $\bullet$ and where $i = \sqrt{-1}$. However, as will be shown below, if we drop the Imag-part, more valuable information concerning the energy dissipation and damping can be extracted, whereby we in fact consider the applied load as

$$\tilde{\sigma}(t) = \sigma_0 \mathrm{e}^{i\omega t} \tag{8.26}$$

in the following. Furthermore, we realise that the resulting strain will oscillate with the same frequency, but that it due to the rate-dependence may follow the stress with a certain delay, or *phase-lag*, δ such that

$$\tilde{\sigma}(t) = \sigma_0 \mathrm{e}^{i\omega t} \rightarrow \tilde{\varepsilon}(t) = \varepsilon_0 \mathrm{e}^{i(\omega t - \delta)} \tag{8.27}$$

If we insert the expression for $\tilde{\sigma}(t)$ and $\tilde{\varepsilon}(t)$ into the differential equation of the Zener model, Eq. (8.22), we obtain

$$\tilde{\sigma}(t)\left[1 + \frac{\mu_1}{k_1}(i\omega)\right] = \left[k_0 + \frac{\mu_1}{k_1}(k_0 + k_1)(i\omega)\right]\tilde{\varepsilon}(t) \tag{8.28}$$

which, if we multiply by $1 - \frac{\mu_1}{k_1}(i\omega)$, can be reformulated to obtain the following relation between the stress and strain:

$$\tilde{\sigma}(t) = \left[\frac{k_0 + \lambda_1^2 (k_0 + k_1)\omega^2}{1 + \lambda_1^2 \omega^2} + i\frac{\lambda_1 k_1 \omega}{1 + \lambda_1^2 \omega^2}\right]\tilde{\varepsilon}(t) \tag{8.29}$$

or

$$\tilde{\sigma}(t) = E^*(\omega)\tilde{\varepsilon}(t) \tag{8.30}$$

where $E^*(\omega)$ is the *complex* Young's modulus

$$E^*(\omega) = E'(\omega) + iE''(\omega) \tag{8.31}$$

with

$$E'(\omega) = \frac{k_0 + \lambda_1^2 (k_0 + k_1)\omega^2}{1 + \lambda_1^2 \omega^2} \tag{8.32}$$

$$E''(\omega) = \frac{\lambda_1 k_1 \omega}{1 + \lambda_1^2 \omega^2}. \tag{8.33}$$

Here, $E'(\omega)$ is the so-called *storage modulus* and $E''(\omega)$ is the so-called *loss modulus*. By introducing the frequency-dependent loss-factor $\eta(\omega)$, which is a measure of the relative damping properties of the material, Eq. (8.31) can be reformulated as

$$E^*(\omega) = E'(\omega)(1 + i\eta(\omega)) \tag{8.34}$$

where, consequently, $\eta(\omega)$ is defined as

$$\eta(\omega) = \frac{E''(\omega)}{E'(\omega)}. \tag{8.35}$$

In Figure 8.5, the generic dependence of $E'(\omega)$ and $E''(\omega)$ on ω is shown. It can be seen that for low frequencies ($\omega \rightarrow 0$) the storage modulus approach the long-term stiffness ($E'(\omega) \rightarrow k_0$) whereas the loss modulus approach zero ($E''(\omega) \rightarrow 0$). Thus, as expected the rate-independent response is obtained for low loading rates (=low frequencies). On the other hand, for large frequencies ($\omega \rightarrow \infty$) the storage modulus approach the dynamic stiffness $E'(\omega) \rightarrow k_0 + k_1$ meaning that the response is physically acceptable also

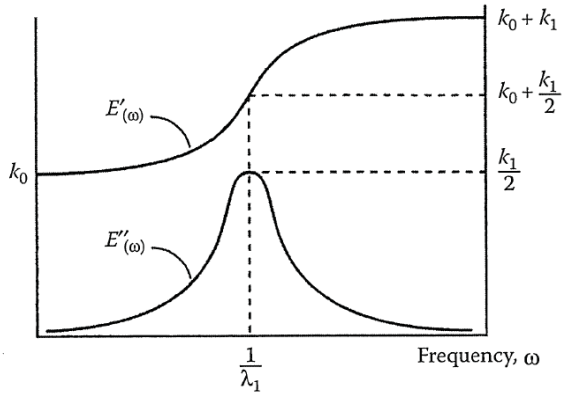

Figure 8.5: Variation of storage modulus, $E'(\omega)$, and loss modulus, $E''(\omega)$, with frequency for the Zener model (from Gibson, *Principles of Composite Material Mechanics (2nd ed.)*, CRC Press, 2007, Figure 8.33).

at high loading-rates. In addition, it can be seen that the loss modulus is maximised for an angular frequency of $1/\lambda_1$.

It should also be noted that the complex Young's modulus can be written as:

$$E^*(\omega) = |E^*(\omega)|\, \mathrm{e}^{i\alpha} \tag{8.36}$$

where

$$|E^*(\omega)| = \sqrt{E'^2 + E''^2} \tag{8.37}$$

$$\alpha = \arctan\left(\frac{E''(\omega)}{E'(\omega)}\right) \tag{8.38}$$

which, inserted into $\tilde{\sigma}(t) = E^*(\omega)\tilde{\varepsilon}(t)$, yields

$$\tilde{\sigma}(t) = \sigma_0\, \mathrm{e}^{i\omega t} = |E^*(\omega)|\, \mathrm{e}^{i\alpha} \varepsilon_0\, \mathrm{e}^{i(\omega t - \delta)} \Rightarrow \tag{8.39}$$

$$\delta = \alpha = \arctan\left(\frac{E''(\omega)}{E'(\omega)}\right) \tag{8.40}$$

$$\varepsilon_0 = \frac{\sigma_0}{|E^*(\omega)|} \tag{8.41}$$

8.1.5.1 Generalisation

It can be shown that Eq. (8.30) can be generalised to the following form

$$\tilde{\sigma}_i(t) = C^*_{ij}(\omega)\tilde{\varepsilon}_j(t) \tag{8.42}$$

where

$$C^*_{ij}(\omega) = i\omega C_{ij}(\omega) \tag{8.43}$$

in which $C_{ij}(\omega)$ is the *Fourier transform* of the relaxation stiffness tensor $C_{ij}(t)$ as

$$C_{ij}(\omega) = \int_{-\infty}^{\infty} C_{ij}(\tau)\, \mathrm{e}^{-i\omega\tau}\, \mathrm{d}\,\tau \tag{8.44}$$

Thus, in the 1D case, $E^*(\omega)$ can be directly obtained e.g. for the Zener model by taking the Fourier transform of Eq. (8.24) as

$$E^*(\omega) = i\omega \int_{-\infty}^{\infty} \left(k_0 + k_1 \mathrm{e}^{-\tau/\lambda_1}\right)\, \mathrm{e}^{-i\omega\tau}\, \mathrm{d}\,\tau \tag{8.45}$$

[1] Since $\sigma_0 \mathrm{e}^{i\omega t} = \sigma_0\,(\cos(\omega t) + i\sin(\omega t))$

8.2 Application to fibre composites - damping

Making use of the derivations above, we can now address the dynamic response and damping properties of a fibre composite laminate in which the fibres can be seen as more or less purely elastic whereas the matrix material (if being a polymer) behaves viscoelastically.

First, we note that in order to enable a simple procedure for the combination of the material properties (homogenisation of properties), the following conditions must be satisfied (cf. also Figure 8.6):

- The fibre dimension (diameter) d must be 'much smaller' than the characteristic length of the laminate L, i.e. $d << L$. This is in fact a necessary condition also for the preceding discussion regarding homogenisation of the elastic properties.
- The dimension (diameter) d must be 'much smaller' than the wave length of the oscillations, i.e. $d << \lambda$, meaning that the applicability of the approach presented below is limited to sufficiently low frequencies. What the actual limit is can only be determined by comparisons between the predicted response and experimental measurements of the same.

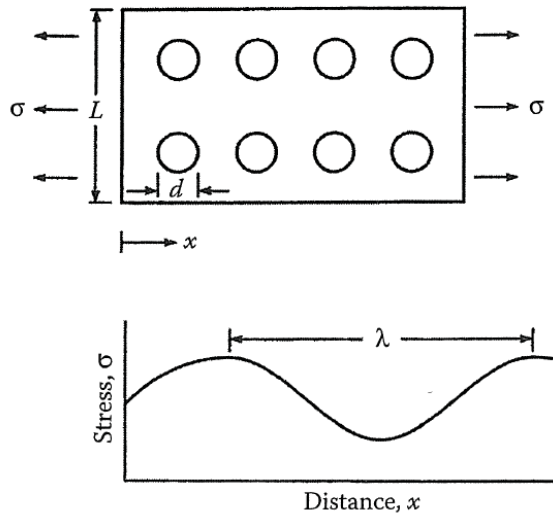

Figure 8.6: Critical dimensions for the validity of the homogenisation (from Gibson, *Principles of Composite Material Mechanics (2nd ed.)*, CRC Press, 2007, Figure 8.6).

Assuming that the requirements specified above are met, we can continue to characterise the dynamic response and damping properties of the laminate. First, we note that, when subjected to sinusoidal loading, we have the following situation

$$\tilde{\sigma}_i^f(t) = C_{ij}\tilde{\varepsilon}_j^f(t) = [\bar{Q}_{ij}]_f\tilde{\varepsilon}_j^f(t) \qquad \text{for the fibres} \tag{8.46}$$

$$\tilde{\sigma}_i^m(t) = C_{m,ij}^*(\omega)\tilde{\varepsilon}_j^m(t) \qquad \text{for the matrix} \tag{8.47}$$

$$\tilde{\sigma}_i^c(t) = C_{c,ij}^*(\omega)\tilde{\varepsilon}_j^c(t) \qquad \text{for the composite} \tag{8.48}$$

in which $[\bar{Q}_{ij}]_f$ is the normal tensor relating fibre strains to fibre stresses, $C_{m,ij}^*(\omega)$ is the complex stiffness for the matrix and $C_{c,ij}^*(\omega)$ is the homogenised complex stiffness for the composite, which can be obtained by the ordinary homogenisation rules used for the elastic properties. What this means is that E_m is replaced by E_m^* in the models to predict the different moduli etc. Thus, the general procedure is as follows:

1. Determine $E_m^*(\omega) = E_m'(\omega) + iE_m''(\omega)$
2. utilise $E_m^*, \nu_m, E_f, \nu_f, V_f$ to determine $[\mathbf{Q}^*](E_L^*, E_T^*, G_{LT}^*, \nu_{LT}^*, \nu_{TL}^*)$
3. For each ply k, transform $[\mathbf{Q}^*]$ to obtain $[\overline{\mathbf{Q}}^*]_k = [T_1]_k^{-1}[\mathbf{Q}^*][T_2]_k = [\overline{\mathbf{Q}}'(\omega) + i\overline{\mathbf{Q}}''(\omega)]_k$

4. Utilise $[\overline{\mathbf{Q}}^*]_k$ to compute $[\mathbf{A}^*] = [\mathbf{A}'(\omega) + i\mathbf{A}''(\omega)], [\mathbf{B}^*] = [\mathbf{B}'(\omega) + i\mathbf{B}''(\omega)]$ and $[\mathbf{D}^*] = [\mathbf{D}'(\omega) + i\mathbf{D}''(\omega)]$ matrices to obtain the relation
$$\left\{ \begin{array}{c} \tilde{\mathbf{N}}(t) \\ \tilde{\mathbf{M}}(t) \end{array} \right\} = \left[\begin{array}{cc} \mathbf{A}^* & \mathbf{B}^* \\ \mathbf{B}^* & \mathbf{D}^* \end{array} \right] \left\{ \begin{array}{c} \tilde{\boldsymbol{\varepsilon}}^0(t) \\ \tilde{\mathbf{k}}(t) \end{array} \right\}$$

5. Applied to a specific kinematical representation of *e.g.* a plate (*e.g.* Mindlin theory), also a complex stiffness matrix can be computed on the structural level as
$$\mathbf{K}^* = \mathbf{K}'(\omega) + i\mathbf{K}''(\omega).$$
In this case, $\mathbf{K}''(\omega)$ is nothing but a frequency dependent structural damping matrix $\mathbf{C}^{mat}(\omega)$ due to internal (material) damping., cf. structural dynamics. Is should however be remarked that this material damping due to the viscoelastic material response is only one part of the total structural damping.

It should be remarked that it is not straightforward to realise or prove that the approach above holds, but several experimental comparisons prove a very good agreement between predicted and experimentally measured behaviour, cf. e.g. Figure 8.7.

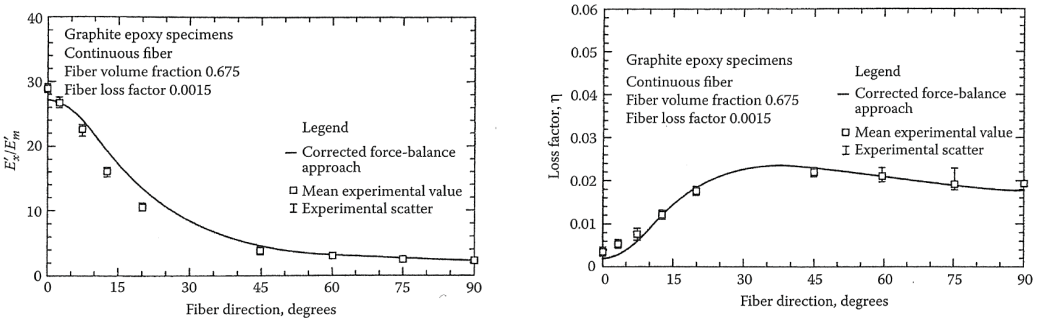

a) b)

Figure 8.7: Predicted and measured a) off-axis storage modulus ratio, E'_x/E'_m and b) loss factor η of graphite/epoxy for various fibre orientations (from Suarez, Gibson, Sun, Chaturvedi. *Experimental Mechanics*, 26(2):175–184, 1986).

8.2.1 Example: In-plane sinusoidal loading of a symmetric laminate

Considering a symmetric laminate subjected to an in-plane load $\tilde{\mathbf{N}}(t) = \{1, 0, 0\}^T \, \mathrm{e}^{i\omega t}$ N/m and zero moment ($\tilde{\mathbf{M}}(t) = \mathbf{0}$), we note that the time-varying mid-plane strains can be obtained as
$$\tilde{\boldsymbol{\varepsilon}}^0(t) = [\mathbf{A}^*]^{-1} \tilde{\mathbf{N}}(t) \tag{8.49}$$
Using the following notation
$$[\mathbf{A}^*]^{-1} = \left[\begin{array}{ccc} A_{11}^{*-1} & A_{12}^{*-1} & A_{16}^{*-1} \\ A_{12}^{*-1} & A_{22}^{*-1} & A_{26}^{*-1} \\ A_{16}^{*-1} & A_{26}^{*-1} & A_{66}^{*-1} \end{array} \right]$$
we obtain the different strain components as:
$$\tilde{\varepsilon}_x^0(t) = A_{11}^{*-1} \, \mathrm{e}^{i\omega t} = |A_{11}^{*-1}| \, \mathrm{e}^{i(\omega t - \delta_{11})} \tag{8.50}$$
$$\tilde{\varepsilon}_y^0(t) = A_{12}^{*-1} \, \mathrm{e}^{i\omega t} = |A_{12}^{*-1}| \, \mathrm{e}^{i(\omega t - \delta_{12})} \tag{8.51}$$
$$\tilde{\gamma}_{xy}^0(t) = A_{16}^{*-1} \, \mathrm{e}^{i\omega t} = |A_{16}^{*-1}| \, \mathrm{e}^{i(\omega t - \delta_{16})} \tag{8.52}$$

As can be seen, the different strain component will oscillate with the same frequency but with different amplitudes (e.g. $|A_{11}^{*-1}|$ for $\tilde{\varepsilon}_x^0(t)$) and different phase-lags (e.g. δ_{11} for $\tilde{\varepsilon}_x^0(t)$) where the latter are defined

as

$$\delta_{11} = \arctan\left(\frac{\text{Imag}\left[\text{A}_{11}^{*-1}\right]}{\text{Real}\left[\text{A}_{11}^{*-1}\right]}\right) \tag{8.53}$$

$$\delta_{12} = \arctan\left(\frac{\text{Imag}\left[\text{A}_{12}^{*-1}\right]}{\text{Real}\left[\text{A}_{12}^{*-1}\right]}\right) \tag{8.54}$$

$$\delta_{16} = \arctan\left(\frac{\text{Imag}\left[\text{A}_{16}^{*-1}\right]}{\text{Real}\left[\text{A}_{16}^{*-1}\right]}\right) \tag{8.55}$$

In the present case, since the amplitude of the force is unity, the amplitudes of the strain components correspond to the so-called *amplification factors* ($|A_{ij}^{*-1}|$), which in general relate the amplitude in force to the amplitude in strain.

To investigate the frequency dependency of the amplification factors, we consider the special case of a $[90/0/45]_S$-laminate of thickness $h = 12\,\text{mm}$ with volume fraction of fibres $V_f = 0.6$ with the following properties:

Fibres:
$E_f = 350$ GPa, $\nu_f = 0.2$

Matrix (represented by the Zener model):
$k_0 = 3.5$ GPa, $k_1 = 3.5$ GPa, $\mu_1 = 1$ MPa s, $\nu_m = 0.35$

It can be seen from Figure 8.8a that damping results in that the amplification factors decrease with angular frequency giving the largest amplitudes for really slow loading. Furthermore, from Figure 8.8b, the phase-lag of $\tilde{\varepsilon}_x^0(t)$ is evident (there is a time-shift between the oscillations in force and in strain) in the plot showing the normalised force and normalised strain.

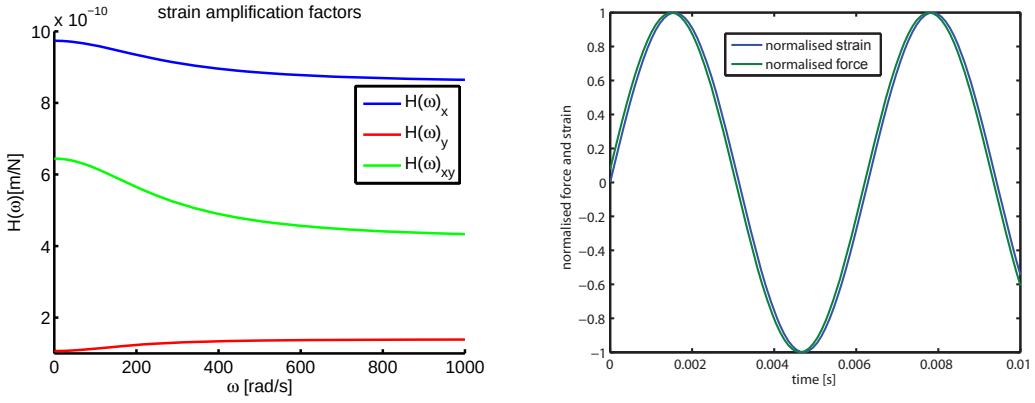

a) b)

Figure 8.8: a) Predicted amplification factors ($H(\omega)_x = |A_{11}^{*-1}|$, $H(\omega)_y = |A_{12}^{*-1}|$ and $H(\omega)_{xy} = |A_{16}^{*-1}|$) and b) predicted normalised x-component of strain $\tilde{\varepsilon}_x^0(t)/|\varepsilon_x^0|$ plotted together with the normalised force $\tilde{N}_x(t)/|N_x|$.

8.2.2 Example: Sinusoidal bending of a symmetric laminate

In order to study the effect of laminate lay-up on the damping properties, we consider two symmetric laminates $[90/0]_S$ and $[0/90]_S$ subjected to a bending moment load $\tilde{\mathbf{M}}(t) = \{1, 0, 0\}^T \, \text{e}^{i\omega t}$ Nm/m and zero in-plane load ($\tilde{\mathbf{N}}(t) = \mathbf{0}$). For this case, we note that the time-varying curvatures can be obtained as

$$\tilde{\mathbf{k}}(t) = [\mathbf{D}^*]^{-1}\tilde{\mathbf{M}}(t) \tag{8.56}$$

Using the following notation

$$[\mathbf{D}^*]^{-1} = \begin{bmatrix} D_{11}^{*-1} & D_{12}^{*-1} & D_{16}^{*-1} \\ D_{12}^{*-1} & D_{22}^{*-1} & D_{26}^{*-1} \\ D_{16}^{*-1} & D_{26}^{*-1} & D_{66}^{*-1} \end{bmatrix}$$

we obtain the different curvature components as:

$$\tilde{k}_x(t) = D_{11}^{*-1}\,\mathrm{e}^{i\omega t} = |D_{11}^{*-1}|\,\mathrm{e}^{i(\omega t-\delta_{11})} \tag{8.57}$$

$$\tilde{k}_y(t) = D_{12}^{*-1}\,\mathrm{e}^{i\omega t} = |D_{12}^{*-1}|\,\mathrm{e}^{i(\omega t-\delta_{12})} \tag{8.58}$$

$$\tilde{k}_{xy}(t) = D_{16}^{*-1}\,\mathrm{e}^{i\omega t} = |D_{16}^{*-1}|\,\mathrm{e}^{i(\omega t-\delta_{16})} \tag{8.59}$$

As can be seen, the different curvature component will oscillate with the same frequency but with different amplitudes (e.g. $|D_{11}^{*-1}|$ for $\tilde{k}_x(t)$) and different phase-lags (e.g. δ_{11} for $\tilde{k}_x(t)$) where the latter are (in the bending case) defined as

$$\delta_{11} = \arctan\left(\frac{\mathrm{Imag}\,[\mathrm{D}_{11}^{*-1}]}{\mathrm{Real}\,[\mathrm{D}_{11}^{*-1}]}\right) \tag{8.60}$$

$$\delta_{12} = \arctan\left(\frac{\mathrm{Imag}\,[\mathrm{D}_{12}^{*-1}]}{\mathrm{Real}\,[\mathrm{D}_{12}^{*-1}]}\right) \tag{8.61}$$

$$\delta_{16} = \arctan\left(\frac{\mathrm{Imag}\,[\mathrm{D}_{16}^{*-1}]}{\mathrm{Real}\,[\mathrm{D}_{16}^{*-1}]}\right) \tag{8.62}$$

To investigate the lay-up dependency on the amplification factors (and thereby the damping properties), we consider two laminates with different lay-up but with the same total thickness of 8 mm and the constituent properties:

Fibres:
$E_f = 350$ GPa, $\nu_f = 0.2$

Matrix (represented by the Zener model):
$k_0 = 3.5$ GPa, $k_1 = 3.5$ GPa, $\mu_1 = 10$ MPa s, $\nu_m = 0.35$

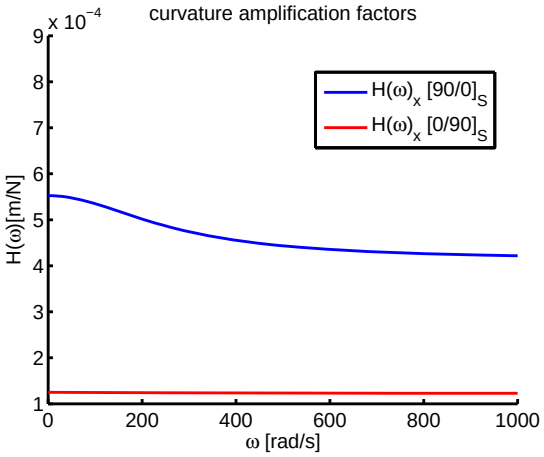

Figure 8.9: Predicted amplification factor ($H_x^{\kappa}(\omega) = |D_{11}^{*-1}|$) for the $[0/90]_S$ and $[90/0]_S$ laminates.

What is interesting to note in Figure 8.9 is the expected weaker response when the upper and lower plies has fibres in the 90°-direction ($[90/0]_S$), but also that a pronounced frequency dependency is obtained whereas in the reversed case ($[0/90]_S$), the amplification factor $H(\omega)_x = |D_{11}^{*-1}|$ is more or less constant.

This means that more damping is obtained whenever plies with fibres oriented 90° are placed at (or close to) the top and bottom of the laminate. Thereby, it can be concluded that, not only the stiffness properties but also the damping properties may be tailored by changing the order of the plies.

Chapter 9

A brief introduction to cohesive zone modelling of delamination propagation

9.1 Preliminaries

We will study how a cohesive zone modelling approach works in practice under the following simplified conditions:

- The problem studied is a double cantilever beam test modelled in 2D with uniform width and uniform thickness of the laminate.
- A centrally placed delamination propagates from a centrally placed initial notch.
- Each ply is explicitly modelled through the thickness with separate elements.
- The notch is modelled such that elements above and below the notch have separate nodes along the interface which corresponds to two overlapping traction free external surfaces of the domain.
- The propagating delamination is modelled by a so-called cohesive zone connecting the upper and lower elements along the propagation path. This can also be viewed as having separate interface elements sharing the nodes of the elements on either side of the propagation path.

9.2 A simple prototype cohesive zone model for mode I loading

A simple form of a cohesive zone model for pure mode I loading (see Figure 9.1a), i.e. a model that describes the relation between the resulting normal traction and the given normal separation (the displacement discontinuity) over a delamination surface, can be seen in Figure 9.1b . As can be seen, the model has an initial elastic response (with a given stiffness K) followed by a linear softening response where the latter represents the degrading load carrying capacity of the interface as the plies separate.

As explained earlier, the area under the traction-separation law represents the critical energy release rate of the material (or the fracture toughness) G_{Ic}. Furthermore, the traction is maximum for an opening separation d_0 with the maximum value σ_{nf} and the material is considered as fully degraded (or fully "damaged") at a separation distance of d_{nf}. In between d_0 and d_{nf}, the degradation of the interface is described by a damage variable α ranging from 0 to 1 where $\alpha = 0$ represents the pristine interface with full load carrying capacity and $\alpha = 1$ represents a fully damaged interface with no load carrying capacity (traction is zero). Thus, for any opening (or normal displacement discontinuity) d_n in a point along the delaminating interface, we can find the resulting normal traction as

$$t_n = (1 - \alpha)Kd_n \tag{9.1}$$

To find d_0 and d_{nf} we simply consider the following equalities:

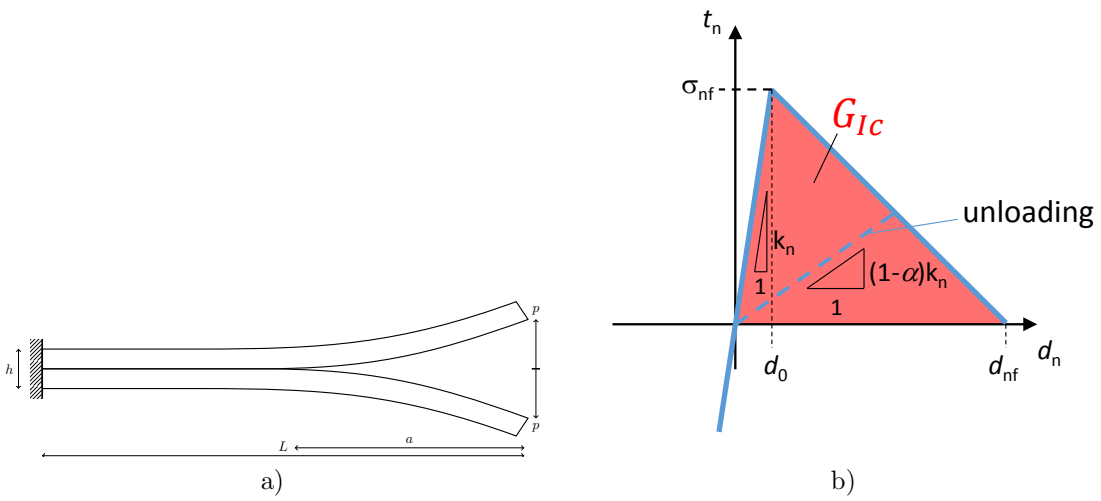

Figure 9.1: a) sketch of double cantilever beam loaded in pure mode I. b) Mode I cohesive zone model with linear softening.

$$\sigma_{nf} = Kd_0 \Rightarrow d_0 = \frac{\sigma_{nf}}{K} \tag{9.2}$$

$$G_{Ic} = \frac{1}{2}\sigma_{nf} d_{nf} \Rightarrow d_{nf} = \frac{2G_{Ic}}{\sigma_{nf}} \tag{9.3}$$

9.2.1 How to calculate the damage variable

We know that in every point, we can calculate the resulting traction according to Eq. (9.1). But, we can also find the traction as

$$t_n = \sigma_{nf} - \left(\frac{\sigma_{nf}}{d_{nf} - d_0}\right)(d_n - d_0) \tag{9.4}$$

Equating Eq. (9.1) and Eq. (9.4) gives after some elaboration

$$\alpha = 1 - \frac{d_0}{d_n}\frac{(d_{nf} - d_n)}{(d_{nf} - d_0)} \tag{9.5}$$

The typical traction and damage evolution as function of crack opening displacement is shown in Figure 9.2 Please note the rapid initial evolution in this model.

9.3 The cohesive zone contribution to the finite element load vector

The weak form of a 2D elasticity problem for a body Ω with external boundary $\Gamma_{ext} = \Gamma_{ext,D} \cup \Gamma_{ext,N}$ (one Dirichlet and one Neumann part) and internal traction loaded delamination surfaces Γ^+_{int} and Γ^-_{int} (upper and lower surfaces of the interface Γ_{int}), see Figure 9.3 , can be written on matrix form as:

$$\int_\Omega \left(\tilde{\boldsymbol{\nabla}}\delta\mathbf{u}\right)^T \boldsymbol{\sigma}\, d\Omega = \int_{\Gamma_{ext,N}} \delta\mathbf{u}^T\mathbf{t}\, d\Gamma + \int_{\Gamma^+_{int}} \delta\mathbf{u}^T\mathbf{t}^+\, d\Gamma + \int_{\Gamma^-_{int}} \delta\mathbf{u}^T\mathbf{t}^-\, d\Gamma, \quad \forall\delta\mathbf{u} \in \mathbf{V}_{\delta u} \tag{9.6}$$

We note that the term in the left hand side and the first term in the right hand side are standard terms for problems without any cracks forming in the body, whereby we pay attention only to the additional terms including the effect of the cohesive zone model in terms of the cohesive tractions $\mathbf{t}^+$ and $\mathbf{t}^-$ on the upper and lower delamination crack surface respectively.

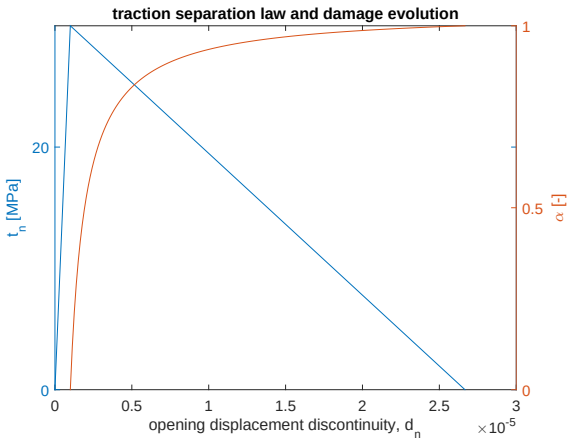

Figure 9.2: Typical normal traction (d_n) and damage (α) evolution as function of normal crack opening displacement (d_n) for a cohesive zone model with the folowing material parameters: $K = 3 \times 10^{13}$ N/m^3, $\sigma_{nf} = 30$ MPa and $G_{Ic} = 400$ J/m^2.

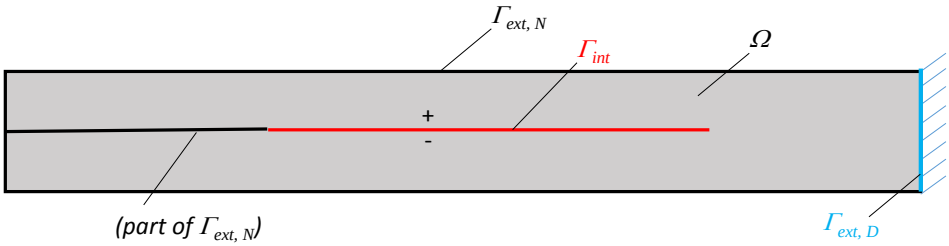

Figure 9.3: Sketch of domain Ω with external boundary Γ_{ext} and an internal traction interface Γ_{int}.

In the finite element formulation (using Galerkin's method), the external load contribution from these new "cohesive" terms can be written as:

$$\mathbf{f}_b^{coh} = \int_{\Gamma_{int}^+} \mathbf{N}_+^T \mathbf{t}^+ \, d\Gamma + \int_{\Gamma_{int}^-} \mathbf{N}_-^T \mathbf{t}^- \, d\Gamma \tag{9.7}$$

where $\mathbf{N}_+$ and $\mathbf{N}_-$ denotes the standard shape function matrices evaluated above (+) and below (-) the delamination interface respectively. Please note that these will be different since elements above and below the delamination interface do not share nodes.

Thus, for each matching pair of elements above and below the delamination interface, the procedure to calculate the load contribution will be the same. For this purpose, we here further simplify the discussion and consider only the contribution from the cohesive tractions along the interface segment shared by the elements 1 and 2, see Figure 9.4 for definitions.

With the node numbering of these two elements as indicated in Figure 9.4, we can now write the explicit expressions for the contribution to the external load vector as

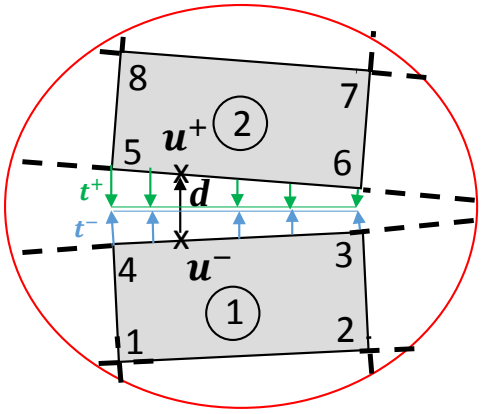

Figure 9.4: Two continuum 2D element sharing a cohesive segment. Element ① has nodes 1-4 and is here defined to be on the minus (-) side of the interface and Element ② has nodes 5-8 and is here defined to be on the plus (+) side of the interface.

$$\mathbf{f}_b^{coh,e} = \int_{\Gamma_{int}^-} \begin{bmatrix} 0 & 0 \\ 0 & 0 \\ 0 & 0 \\ 0 & 0 \\ N_3 & 0 \\ 0 & N_3 \\ N_4 & 0 \\ 0 & N_4 \\ 0 & 0 \\ 0 & 0 \\ 0 & 0 \\ 0 & 0 \\ 0 & 0 \\ 0 & 0 \\ 0 & 0 \\ 0 & 0 \end{bmatrix} \mathbf{t}^- \, d\Gamma + \int_{\Gamma_{int}^+} \begin{bmatrix} 0 & 0 \\ 0 & 0 \\ 0 & 0 \\ 0 & 0 \\ 0 & 0 \\ 0 & 0 \\ 0 & 0 \\ 0 & 0 \\ N_5 & 0 \\ 0 & N_5 \\ N_6 & 0 \\ 0 & N_6 \\ 0 & 0 \\ 0 & 0 \\ 0 & 0 \\ 0 & 0 \end{bmatrix} \mathbf{t}^+ \, d\Gamma = \int_{\Gamma_{int}^-} \begin{bmatrix} 0 \\ 0 \\ 0 \\ 0 \\ N_3 t_x^- \\ N_3 t_y^- \\ N_4 t_x^- \\ N_4 t_y^- \\ 0 \\ 0 \\ 0 \\ 0 \\ 0 \\ 0 \\ 0 \\ 0 \end{bmatrix} d\Gamma + \int_{\Gamma_{int}^+} \begin{bmatrix} 0 \\ 0 \\ 0 \\ 0 \\ 0 \\ 0 \\ 0 \\ 0 \\ N_5 t_x^+ \\ N_5 t_y^+ \\ N_6 t_x^+ \\ N_6 t_y^+ \\ 0 \\ 0 \\ 0 \\ 0 \end{bmatrix} d\Gamma \tag{9.8}$$

since $N_3 - N_6$ will be the only shape functions that are non-zero along the interface considered.

What remains is then:

1. to calculate the cohesive tractions $\mathbf{t}(\mathbf{d}) = \mathbf{t}^- = -\mathbf{t}^+$ from the displacement discontinuity $\mathbf{d} = \mathbf{u}^+ - \mathbf{u}^-$ (or separation distance) using a cohesive zone model, cf. e.g. Section 9.2 above.

2. to integrate the cohesive traction contribution accurately according to Eq. (9.8) and to assemble the force contributions to the global load vector.

9.3.1 The interface element approach

The steps above can be handled directly from Eq. (9.8), but more convenient can be to consider the cohesive contributions in terms of separate interface elements connecting the 2D elasticity elements above and below the delamination interface.

To see this, we first note that:

$$N_4 = N_5 = N_1^e, \; N_3 = N_6 = N_2^e \text{ along the interface segment} \tag{9.9}$$

where N_1^e and N_2^e are one-dimensional shape functions along the delamination interface as indicated in Figure 9.5 . Due to traction continuity $\mathbf{t}^- = -\mathbf{t}^+$ this also leads to that

$$\int_{\Gamma_{int}^e} N_3 t_x^- \, d\Gamma = -\int_{\Gamma_{int}^e} N_6 t_x^+ \, d\Gamma = \int_{\Gamma_{int}^e} N_2^e t_x(\mathbf{d}) \, d\Gamma \tag{9.10}$$

$$\int_{\Gamma_{int}^e} N_3 t_y^- \, d\Gamma = -\int_{\Gamma_{int}^e} N_6 t_y^+ \, d\Gamma = \int_{\Gamma_{int}^e} N_2^e t_y(\mathbf{d}) \, d\Gamma \tag{9.11}$$

$$\int_{\Gamma_{int}^e} N_4 t_x^- \, d\Gamma = -\int_{\Gamma_{int}^e} N_5 t_x^+ \, d\Gamma = \int_{\Gamma_{int}^e} N_1^e t_x(\mathbf{d}) \, d\Gamma \tag{9.12}$$

$$\int_{\Gamma_{int}^e} N_4 t_y^- \, d\Gamma = -\int_{\Gamma_{int}^e} N_5 t_y^+ \, d\Gamma = \int_{\Gamma_{int}^e} N_2^e t_y(\mathbf{d}) \, d\Gamma \tag{9.13}$$

from which we can conclude that it is sufficient to calculate the interface element cohesive load vector

$$\mathbf{f}_b^{int,e} = \int_{\Gamma_{int}^e} \begin{bmatrix} N_1^e t_x(\mathbf{d}) \\ N_1^e t_y(\mathbf{d}) \\ N_2^e t_x(\mathbf{d}) \\ N_2^e t_y(\mathbf{d}) \end{bmatrix} d\Gamma \tag{9.14}$$

and then assemble the contribution (with the correct sign) to the right positions of $\mathbf{f}_b^{coh,e}$ in Eq. (9.8).

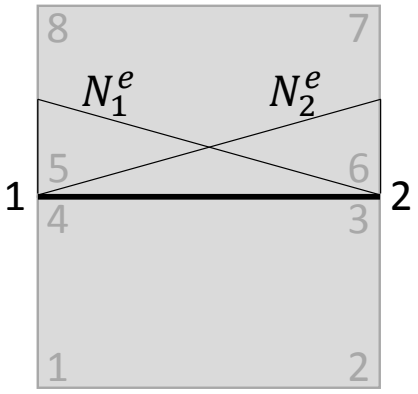

Figure 9.5: Sketch of the cohesive interface element with local nodes 1 and 2 and how these relate to the continuum element nodes for element ① and ② shown in grey.

$\mathbf{f}_b^{int,e}$ is calculated for each cohesive segment using numerical integration in 1D. This can be done according to the following procedure:

- initialise $\mathbf{f}_b^{int,e} = \begin{bmatrix} 0 \\ 0 \\ 0 \\ 0 \end{bmatrix}$
- Loop over the number of integration points of the segment and add contributions to $\mathbf{f}_b^{int,e}$. For each integration point:
  - Calculate the displacement discontinuity $\mathbf{d} = \mathbf{u}^+ - \mathbf{u}^-$ in the integration point
  - Calculate $\mathbf{t}(\mathbf{d})$ from the cohesive zone model
  - Evaluate N_1^e and N_2^e in the integration point

– Add the contribution to the load vector

$$\mathbf{f}_b^{int,e} = \mathbf{f}_b^{int,e} + \begin{bmatrix} N_1^e t_x(\mathbf{d}) \\ N_1^e t_y(\mathbf{d}) \\ N_2^e t_x(\mathbf{d}) \\ N_2^e t_y(\mathbf{d}) \end{bmatrix} \times gw$$

where gw is the corresponding Gauss weight of the integration point. As an example, if two Gauss points are used $gw = \frac{L_e}{2}$ where L_e is the length of the segment

- Assemble the components of $\mathbf{f}_b^{int,e}$ (with the correct sign) into the proper positions of $\mathbf{f}_b^{coh,e}$